Stratal and Petrophysical Complexity Expressed in Seismic Reflection Patterns within Isolated Carbonate Platforms

By:

Adrienne Michele Duarte

Submitted to the graduate degree program in Geology and the Graduate Faculty of the University of Kansas in partial fulfillment of the requirements from the degree of Master of Science.

_____

Chair Dr. Eugene C. Rankey

_____

Dr. Evan K. Franseen

_____

Dr. George P. Tsoflias

Date Defended: August 28, 2018

The Thesis Committee for Adrienne Michele Duarte
Certifies that this is the approved version of the following thesis:

Stratal and Petrophysical Complexity Expressed in Seismic Reflection Patterns within Isolated Carbonate Platforms

_____

Chair Dr. Eugene C. Rankey

_____

Dr. Evan K. Franseen

_____

Dr. George P. Tsoflias

Date Approved: August 28, 2018

ABSTRACT

Seismic data are fundamental tools for evaluating and exploiting hydrocarbon resources, yet how the heterogeneous nature of carbonates complicates imaging, interpretation, and predictability of reservoir properties from seismic data is poorly understood. To test the hypothesis that changes in geologic inputs create a statistically distinct impact on seismic character of isolated platforms, this project generated synthetic seismic volumes from geologic models in which geologic heterogeneities (e.g. vertical and lateral trends in facies, porosity, and impedance) were isolated and varied, and their seismic impacts evaluated. Twenty-eight geologic scenarios, each of which addresses a single variable of geologic heterogeneity, form the basis for qualitatively illustrating the influence of stratal and petrophysical complexity on seismic volumes. The geological and petrophysical inputs are derived from modern and ancient analogs that capture a range of depositional and petrophysical variability. Subtle seismic reflection patterns captured by seismic attributes facilitate quantitative insights for understanding the relationship between geology and seismic character. Exploring statistical distinctions among scenarios reveals the capability for attributes to predict rock properties (e.g., average porosity) accurately in certain geological models.

Qualitative results illustrate the seismic character of models in which stratigraphic architecture and petrophysical complexity varied reveals marked differences in phase and amplitude leading to both accurate and inaccurate geological interpretations. Quantitative results illustrate that as the type of geological heterogeneity changes, the quality of prediction between attributes and average porosity (expressed on a trace-by-trace, and net pore volume basis) also varies, emphasizing the importance of geology on attributes. These results provide insights into

the complex controls on the seismic character of isolated platforms and potential pitfalls in interpretation.

ACKNOWLEDGEMENTS

I would like to thank Dr. Eugene Rankey, for serving as both my graduate and undergraduate advisor, mentor, and friend throughout my years at The University of Kansas. I would also like to thank Dr. George Tsoflias for serving on my committee, and for his thoughtful discussions and providing comments to improve the quality of this work. I would like to thank Dr. Evan Franseen for serving on my committee, providing comments to improve the quality of this work, and for his advice and mentorship. I would also like to thank Hassan Eltom for introducing me to Petrel software and teaching me think like a modeler. I would like to thank the Rankey Research Group, both current and graduated students for their support, and "cooperate to graduate" mentality: Michelle Mary, Thomas Neal, Alexa Goers, Hamilton Goodner, Hannah Hubert, and Maritha Konetchy; and special thanks to Steven Herbst for always being available to brainstorm ideas and help with Petrel. I would like to thank Dr. Steve Hasiotis for his mentorship and support throughout my time at The University of Kansas, he and his class are one of the reasons I declared my geology major my first semester of college. I also would like to thank Dr. Diane Kamola for her advice and support as a professor and friend. I would like to thank my family for their continuous support throughout this entire process. I would also like to thank my new family, Mr. Steve and Mrs. Jerri Sitek, for their endless generosity and support, especially toward the end of the writing and editing process. Finally, I would like to thank my fiancé, Brian Sitek, for his emotional and mental support by keeping me grounded. Support for this project came from the Kansas Interdisciplinary Carbonates Consortium (KICC) and the University of Kansas Geology Department.

TABLE OF CONTENTS

Abstract iii
Acknowledgements v
Table of Contents vi
Introduction 1
Modeling the Seismic Character of Geological Variability 2
Geological Inspiration 3
Modeling Geological Heterogeneities 4
Modeling Framework 6
Analysis of Models 9
Seismic Expression of Geological Heterogeneity within Isolated Platforms: Qualitative Character 9
Base Case and Null Hypothesis Scenarios 9
Stratigraphic Architecture 11
Petrophysical Complexities 14
Seismic Expression of Geological Heterogeneity within Isolated Platforms: Quantitative Signatures of Stratigraphy and Porosity 17
Implications for Seismic Interpretation 19
Implications for Seismic Interpretation: 1. Qualitative Aspects 20
Implications for Seismic Interpretation: 2. Quantitative Considerations 23
Implications for Seismic Interpretation: 3. Comparison with Extant Isolated Platforms 25
Conclusions 29
References 31
Figures 42
Tables 55
Appendix 1. Geologic Models and Synthetic Seismic Volumes 59
Appendix 2. Quantitative Characterization of Seismic Character 66
Appendix 3. Prediction of Rock Properties from Seismic Data 78
Appendix 4. Tables 90
Appendix 5. Plots of Multivariate Regressions 91
Appendix 6. Plots of Variable Amplitude Seismic Traces 92

INTRODUCTION

Isolated platforms can be found globally and throughout geologic time. These geologic features provide a record of depositional processes important in carbonate systems, and may serve as prolific hydrocarbon-producing carbonate reservoirs in strata of many geologic ages and locations (e.g., Miocene Central Luconia Province, Malaysia - Epting 1980, 1989; Zampetti et al., 2003, 2004, Malampaya platform, Philippines - Grötsch and Mercadier, 1999; Fournier et al., 2004, 2005; Neuhaus et al., 2004; Fournier and Borgomano, 2007, Natuna Platform and updip Segitiga Platform, Indonesia - May and Eyles 1985; Rudolph and Lehmann 1989; Bachtel et al., 2004, Jurassic Djebel Bou Dahar platform, Morocco – Campbell and Stafleu, 1992, Devonian Western Canadian Basin pinnacles - Watts, 1987, Silurian Niagaran pinnacles, Michigan Basin - Huh et al., 1977, and many more globally). Many carbonate reservoirs in isolated platforms include considerable geological and geophysical heterogeneity, driven by variable stratigraphic architecture (Sarg, 1988), diagenesis (e.g., Jones and Xiao, 2006), porosity-permeability-velocity relations (e.g., Ehrenberg, 2004), and structural deformation (e.g., Yose et al., 2001; Elvebakk et al., 2002; Ting et al., 2011). Furthermore, detailed and quantitative understanding of the impacts of distinct types of variability on predictability of reservoir properties from seismic data is explored poorly in the literature.

Synthetic seismic models provide a means to explore this variability, and to better understand controls on seismic character of carbonate systems (e.g., Campbell and Stafleu 1992; Anselmetti et al., 1997; Eberli et al., 2004; Zeller et al., 2014). To further constrain geological controls, many studies have focused on exploring the likely seismic expression of specific, well studied outcrops (e.g., Stafleu and Sonnenfeld, 1995; Bourgeois et al., 2004; Janson et al., 2007; Favliene et al., 2010; Kleipool et al., 2017). Many of these stratigraphic-seismic models

carefully honor stratal architecture and geometry. As a simplification, these studies model invariant geologic properties throughout each geobody (that is, each facies body includes uniform acoustic impedance), and do not consider alternative geological scenarios.

This project utilizes a distinct, systematic approach. Instead of attempting to understand the seismic character of one specific reservoir system or outcrop analog, it considers the seismic signatures of a spectrum of possible geological systems. As such, it is not "constrained" by data specific to one area or geological age. Rather, this project models a range of idealized isolated platforms so that critical comparison of model inputs and seismic attributes captures diverse seismic reflection patterns related to a range of possible geological heterogeneity. In doing so, this study explicitly tests the hypothesis that geologic (e.g., model) inputs create statistically distinct impacts on seismic character within isolated platforms.

The aim of this paper is to enhance understanding of how differences in seismic character reflect changes in stratigraphic and petrophysical properties of isolated carbonate platforms. By generating a suite of 'what if' synthetic volumes, various types of geological heterogeneity (e.g., vertical and lateral trends in facies, porosity, and impedance) can be isolated and varied, and their impacts on seismic character can be evaluated. The results reveal pronounced differences in seismic character among models, as well as predictability of porosity as geological heterogeneity is varied.

MODELING THE SEISMIC CHARACTER OF GEOLOGICAL VARIABILITY

Through their influences on absolute values or spatial variability in impedance, a spectrum of parameters influence the seismic character of isolated carbonate platforms (Sarg and Schuelke, 2003; Eberli et al., 2004). A complete consideration of all possible scenarios is impossible.

Instead, rather than focusing on parameters such as structural modification (faults and fractures), slope facies heterogeneity, or fluid properties, this study focuses on assessing the importance of sedimentologic and stratigraphic influences (and implicitly, diagenetic factors) on platform-top systems. The general philosophy is not to model every possible isolated platform or all possible combinations of all parameters. Instead, the conceptual and numerical models aim to create simple, idealized models to better understand how seismic data reflect changes in key geologic properties in fully controlled systems, focusing on facies variability (dimensions, spatial distribution, and vertical stacking pattern) and facies-based porosity trends (absolute values and range) that impact the interiors of carbonate platform systems. Note that this manuscript describes "facies" by reference to an environment of deposition (slope, reef, reef sand apron, and platform interior) for simplicity; the assumption is that the products of different environments would have distinct sedimentological (and diagenetic) character, and hence distinct petrophysical signatures. Future studies can build upon results of this study to incorporate other variables (mentioned above) that impact seismic character.

Geological Inspiration

Although this project models idealized platforms, the geological and petrophysical inputs are derived from modern and ancient analogs that capture a range of depositional and petrophysical variability (Table 1). Devonian (Nisku) pinnacles of the Western Canadian Sedimentary Basin and Miocene platforms of the Central Luconia province, South China Sea, provide input into the examples of ranges of average porosity (mean Devonian $\phi = 9\%$; Watts, 1987 and mean Miocene $\phi = 26\%$; Rudolph and Lehmann 1989; Grötsch and Mercadier, 1999; Fournier et al., 2004; Neuhaus et al., 2004, respectively), stratigraphic vertical trends in porosity (e.g., shallowing- and

deepening-upward intervals), and stratigraphic parameters (such as vertical and spatial facies distribution) to ensure geologically plausible scenarios. However, no single scenario is intended to explicitly model the specific details for either Devonian or Miocene analogs.

High-resolution satellite imagery of platforms of the South China Sea (Rankey, 2016) show spatial distributions of modern geomorphic elements and serve as modern analogs for spatial distribution and widths of facies. Geomorphic elements can have a wide range of widths and distributions, however, the probability of occurrence is linked to location on the platform (Rankey 2016). Both modern and subsurface analogs in the South China Sea (Epting 1980, 1989; May and Eyles 1985; Rudolph and Lehmann 1989; Grötsch and Mercadier, 1999; Zampetti et al., 2003, 2004; Fournier et al., 2004, 2005; Neuhaus et al., 2004; Fournier and Borgomano, 2007; Bachtel et al., 2004) provided guidance for constructing varieties of stratigraphic architecture.

Modeling Geological Heterogeneities

Because they are fully constrained, forward synthetic seismic models of a suite of scenarios with different geological properties provide a means to explore geological controls on seismic character. The scenarios capture geological heterogeneities at a range of scales (Figure 1), as might be present in isolated platform systems. Heterogeneities considered here can be grouped into two primary classes: 1) stratigraphic architecture (e.g., layer-cake, clinoform, and stochastic facies distributions; facies and zonal stacking patterns; facies dimensions; presence or absence of low-porosity zones), and 2) petrophysical properties (average and range of porosity within and among facies, and trends in porosity).

Stratigraphic architecture is a primary control on seismic character (Payton, 1977; Hubbard et al., 1985; Eberli et al., 2004; Hart, 2008; Kleipool et al., 2017). As used here, and as modeled, architecture includes variations in facies dimensions (the plan-view extent and orientation of a facies body), spatial distribution (facies belts and facies mosaics - e.g., Wright and Burgess, 2005; Rankey, 2016), and both facies and zonal stacking patterns. Zonal stacking patterns in this study are captured in zones 100 m thick and control the margins of the platform. Facies stacking patterns herein refers to the arrangement of facies within zones (e.g., prograding, aggrading, and retrograding); these zone might be considered of the scale as parasequence sets (Van Wagoner et al., 1988; Lehrmann and Goldhammer, 1999). Some scenarios tested the impact of inclusion of 15-m thick, low-porosity layers (e.g., dense flooding or diagenetically altered intervals; Neuhaus et al., 2004; Zampetti et al., 2004; Warrlich et al., 2008). Facies stacking patterns include two depositional geometries, layer cake (e.g., Borgomano et al., 2008) and clinoformal (e.g., Droste and Van Steenwinkel, 2004; Masaferro et al., 2004; and Neuhaus et al., 2004). A null-hypothesis scenario in the stratigraphic architecture group is the absence of any stratigraphic organization, here generated by stochastic facies distribution in three dimensions.

In addition to stratigraphic architecture, petrophysical properties also impact seismic character. As used here, changes in petrophysical properties refer to variations in mean porosity, and stratigraphic trends in porosity (e.g., increasing- or decreasing-upward porosity). These changes are explored systematically using ‘greenhouse’ and ‘icehouse’ end-member inputs to the conceptual models. For example, mean porosity for ‘Devonian’ low-porosity greenhouse end-member analogs is 9%, whereas mean porosity of the ‘Miocene’ high-porosity icehouse end member is 26% (Watts, 1987; Rudolph and Lehmann 1989; Grötsch and Mercadier, 1999).

Furthermore, each facies includes distinct mean porosity, and porosity variability ranges between high (+/- 10 p.u.) and low (+/- 5 p.u.) variance end members. Vertical changes in porosity (such as an upwards increase or decrease in porosity) across varying stratigraphic thicknesses mimic porosity trends from the Devonian Nisku pinnacles and Miocene South China Sea platform analogs (Watts, 1987; Rudolph and Lehmann 1989; Bachtel et al., 2004; Fournier et al., 2004; Neuhaus et al., 2004).

Modeling Framework

To explore the role of the geological heterogeneity on seismic expression of isolated carbonate platforms, a suite of scenarios systematically captures an array of geologic variability. Each scenario includes three parts: an idealized geologic model, a synthetic seismogram, and extracted attributes. Each geologic model represents a realization intended to isolate specific type(s) of heterogeneity that occur in isolated platform reservoirs. The dimensions of each model are 3 km long x 200 m wide x 500 m thick, with cell dimensions (I, J, K) of 20 m x 20 m x 1 m (481,500 cells). Each synthetic 3D volume also could be considered as ten equi-probable realizations of synthetic 2D seismic lines through the platform.

All models include one isolated carbonate platform (300 m thick), consisting of three 100 m-thick stratigraphic zones, underlain and overlain by high-impedance shale (100 m thick each). Within each stratigraphic zone, four facies (slope, reef, reef sand apron, and platform interior) that represent depositional environments recognized in modern and ancient rock record are distributed using Petrel's truncated Gaussian simulation with trends method (Figure 1). The middle carbonate zone isolates the heterogeneity of interest. Horizontal-parallel layering within stratigraphic zones of most facies models is utilized to mimic layer-cake facies geometry

commonly interpreted within platform interiors (e.g., Borgomano et al., 2008). In contrast, in clinoform-based models, layers follow an inclined stratigraphic surface to create clinoform geometries (e.g., Masaferro et al., 2004).

Within this stratigraphic and facies framework, porosity is distributed by facies. Although porosity is the end product of both depositional (e.g., Anselmetti and Eberli, 2001; and Fournier and Borgomano, 2007) and diagenetic processes (e.g., Ehrenberg, 2004), the mean and range commonly are distinct among depositional facies (Watts et al., 1994; Yose et al., 2001; Atchley et al., 2006; Fournier and Borgomano, 2007). As such, porosity was distributed by facies, using Gaussian distribution within the volume (Grötsch and Mercadier, 1999; Ehrenberg, 2004; Falivene et al., 2010; Janson and Fomel, 2011) in all cases but one. The exception to this facies-based method used stochastic distribution, which simulated an end-member conceptual null model of processes in which porosity was unrelated to facies, as if "random" diagenesis were the control.

Wylie's time average equation provided a means to estimate acoustic velocity from porosity (Anselmetti et al., 1997; Eberli et al., 2003) for each cell in each model. Since velocity can vary at a given porosity (and porosity can vary at a given velocity) in carbonates (Anselmetti and Eberli, 1999), models incorporate internal variability to mimic changes in porosity-velocity relations (Wang, 1997) using a mean value and standard deviation to populate porosity for a given facies. Density was calculated from porosity, assuming a limestone matrix (Mavko et al., 2009). The product of density and velocity simulated in this way provide acoustic impedance. In all models, fluid type (as water), was held constant, and hence not evaluated as an influence.

The synthetic seismic response was calculated by 1D convolution of the impedance volume (e.g., Dubrule et al., 1998) with a zero-phase, SEG-normal polarity Ricker wavelet

(Ricker, 1953) of length 128 ms and sample rate 2 ms. Although lower than many industry surveys, the central frequency (10 Hz) was set so that the resolvable limit is approximately the thickness of the zone of interest (100 m), given an average velocity of 4,000 m/s. *(Wavelength = Average Velocity / Frequency = 4000 m/s / 10 Hz = 400 m; Resolvable Limit = Wavelength / 4 = 400 / 4 = 100 m).* Though models at or near the resolvable limit might be influenced by tuning effects (Widess, 1973), other higher-resolution models (not illustrated here) effectively imaged the geometries and internal variability directly, and thus were of less interest. Although the models (as constructed) assess variability in a 100 m-thick zone at 10 Hz, the responses scale; that is, model response would replicate a 50 m-thick zone (with 0.5 m-thick cells) at 20 Hz, or 20 m-thick zone (with 0.2 m thick cells) at 50 Hz.

Seismic attributes measure quantitative signal characteristics such as amplitude and signal shape, and thus quantitatively capture variability in seismic data (Rijks and Jauffred, 1991; Matteucci, 1996; Chopra and Marfurt, 2008; Hart, 2013). In this study, the analysis considered only attributes from the area of platform-top facies within the middle carbonate stratigraphic zone (e.g., interval in which geology varied) and used surface inputs as boundaries. Even though slope facies can have economic importance (e.g., Enos, 1985; Collins et al., 2013; Kosa et al., 2015), platform-marginal slopes were not assessed because they have distinct imaging challenges (e.g., high dips, related to elevated depositional gradient) that would require different modeling strategies, and therefore, would deter focus from the idealized and fully constrained models (studies that focus primarily on modeling slope margins include Rudolph et al., 1989; Biddle et al., 1992; Bracco-Gartner et al., 2004; Collins et al., 2013, to list a few). The number of seismic traces for each synthetic volume used for subsequent analysis ranged between 660 and 784, depending on stratigraphic architecture. For example, the progradational zonal stacking pattern

included a larger platform interior than the aggradational platform, and thus included more traces. Additionally, a subset of extractions included an extended interval of 20 ms above and below the stratigraphic surfaces, to evaluate how extraction interval could impact attributes.

Analysis of Models

The net products of the seismic modeling include an idealized, and fully constrained geologic model and synthetic volume for each of the 28 geological scenarios. These scenarios also are associated explicitly with a suite of seismic attributes extracted from the middle zone in which the geological controls are systematically varied. To directly relate the model input and geologic parameters to their seismic expression, and assess the 'predictability' of geology, the suite of scenarios are evaluated both qualitatively (i.e., visual comparison of seismic expression among scenario groups and published reservoir analogs) and quantitatively (i.e., statistical analyses of attributes and their ability to predict a known geological input).

SEISMIC EXPRESSION OF GEOLOGICAL HETEROGENEITY WITHIN ISOLATED PLATFORMS: QUALITATIVE CHARACTER

Forward synthetic seismic models of a suite of 28 geologic scenarios form a basis for qualitatively evaluating the influence of stratigraphic architecture and petrophysical complexity on seismic character (Figures 2, 3). These data are assessed qualitatively (this section) and quantitatively (next section). For consistency, all models are compared to a simple "base case" geological scenario (Figure 2).

Base Case and Null Hypothesis Scenarios

Geological parameters for the base case scenario represent an aggradational zonal facies stacking pattern, distributed with layer-cake geometry (Figure 2A). Within Zone 2 (Z2 on figures, the zone of interest), geological heterogeneity changes, but all other zones (Zones 1 and 3, Z1 and Z3 on figures) are modeled as constant and are not evaluated. Each facies has a different mean porosity (Table 2; Figure 2B) and mean impedance (Figure 2C).

Seismically, the volume includes high- to low-amplitude discontinuous-inclined reflectors (Figure 2D) near the margins. Although the geologic model includes only parallel facies stratal geometry, the varying dip angles of reflectors capture the subtle change in facies stacking patterns on either end of the platform (i.e., lack of contrast in the impedance between zones). The area of stacked platform interior facies has the lowest amplitude, consistent with the low impedance contrasts (Figure 2C). In comparison, areas with facies transitions (platform interior to reef sand apron; reef sand apron to reef) are reflected in the seismic volume by high amplitude. Because the porosity (and impedance) contrast between the reef sand apron and platform interior is greater than the difference between the reef and reef sand apron, the platform interior-reef sand apron facies transition has higher amplitude than the reef sand apron-reef facies transition. Another explanation could result from tuning effects, which increases the amplitudes in the reef sand apron facies.

An alternative scenario simulates a null-hypothesis geologic model of "random" distribution of porosity through the volume (e.g., non-geological heterogeneity; porosity is unrelated to facies, and distributed stochastically) (Figure 3A and B). In this scenario, no trends in facies or porosity occurs within Zone 2, but the two other zones include an aggradational stacking pattern. Within Zone 2, mean and range of porosity in all cells is the same as the base case.

The absence of any stratigraphic organization within Zone 2 results in stochastic distribution of impedance contrasts. Not surprisingly, therefore, the seismic data in Zone 2 include sub-parallel to wavy reflectors of moderate amplitude (Figure 3A), with less continuity and a more chaotic appearance than is present in the base case.

Stratigraphic Architecture

Five scenarios within the stratigraphic architecture group consider changes in facies dimensions and distribution, as well as facies and zonal stacking pattern, but hold average porosity (and thus impedance) by facies constant. This suite of scenarios isolates and explores the seismic expressions of 1) distinct zonal stacking patterns (progradational; aggradational [i.e., base case scenario]; and retrogradational), 2) the addition of a 15-m thick impedance (e.g. shale) cap on the middle zone, and 3) intra-zonal depositional geometries within Zone 2 (layer cake and clinoform) (Figure 3C-J and Table 3).

Zonal Stacking Patterns. Scenarios with progradational, aggradational, and retrogradational zonal stacking patterns all have layer-cake facies distribution. They are distinct in that: 1) the progradational zonal stacking pattern (Figure 3C) includes facies that build basinward in each zone; 2) the aggradational zonal stacking pattern (Figure 2A; the base case scenario) has facies that stack vertically; and 3) the retrogradational zonal stacking pattern (Figure 3F) includes zones that step back (platformward) relative to the underlying zone.

As these geologic models include facies of the same dimensions and with the same average porosity (and therefore the same average impedance), their seismic character includes some similarities (compare Figure 3D and E; Figure 2D). For example, in all models, platform interior areas include the lowest amplitude reflectors, and the highest amplitude reflectors occur

at the boundary between the reef sand apron and platform interior facies. Each of these distinctions are controlled by the specifics of the distribution and magnitude of impedance contrasts within and among facies and potentially tuning effects. Transitions between facies are major impedance contrasts and thus form high-amplitude reflectors, whereas intra-facies contrasts are less pronounced and hence include low-amplitude reflectors.

In detail, nonetheless, the data reveal pronounced differences. For example, although the boundary between the reef sand apron and platform interior facies is high amplitude, the phase of the wavelet varies (e.g., compare Figure 3D and E) as a function of zone and facies stacking patterns (which in turn controls impedance, and impedance contrasts). In the progradational model, for example, the boundary is a trough, due to the decrease in impedance from overlying platform interior to underlying reef sand apron. In the retrogradational model, it forms a peak caused by the downward increase in impedance from reef sand apron to platform interior. The aggradational model (base case scenario; Figure 2D) does not show a comparable reflector at the facies boundary because the position of the facies boundary does not change at this resolution, rather the facies change results in inclined reflectors.

Beyond changes in amplitude and phase, the stratal geometries suggested by the seismic vary markedly. For example, the progradational model has reflectors dipping away from the shelf margin (Figure 3D), the aggradation model has several reflectors that appear to dip at lower angle into the interior (Figure 2D), and the retrogradational model has a pronounced basinward-dipping reflector that appears to be progressively onlapped (Figure 3E). The dipping reflections are interpreted to be pseudo-geometries (Hubbard et al., 1985; Stafleu and Schlager, 1993; Jason et al., 2007), because all models had layer-cake depositional geometries as part of their input parameters. Some reflectors from these retrogradational model could represent zonal boundaries

at the margin (right side of Figure 3E), due to vertical facies patterns (e.g. reef immediately overlying sand apron facies in underlying zone). Therefore, in platforms where facies transitions are abrupt (e.g., Figure 3E) versus gradual change in facies (either retrogradational or progradational models) some reflectors do represent stratigraphic architecture.

Another possible stratigraphic variation would be the presence of a layer at the top of Zone 2 with distinct petrophysical properties, such as a high-impedance shale layer or a diagenetically altered (e.g., dense, cemented) layer (e.g., Zampetti et al., 2004, 2005). Replacing 15 m of carbonate with "shale" at the top of Zone 2 in the base model changes the impedance contrast (Figure 3G) and, as a result, seismic amplitude at the top of Zone 2 increases relative to the base case (Figure 3H). Nonetheless, as in the base model, amplitude decreases towards the interior of the platform.

Depositional Geometry. A scenario that incorporates clinoform geometries represents an alternative to layer-cake depositional geometry. In this geologic model (Figure 3J), 1-m thick layers in Zone 2 form inclined layers that mimic progradation towards the platform interior (cf. Droste and Van Steenwinkel 2004; Neuhaus et al., 2004). As in all other models, Zones 1 and 3 have layer-cake facies with parallel, horizontal layers.

As in the other seismic models, the highest amplitude reflectors in this model follow the boundary between interfingering of the platform interior and the reef sand apron (Figure 3I), rather than following the clinoforms. The transition between slope and reef facies have a reflector dip in Zone 2 that is basinward, opposite the platformward-oriented clinoforms in the facies volume. However, the transition between reef sand apron and platform interior facies have reflectors that dip towards the platform interior, accurately imaging the platform-oriented clinoforms in the facies volume.

Boundary and Intra-facies Complexities. Several other stratigraphic and petrophysical factors that could influence seismic character were modeled. Many had only minor impact on seismic character, and so are not illustrated (see Appendix 1 for details). These factors explored changes outside of Zone 2 (i.e., boundary effects) and within a single facies inside Zone 2 (i.e., platform interior heterogeneity). For example, one end-member model of platform interior heterogeneity has 25% of the cells within the platform interior populated to simulate randomly distributed patch reefs, with reef petrophysical properties (increase in porosity, 20% vs 12%) (Appendix 1, Figure A1-1I). Seismically, this scenario has the most evident differences from the base case (comparing Appendix 1, Figure A1-1J and Figure 2D), and resembles the scenario with facies stochastically distributed (Figure 3A) within the platform interior area of the volume, but includes lower amplitudes. Scenarios that modeled less than 25% patch reefs in the platform interior had less pronounced differences in seismic character to each other and to the base case scenario. (Appendix 1, Figure A1-1E through H).

Petrophysical Complexities

Scenarios in this suite explore the impact of variations in petrophysical properties. All use the identical base case scenario (aggradational zonal stacking pattern) with depositional layer cake facies geometry, but vary: 1) average porosity, between a low-porosity end member (3-16%, "Devonian," Watts, 1987) and high-porosity end member (16-36%; "Miocene," Grötsch and Mercadier, 1999); and 2) vertical trends in porosity, modeled as upward changes in porosity (e.g., "cleaning-up" trend of upwards-decreasing porosity) at intervals of varying thickness (100 m, two 50 m, and four 25 m packages) (e.g.,Goldhammer et al., 1993; Egenhoff et al., 1999; Droste and van Steenwinkel 2004; Ehrenberg, 2004) (Table 4).

Average Porosity. In this suite of models, average porosity remains distinct among facies, but the absolute values vary between high porosity (16-36%; Figure 3K) and low porosity (3-16%; Figure 3N) (recall, base values range between 9-26%; Figure 2D). Furthermore, each facies has a mean porosity value and range of porosity varies between high (+/- 10 p.u.) and low (+/- 5 p.u.) range. Incorporating a range of porosity to populate a given facies provides internal impedance contrasts that could influence seismic character beyond the impedance contrast at the stratigraphic zone interfaces.

The data reveal that seismic character ranges considerably among the three scenarios, even though they all have the same stratigraphic architecture (comparing Figure 2D; Figure 3L and M). For example, the synthetic volume of the base case scenario (Figure 2D) has two distinct 'reflection-free' regions. These low-amplitude reflectors occur where the reef sand apron and reef facies, both of which have similar impedance, are stacked vertically. This type of seismic expression is absent in the two other scenarios. Instead, the seismic reflectors are either continuous across the reef sand apron and reef facies with lateral changes in amplitude or appear to be truncated by overlying reflectors, which was not part of the geological model (Figure 3L and M). Another difference is in the platform interior, where both scenarios with low and high porosity enhance the impedance contrasts from the base case scenario, and as a result, three new continuous to discontinuous reflectors appear in the platform interior.

In contrast to these differences, two similarities are worth noting. In all three synthetic volumes (comparing Figure 2D; Figure 3L and M), the highest amplitude reflectors occur at the platform interior – reef sand apron boundary. Furthermore, changes in the range in porosity drove almost no immediately obvious differences in seismic character for all three synthetic volumes. These data suggest seismic character is influenced more by inter-facies range of

porosity more than intra-facies range of porosity and so subsequent modeling focused on altering the absolute variables and kept ranges constant.

Stratigraphic Porosity Trends. A suite of six scenarios evaluated the influence of vertical trends in porosity on seismic character. In contrast with the base case scenario, which has no stratigraphic trends in porosity, models included upward increases in porosity ("cleaning up") and upward decreases in porosity ("dirtying up"), manifest within one interval (100 m) (Figure 3O and S), two 50 m intervals (Figure 3R; Appendix 1, Figure A1-2E), and four 25 m intervals (Figure 3V; Appendix 1, Figure A1-3G). Average porosity among facies were modeled 1) with the same porosity as the base case scenario (between 9-26%); and 2) with elevated average porosity (between 16-36%) (Appendix 1, Figures A1-4 and A1-5).

The three different thickness intervals reveal similar seismic amplitude reflectors regardless of stratigraphic trends (upwards-increasing or upwards-decreasing) in porosity. The 100 m (Figure 3P and T) and 25 m (Figure 3U and Appendix 1, Figure A1-3H) intervals have subtle phase differences to one another and with the base case scenario (Figure 2D). Both synthetics from the scenarios with the 50 m dirtying-upward (Appendix 1, Figure A1-2F) and cleaning-upward porosity (Figure 3Q) have two reflectors representing a peak in the platform interior region. However, the cleaning-up synthetic (Figure 3Q) has an additional third reflector near the top of Zone 2 that is lower in amplitude and is less continuous.

The second set of scenarios modeled high average porosity (between 16-36%) with the same vertical porosity intervals, and modeled both cleaning- (Appendix 1, A1-5) and dirtying-upward (Appendix 1, Figure A1-6) successions. Because differences in seismic character, such as amplitude and phase, are not pronounced, data are not shown here, but are available in Appendix 1.

To summarize scenarios in this suite that explored variations in petrophysical properties: 1) regardless of porosity or magnitude of changes in porosity, the reef sand apron – platform interior boundary includes the highest amplitude reflectors in each scenario. An additional explanation for this could result from tuning effects (amplitude changes due to tuning when working with seismic amplitude at the limit of resolution); 2) Marked differences among scenarios are most evident in the platform interior because the platform interior of the base case scenarios had few reflectors and, therefore, the presence of any new reflectors were more notable; and 3) Close similarities among the models with distinct stratigraphic porosity trends emphasizes that fine details of impedance changes at or below resolution may not be discernable or distinguishable.

SEISMIC EXPRESSION OF GEOLOGICAL HETEROGENEITY WITHIN ISOLATED PLATFORMS: QUANTITATIVE SIGNATURES OF STRATIGRAPHY AND POROSITY

Even a cursory glance at the seismic character of models in which stratigraphic architecture and petrophysical complexity varied (Figures 2 and 3) reveals pronounced qualitative differences. To expand the qualitative observations, and to test the hypothesis that geologic variability creates statistically distinct impacts on seismic character of isolated platforms, seismic character can be compared to model inputs explicitly. Exploring statistical distinctions among models reveals the capability for attributes to predict rock properties accurately in certain geological scenarios.

Nine standard attributes were calculated from the 100 m middle zone for each scenario: RMS amplitude, average energy, average magnitude, average peak value, positive to negative ratio (these attributes relate to signal amplitude which is expected to response to impedance (or porosity) contrasts and tuning), average duration of negative loops, average duration of positive

loops, average loop duration, and standard deviation of loop duration (these attributes relate to the frequency of the signal which is expected to respond to layer thickness and gradational changes in porosity) (Taner, 2001). Calculated attributes are shown for each scenario (base case scenario, Appendix 2, Figure A2-1), organized by type of geological variable, stratigraphic architecture (Appendix 2, Figure A2-2), average porosity (Appendix 2, Figure A2-3), vertical porosity trends with mean values consistent with the base case scenario (Appendix 2, Figure A2-4), and at an elevated mean porosity (Appendix 2, Figure A2-5).

For each scenario, a multivariate linear regression used all nine attributes (calculated at each trace) to predict average porosity at the trace location within the zone of interest (see Appendix 5). The results for each regression are presented as a single R^2 value that indicates the amount of variance in average porosity explained by attributes for a given scenario (higher R^2 means stronger correlation) (e.g., Figure 4). The scenario whose attributes had the closest correlation to average porosity was the scenario with a high impedance cap ($R^2 = 0.91$) (Figure 4A). All other scenarios had much lower predictability, such as the base case scenario ($R^2 = 0.28$, Figure 4B), with the lowest predictability from the null hypothesis scenario ($R^2 = 0.15$, Figure 4C). Recall that all three scenarios have the same average porosity for each facies, and therefore have the same impedance (the models vary the organization of impedance contrasts). The lack of organized stratigraphy (Figure 3A and B) resulted in the lowest correlation between attributes and average porosity (Figure 4C). If stratigraphic organization was introduced (e.g., the base case, Figure 2A-C) the correlation strength increased, although not markedly (Figure 4B). The addition of the high impedance cap (Figure 3G and H) resulted in a greater impedance contrast than the base case scenario and therefore impacted the attributes and had the closest correlation to average porosity (Figure 4A). Other types of geological heterogeneity resulted in

varying correlation values (Figure 5). The data illustrate that as the type geological heterogeneity is changed, the R^2 also varies. For example, in all but one, scenarios mimicking petrophysical complexities (Figure 5, blue and yellow bars) had correlation equal to, or better than, the base case scenario.

A different quantitative measure (volumetric, as opposed to trace-by-trace) considers how accurately the total pore volume of the platform might be predicted, and how that varies among geological scenarios. This metric, calculated here as the ratio between predicted net pore volume and actual net pore volume, was calculated by using the sum of regression-predicted porosity versus the sum of the actual porosity, calculated at each trace (phi-h). In this metric, therefore, a value of less than one documents underprediction, a value of greater than one means overprediction. The data for all models (Figure 6) illustrate a range of values with minimum and maximum represented by scenarios with low average porosity (0.71) and high average porosity (1.17), respectively. However, the average ratio for all scenarios is 0.98 (standard deviation of +/- 0.10).

These results show that accuracy of prediction of net pore volume varies among scenarios. Predictions are almost the same despite the model input, suggesting that the errors among traces essentially average out, some overpredict and others underpredict. Interestingly, the quality of porosity prediction on a trace-by-trace basis (quantified by R2; Figure 5) is uncorrelated (R2 = 0) with quality of prediction of net pore volume (quantified by ratio of predicted:actual; Figure 6).

IMPLICATIONS FOR SEISMIC INTERPRETATION

Seismic data represent an important means to unravel the stratigraphic architecture and rock properties of isolated carbonate platforms (Eberli et al., 2002; 2004; Masaferro et al., 2004; Fournier et al., 2007;Janson and Fomel, 2011; Burgess et al., 2013). The challenge of interpreting isolated carbonate platforms lies in their complexity, and unraveling the numerous variables that control that complexity (Grötsch and Mercadier, 1999; Masaferro et al., 2003; Vahrenkamp et al., 2004).

To explore the influence of a range of parameters that can impact seismic expression of carbonate platforms, this study systematically isolates and models a suite of idealized platforms, rather than model one platform in particular. Of course, real platforms are much more complex, and are impacted by a greater number of variables, most of which are not able to be discerned by interpreters. Using fully constrained models provides both qualitative and quantitative insights useful for interpretation of isolated platforms from seismic data.

Implications for Seismic Interpretation: 1. Qualitative Aspects

Seismic stratigraphy and seismic facies analysis commonly utilizes objective assessment of reflector amplitude, geometry, and continuity (Payton, 1977; Hart, 2013). These assessments form the basis for the interpretation of stratal architecture and properties. In an ideal setting, seismic data are calibrated to well and core data, but those data do not sample the complete rock volume, so interpretation of most of the seismic volume may be ambiguous (Rankey and Mitchell, 2003). To highlight potential pitfalls in interpretation, this section illustrates three seismic scenarios in which plausible qualitative seismic stratigraphic interpretation of synthetic models differ from the geologic input.

The first example has seismic reflectors that form apparent mounded geometries, which appear to backstep towards the platform interior (to the right) (Figure 7A and B). This succession (highlighted in blue in Figure 7C) could be interpreted to be onlapped on their platformward flank by several low-amplitude reflectors. Basinward of these mounded geometries, inclined reflectors mimic downlap onto the mounded succession as they prograde, suggesting off-platform progradation. Overall, this line could be interpreted to represent a transgressive (backstepping) – regressive (prograding) succession (the black arrow in Figure 7C).

This interpretation, although plausible based on the seismic data, does not align precisely with the geological model used to generate this synthetic line (Figure 7D) in two ways. First, the seismic data suggest that the three zones collectively include a backstep followed by offlapping succession. In contrast, the geological model included a lower prograding zone, a middle backstepping zone, and an upper prograding zone. Second, at a finer level of detail, the seismic data fail to resolve the platformward progradation within Zone 2 in the model. Instead of representing the stratal geometries, the mounded geometries defined by peaks appear to reflect the facies boundary between the overlying lower impedance reef sand apron and the underlying higher impedance platform interior deposits.

The second example includes several distinct apparent seismic geometries: a) continuous to discontinuous parallel reflectors; b) inclined reflectors dipping platformward c) onlapping reflectors (Figure 8A and B). The oldest part of the succession includes parallel, discontinuous reflectors (dark blue, Figure 8C). These reflectors appear to be downlapped by concave downward reflectors building from near the shelf margin. Both the parallel reflectors and the mounded, downlapping reflectors are onlapped by parallel continuous reflectors (light blue, Figure 8C). Overall, this succession could be interpreted to represent an aggrading platform

margin (reef, reef sand apron, dark blue), which decreases in aerial extent (white), and ultimately is onlapped by a platform interior succession (light blue).

This geologic explanation is plausible based on the interpretation of the seismic line, but it does not match the geologic inputs that generated this line (Figure 8D). In contrast to the explanation of the seismic line, the geological model has three aggrading zones, and within each zone the facies are prograding basinward (to the right). None have facies that prograde platformwards. Reflection character is driven by lower average porosity in Zone 2 than the surrounding zones 1 and 3. The seismic character reflects this change because the reflectors follow the acoustic impedance contrast caused by the change in porosity; the apparent stratal terminations (downlap and onlap) are pseudo-geometries.

A third example includes a number of reflectors with markedly varying amplitudes, and varying geometry (Figure 9A and B). One interpretation of these reflectors could suggest a lower unit that thickens and includes an internal, low amplitude peak towards the margin (light blue, Figure 9C). An overlying set of reflectors defines a medial unit that appears to be mounded near the margin, but extend further platformward than the lower unit (dark blue, Figure 9C). A capping unit essentially fills in this relief (white, Figure 9C).

This geological interpretation (Figure 9C) contrasts with the model inputs (Figure 9D). That is, although the geological model has three zones, broadly analogous to the interpretation, the model includes zones with tabular, sheet-like geometry, and the seismic interpretation suggests marked geometries within and between zones. The seismic data could be interpreted to represent a platformward expansion of reef-reef sand apron from the lower to middle zones; yet, no comparable expansion is in the model. Instead, the middle zone included only random distribution of facies and porosity.

Seismic reflections represent changes in impedance which result from an array of geological factors that impact differences in petrophysical properties. Such variations can be driven by changes in stratigraphic architecture or facies transitions that superimpose rocks of different depositional porosity, or by spatial and vertical changes in diagenesis that modify porosity. Qualitatively, the geological seismic stratigraphic interpretations for the three examples are plausible. Yet, they are demonstrably incorrect, as illustrated by comparison with the model input. These types of incorrect interpretations can result from mis-interpretation of reflectors that do not represent chronostratigraphic surfaces, but instead are facies transitions or merely boundaries between areas of petrophysical contrast (cf. Biddle et al., 1992; Stafleu and Schlager, 1993; Eberli et al., 2002,).

Implications for Seismic Interpretation: 2. Quantitative Considerations

Studies have shown seismic attributes can be used to predict rock properties, which can be useful for understanding petrophysical properties away from well control or if the dataset is limited (Matteucci, 1996; Hart and Balch 2000; Tebo and Hart, 2005, to mention a few). In this study, nine attributes were calculated for every scenario at every trace. The attributes used in the regressions to predict average porosity and net pore volume varied in their accuracy (Figure 5 and 6).

The results (Figure 5) illustrate that different types of geological heterogeneity have varying impact on prediction accuracy. For example, changes in stratigraphic architecture, average porosity, and stratigraphic trends in porosity exhibit quantitative differences on accuracy of predictions of average porosity on a trace-by-trace basis. The scenarios within the stratigraphic architecture group have the same average porosity (Figure 5, red bars) and all have higher correlations than the other classes of geological heterogeneity. Of these scenarios, the

best prediction ($R^2 = 0.91$) of porosity occurs in the model with a high impedance cap. The high impedance layer likely creates an impedance contrast sufficient to markedly impact the reflector. This impact enhances differentiation of even subtle differences in physical properties within the reservoir zone. For example, the platform interior in the base model includes only low-amplitude reflectors, the result of only subtle impedance contrasts (Figure 2D); in marked contrast, the addition of a high impedance layer includes a pronounced reflector evident in the interior (and even through the reef sand apron and reef areas), the result of the pronounced impedance contrast (Figure 3G,H). Such layers that represent a high impedance contrast are evident in many platforms, where they are associated with comparable to flooding surfaces or cemented zones. For example, many Miocene buildups in Southeast Asia include such tight cemented zones that are associated with high-amplitude reflectors (e.g., Masaferro et al., 2004; Zampetti et al., 2004, 2005).

The scenarios that model stratigraphic trends in porosity include different predictabilities. This group consists of models that included intra-facies impedance contrasts driven by vertical increases or decreases in porosity (e.g., Figure 3O-V). In contrast to the predictions from the scenario with the high impedance cap, the results from these scenarios predict porosity less accurately, with the average correlation for the group being $R^2 = 0.34$ (Figure 5, blue bars). These poor results may reflect the relative thinness of the vertical trends, with thicknesses at or below seismic resolution (e.g., Figures 3Q-V). As a result, most of these finer-scale (25, 50, 100 m) impedance contrasts were not imaged directly as high amplitudes, a situation perhaps enhanced by interference. These types of changes would be expected in isolated platforms with shallowing-upward (cleaning-upward) successions, such as parasequence sets or high-frequency sequences, at a thickness less than the resolution of the seismic data. For example, many

Devonian buildups in the Western Canadian Basin include several shallowing-upward successions, but on seismic represent only one or two loops (Anderson and Brown, 1988; Rankey and Mitchell, 2003; Schwab et al., 2004); in such scenarios, accurate prediction of porosity may be challenging.

Finally, the scenarios with high and low average porosity (averages 26% and 9%, respectively) had changes in porosity that enhance the impedance contrasts among zones, favoring higher amplitudes and a greater number of reflectors (Figure 3K-N; Appendix 6). These include correlation coefficients intermediate between the other scenarios (R2 = 0.52 and 0.37, respectively; Figure 5, yellow bars). These types of porosity variations could reflect different diagenesis between different reservoir zones, perhaps associated with distinct subaerial exposure events creating dissolution or cementation that would impact only certain zones (e.g., Ehrenberg, 2004; Masaferro et al., 2004; Zampetti et al., 2004, 2005).

Akin to the predictions on a trace-by-trace basis, the accuracy of prediction of net pore volume varies with changes in the type of geological heterogeneity (Figure 6). However, the range of variability of the ratio between predicted net pore volume and observed net pore volume is much less, with the average ratio for all scenarios 0.98. It thus appears as though the errors are essentially smoothed out - some are higher than predicted, some are less than predicted, but in sum they average out. These results suggest that predictions of porosity at a given location may be much less accurate than predicting the overall pore volume.

Implications for Seismic Interpretation: 3. Comparison with Extant Isolated Platforms

Seismic data provide invaluable insights into complexity in subsurface stratigraphic systems. These data, however, also provide non-unique solutions. For example, Hart (1999) noted, "many different stratigraphic successions could have been produced a given seismic section" (p. 208).

This study did not attempt to model any specific real-world platform. The results, however, can provide insights to understanding geology of actual platforms imaged in seismic data by constraining the range of potential geological interpretations from seismic data and pointing out pitfalls. This section highlights comparisons between real seismic data and synthetic volumes generated from constrained geological models, and how a range of interpretations may be possible.

One example of data from a real platform is from Central Luconia Province, Malaysia. Here, Jintan, a 30-km by 50-km wide, Middle Miocene platform includes a well-documented succession (e.g., Vahrenkamp et al., 2004). Vahrenkamp et al. (2004) used cores, logs, and seismic to interpret sequence stratigraphy of the succession. Above the karst surface that terminated the larger platform, a smaller (8 x 12 km) backstepped platform includes two sequences. Within this backstepped succession, parallel, low-amplitude reflectors pass laterally into a platform-marginal succession of dipping reflectors, interpreted to represent progradation into a smaller intraplatform depression (Figure 10A) (Vahrenkamp et al., 2004).

The dipping reflections in the Jintan seismic line (Figure 10A) are similar to two of the synthetic volumes, in that they also have inclined reflectors. The first synthetic was generated from a scenario that modeled a progradational platform margin (Figure 10B and C). The geologic facies model is similar to the Jintan conceptual model in that both margins prograde into the basin and pass laterally into platform interiors. Seismically, they both include low-amplitude interiors and dipping platform-marginal reflectors. They differ in several ways,

however. For example, the inclined reflectors in the seismic model appear to have visibly lower amplitudes than those from the Jintan seismic volume. Additionally, the transition from the dipping reflectors to the lower-amplitude platform interior region is characterized by a sharp decrease in amplitude in the real-world data, but by a zone of high amplitudes in the model.

Both of these likely represent distinct distributions of petrophysical properties in different regions of the platform. That is, in the Jintan seismic data, the highest amplitudes are in the area of the dipping reflectors. These amplitudes likely reflect high impedance contrasts in slope and marginal facies. In contrast, the model includes only low amplitudes in the slope, consistent with the low impedance contrasts. Similarly, the highest amplitudes in the model represent the contrasts in impedance between facies (most notably reef sand apron and platform interior). The absence of comparable reflectors in the Jintan seismic suggests that impedance contrasts between these facies are less pronounced.

Comparison with a second synthetic illustrates the possible non-uniqueness of geometries. In this scenario, broadly comparable, basinward-dipping clinoforms were generated from the scenario with an almost mounded marginal geometry, but that included platformward-prograding clinoforms (Figure 10D and E). In this synthetic, the basinward-dipping reflections are pseudo-geometries, reflections that do not mimic the underlying geology. These seismic signatures can have non-unique, and very divergent, geological interpretations.

A second illustrative example is provided by another, unidentified Central Luconia Buildup documented by Masaferro et al. (2003). This 600-m thick buildup is a Middle Miocene platform with five reservoir zones (Masaferro et al., 2003). The seismic character on the left side of the platform includes mounded reflections, reflectors that onlap the mounded geometries, low-

amplitude reflections that downlap the platform interior, and flat lying, continuous reflectors, including a high-amplitude event that persists across the platform (Figure 11 A and B).

Two plausible, but different, interpretations of this Luconia buildup suggest two alternative geological explanations (Figure 11C and D). The first interpretation (Figure 11C) includes stacked mounded reflectors near the margin (Figure 11C, colored red). These reflectors appear to be onlapped by subhorizontal, parallel reflectors of the platform interior (Figure 11C, colored light blue). Overall, this succession could be interpreted to represent an aggrading reef – reef sand apron margin that was buried subsequently by platform interior units. An alternative interpretation (Figure 11D) includes stacked mounded reflectors near the margin (colored red). Platformward of the stacked mounded reflectors are continuous flat-lying reflectors that appear to terminate against the mounded seismic features. Instead of representing onlap, however, these geometries could alternatively reflect pseudo-onlap generated by a facies change between the aggrading reef – reef sand apron and aggrading platform interior (comparable to that illustrated in Figure 8C).

The objective of this study was to isolate and evaluate variables and their impact on seismic character. Real examples do not afford that luxury, and many variables can change simultaneously. An example of this complexity is illustrated by Malampaya, a field offshore Philippines. The Malampaya buildup is a 5 km by 1-2 km, 700-m thick platform and includes the early Oligocene to early Miocene Nido Limestone reservoir. This buildup includes quality well logs, core, and seismic data, and has been well documented (e.g., Grötsch and Mercadier, 1999; Fournier et al., 2004, 2005; Neuhaus et al., 2004; Fournier and Borgomano, 2007). The platform includes three units, the Lower Nido (a progradational succession), a Middle Nido and Upper Nido (an aggradational succession separated by a cemented surface, the Intra-Nido

marker), and capping backstepping and subsequent drowning succession (Grötsch and Mercadier, 1999).

The seismic character of Malampaya includes several aspects that appear analogous to the synthetic lines. First, the seismic data clearly show downlapping reflectors on the east side of the platform (right side, yellow arrows, Figure 12A), a pattern that has been interpreted as a platform backstep at that margin (Figure 12B). Similar downlapping reflectors (Figure 12C, yellow arrows) are evident in the modeled backstepping platform margin (Figure 12D).

A second example of similar seismic character between Malampaya and the same synthetic scenarios is the presence of a high-amplitude, continuous, peak-trough combination within the succession that cuts across all facies across the platform. Grötsch and Mercadier (1999) documented that this Intra-Nido marker (Figure 12A, green line) corresponded to a tight, cemented layer in core. A similar high amplitude, continuous, peak-trough combination (Figure 12E, green arrow) was generated from a scenario that added a high impedance cap to Zone 2 (Figure 12F). The results of this study would suggest that porosity predictions in the zone underlying this reflector might be more accurate than those predictions from other zones.

CONCLUSIONS

The stratigraphy of isolated carbonate platforms represents the net product of a complex combination of geological variables; seismic data represent a primary means to understand these products, and predict in the subsurface. To explore the use of seismic data for reservoir interpretation and characterization, this study used a suite of synthetic volumes designed to isolate a specific type of possible geologic heterogeneity, evaluated their role on seismic

character, and assessed the impact on interpretations of stratal architecture and predictions of porosity of isolated platforms.

Evaluating the seismic character of a range of geological heterogeneity realized within several models enhanced the understanding of how geology influences seismic character for interpretation of complex isolated platforms. Specifically, results indicate that:

- **Seismic reflectors do not always represent timelines or stratigraphic surfaces.** Reflectors result from impedance contrasts at facies boundaries or interference patterns, or from impedance contrasts at stratal surfaces. These dynamics emphasize the non-unique interpretation of seismic geometries. For example, models indicate how mounded geometries may, or may not, represent buildups, or relief in general.
- **Geological variability markedly impacted the accuracy of predictions of porosity.** The strongest predictability (measured by correlation between attributes and porosity) occurred in models that altered stratigraphic architecture. The weakest predictability was in the null model of random facies (and porosity distribution). Stratigraphic trends in porosity, such as would be caused by cleaning-upward trends below seismic resolution, had intermediate impact.

These points may seem evident, however, this study emphasizes the fact that low resolution seismic reflectors do not always reflect geology, they can be generated by tuning effects which can lead to misinterpretations. To better understand the subsurface from seismic data, interpreters can use the models generated in this study to constrain the realm of possible geological interpretations for a given dataset. From there, geological interpretations can be modeled using detailed analyses and compared against analogs to better predict the geology.

REFERENCES

Anderson, N. L., and Brown, R. J., 1988, The seismic signatures of some western Canadian Devonian reefs: Journal of the Canadian Society of Exploration Geophysicsts, v. 23, p. 7-26.

Anselmetti, F. S., Eberli, G. P., and Bernoulli, D., 1997, Seismic modeling of a carbonate platform margin (Montagna della Maiella, Italy): Variations in seismic facies and implications for sequence stratigraphy, *in* Palaz, I., and Marfurt, K. J. (Eds.), Carbonate seismology: SEG Geophysics Development Series, v. 6, p. 373-406.

Anselmetti, F. S., and Eberli, G. P., 1999, The velocity-deviation log: A tool to predict pore type and permeability trends in carbonate drill holes form sonic and porosity or density logs: AAPG Bulletin, v. 83, p. 450-466.

Anselmetti, F. S., and Eberli, G. P., 2001, Sonic velocity in carbonates – A combined product of depostional lithology and diagenetic alterations, *in* Ginsburg, R. N. (Ed.), Subsurface geology of a prograding carbonate platform margin, Great Bahama Bank: Results of the Bahamas Drilling Project: SEPM Special Publication, v. 70, p. 193-216.

Atchley, S. C., West, L. W., and Sluggett, J. R., 2006, Reserves growth in a mature oil field: The Devonian Leduc Formation at Innisfail field, south-central Alberta, Canada: AAPG Bulletin, v. 90, p. 1153-1169.

Bachtel, S. L., Kissling, R. D., Martono, D., Rahardjanto, S. P., Dunn, P. A., and MacDonald, B. A., 2004, Seismic stratigraphic evolution of the Miocene-Pliocene Segitiga Platform, East Natuna Sea, Indonesia: The origin, growth, and demise of an isolated carbonate platform, *in* Eberli, G. P., Masaferro, J. L., and Sarg, J. F. (Eds.), Seismic imaging of carbonate reservoirs and systems: AAPG Memoir 81, p. 309-328.

Biddle, K. T., Schlager, W., Rudolph, K. W., and Bush, T. L., 1992, Seismic model of a progradational carbonate platform, Picco di Vallandro, the dolomites, northern Italy: AAPG Bulletin, v. 76, p. 14-30.

Borgomano, J. R. F., Fournier, F., Viseur, S., and Rijkels, L., 2008, Stratigraphic well correlations for 3-D static modeling of carbonate reservoirs: AAPG Bulletin, v. 92, p. 789-824.

Bourgeois, A., Joseph, P., and Lecomte, J.C., 2004, Three-dimensional full wave seismic modelling versus one-dimensional convolution: the seismic appearance of the Grès d'Annot turbidite system, *in* Joseph, P., and Lomas, S. A. (Eds.), Deep-water sedimentation in the Alpine Basin of SE France: New perspectives on the Grès d'Annot and related systems: Geological Society of London, Special Publications, v. 221, p. 401-417.

Bracco-Gartner, G. L., Morsilli, M., Schlager, W., and Bosellini, A., 2004, Toe-of-slope of a Cretaceous carbonate platform in outcrop, seismic model and offshore seismic data (Apulia, Italy): International Journal of Earth Sciences, v. 91, p. 315-330.

Burgess P. M., Winefield, P., Minzoni, M., and Elders, C., 2013, Methods for identification of isolated carbonate buildups from seismic reflection data: AAPG Bulletin, v. 97, p. 1071-1098.

Campbell, A. E., and Stafleu, J., 1992, Seismic modeling of an Early Jurassic, drowned carbonate platform: Djebel Bou Dahar, High Atlas, Morocco: AAPG Bulletin, v. 76, p. 1760-1777.

Chopra, S., and Marfurt, K. J., 2008, Emerging and future trends in seismic attributes: The Leading Edge, v. 27, p. 298-318.

Collins, J., Narr, W., Harris, P.M., Playton, T., Jenkins, S., Tankersley, T., and Kenter, J.A.M., 2013, Lithofacies, depositional environments, burial diagenesis, and dynamic field behavior in a Carboniferous slope reservoir, Tengiz Field (Republic of Kazakhstan), and comparison with outcrop analogs, *in* Verwer, K., Playton, T. E., and Harris, P. M. (Eds.), Deposits, architecture and controls of carbonate margin, slope and basinal settings: SEPM Special Publication, v. 105, p. 50-83.

Droste, H., and Van Steenwinkel, M., 2004, Stratal geometries and patterns of platform carbonates: The Cretaceous of Oman, *in* Eberli, G. P., Masaferro, J. L., and Sarg, J. F. (Eds.), Seismic imaging of carbonate reservoirs and systems: AAPG Memoir 81, p. 185-206.

Dubrule, O., Thibaut, M., Lamy, P., and Haas, A., 1998, Geostatistical reservoir characterization constrained by 3D seismic data: Petroleum Geoscience, v. 4, p. 121-128.

Eberli, G. P., Anselmetti, F. S., Kroon, D., Sato, T., and Wright, J. D., 2002, The chronostratigraphic significance of seismic reflections along the Bahamas transect: Marine Geology, v. 185, p. 1-17.

Eberli, G. P., Baechle, G. T., Anselmetti, F. S., and Incze, M. L., 2003, Factors controlling elastic properties in carbonate sediments and rocks: The Leading Edge, v. 22, p. 654-660.

Eberli, G. P., Masaferro, J. L., and Sarg, J. F., 2004, Seismic imaging of carbonate reservoirs and systems *in* Eberli, G. P., Masaferro, J. L., and Sarg, J. F. (Eds.), Seismic imaging of carbonate reservoirs and systems: AAPG Memoir 81, p. 1-9.

Eberli, G. P., Anselmetti, F. S., Betzler, C., Van Konijnenburg, J. -H., and Bernoulli, D., 2004, Carbonate platform to basin transitions on seismic data and in outcrops: Great Bahama Bank and the Maiella Platform margin, Italy, *in* Eberli, G. P., Masaferro, J. L., and Sarg, J. F. (Eds.), Seismic imaging of carbonate reservoirs and systems: AAPG Memoir 81, p. 207-250.

Egenhoff, S. O., Peterhänsel, A., Bechstädt, T., Zühlke, R., and Grötsch, J., 1999, Facies architecture of an isolated carbonate platform: tracing the cycles of the Latemàr (Middle Triassic, northern Italy), Sedimentology, v. 46, p. 893-912.

Ehrenberg, S. N., 2004, Factors controlling porosity in Upper Carboniferous-Lower Permian carbonate strata of the Barents Sea: AAPG Bulletin, v. 88, p. 1653-1676.

Elvebakk, G., Hunt, D. W., and Stemmerik, L., 2002, From isolated buildups to buildup mosaics: 3D seismic sheds new light on upper Carboniferous-Permian fault controlled carbonate buildups, Norwegian Barents Sea: Sedimentary Geology, v. 152, p. 7-17.

Enos, P., 1985, Cretaceous debris reservoirs, Poza Rica Field, Vera Cruz, Mexico, *in* Roehl, P.O., and Choquette, P.W. (Eds.), Carbonate petroleum reservoirs: New York, Springer Verlag, p. 455-470.

Epting, M., 1980, Sedimentology of Miocene carbonate buildups, central Luconia, offshore Sarawak: Bulletin Geological Society of Malaysia, v. 12, p. 17-30.

Epting, M., 1989, The Miocene carbonate buildups of central Luconia, offshore Sarawak, *in* Bally, A.W., (Ed.), Atlas of seismic stratigraphy: AAPG (Tulsa), Studies in geology, p. 168-173.

Favliene, O., Arbués, P., Ledo, J., Benjumea, B., Muñoz, J.A., Fernández, O., and Martínez, S., 2010, Synthetic seismic models from outcrop-derived reservoir-scale three-dimensional facies models: The Eocene Ainsa turbidite system (southern Pyrenees): AAPG Bulletin, v. 94, p. 317-343.

Fournier, F., Montaggioni, L. M., and Borgomano, J., 2004, Paleoenvironments and high-frequency cyclicity from Cenozoic south-east Asian shallow-water carbonates: a case study

from the Oligo-Miocene buildups of Malampaya (Offshore Palawan, Philippines): Marine and Petroleum Geology, v. 21, p. 1-21.

Fournier, F., Borgomano, J., and Montaggioni, L.M., 2005, Development patterns and controlling factors of Tertiary carbonate buildups: Insights from high-resolution 3D seismic and well data in the Malampaya gas field (Offshore Palawan, Philippines): Sedimentary Geology, v. 175, p. 189-215.

Fournier, F., and Borgomano, J., 2007, Geological significance of seismic reflections and imaging of the reservoir architecture in the Malampaya gas field (Philippines): AAPG Bulletin, v. 91, p. 235-258.

Goldhammer, R. K., Lehman, P. J., and Dunn, P. A., 1993, The origin of high-frequency platform carbonate cycles and third-order sequences (Lower Ordovician El Paso GP, West Texas): Constraints from outcrop data and stratigraphic modeling: Journal of Sedimentary Petrology, v. 63, p. 318-359.

Grötsch, J., and Mercadier, C., 1999, Integrated 3-D reservoir modeling based on 3-D seismic: The Tertiary Malampaya and Camago Buildups, Offshore Palawan, Philippines: AAPG Bulletin, v. 83, p. 1703-1728.

Hart, B. S., 1999, Definition of subsurface stratigraphy, structure and rock properties from 3-D seismic data: Earth-Science Reviews, v. 47, p. 189-218.

Hart, B. S, and Balch, R. S., 2000, Approaches to defining reservoir physical properties from 3-D seismic attributes with limited well control: An example from the Jurassic Smackover Formation, Alabama: Geophysics, v. 65, p. 368-376.

Hart, B. S., 2008, Stratigraphically significant attributes, The Leading Edge, v. 27, p. 320-324.

Hart, B. S., 2013, Whither seismic stratigraphy?: Interpretation, v. 1, p. SA3-SA20.

Hubbard, R. J., Pape, J., and Roberts, D. G., 1985, Depositional sequence mapping as a technique to establish tectonic and stratigraphic framework and evaluate hydrocarbon potential on a passive continental margin, *in* Berg, O. R., and Woolverton, D. G. (Eds.), Seismic stratigraphy II: An integrated approach to hydrocarbon exploration: AAPG Special Publications, v. 39, p. 79-91.

Huh, J. M., Briggs, L. I., and Gill, D., 1977, Depositional environments of pinnacle reefs, Niagara and Salina Groups, Northern Shelf, Michigan Basin, *in* Fisher, J. H. (Ed.), Reefs and evaporites- concepts and depositional models: AAPG Special Publications, v. 5, p. 1-21.

Janson, X., Eberli, G. P., Bonnafee, F., Gaumet, F., and De Casanove, V., 2007, Seismic expressions of a Miocene prograding carbonate margin, Mut Basin, Turkey: AAPG Bulletin, v. 91, p. 685-713.

Janson, X., Kerans, C., Bellian, J., and Fitchen, W., 2007, Three-dimensional geological and synthetic seismic model of Early Permian redeposited basinal carbonate deposits, Victorio Canyon, west Texas: AAPG Bulletin, v. 91, p. 1405-1436.

Janson, X., and Fomel, S., 2011, 3-D forward seismic model of an outcrop-based geocellular model, *in* Martinsen, O. J., Pulham, A., Haughton, P. D. W., and Sullivan, M. D. (Eds.), Outcrops revitalized: Tools, techniques and applications: SEPM Concepts in Sedimentology and Paleontology, v. 10, p. 87-106.

Jones, G. D., and Xiao, Y., 2006, Geothermal convection in the Tengiz carbonate platform, Kazakhstan: Reactive transport models of diagenesis and reservoir quality: AAPG Bulletin, v. 901, p. 1251-1272.

Kleipool, L. M., De Jong, K., De Vaal, E. L., and Reijmer, J. J. G., 2017, Seismic characterization of switching platform geometries and dominant carbonate producers (Miocene, Las Negras, Spain): Sedimentology, v. 64, p. 1676-1707.

Kosa, E., Warrlich, G. M. E., and Loftus, G., 2015, Wings, mushrooms, and Christmas trees: The carbonate seismic geomorphology of Central Luconia, Miocene – present, offshore Sarawak, northwest Borneo: AAPG Bulletin, v. 99, p. 2043-2075.

Lehrmann, D. J., and Goldhammer, R. K., 1999, Secular variation in parasequence and facies stacking patterns of platform carbonates: A guide to application of stacking pattern analysis in strata of diverse ages and settings, *in* Harris, P. M., Saller, A. H., and Simo, J. A. (Eds.), Advances in carbonate sequence stratigraphy: Applications to reservoirs, outcrops, and models: SEPM Special Publications, v. 63, p. 187-226.

Masaferro, J. L., Bourne, R., and Jauffred, J. C., 2003, 3D visualization of carbonate reservoirs: The Leading Edge, March, p. 19-25.

Masaferro, J. L., Bourne, R., and Jauffred, J. C., 2004, Three-dimensional seismic volume visualization of carbonate reservoirs and structures, *in* Eberli, G. P., Masaferro, J. L., and Sarg, J. F. (Eds.), Seismic imaging of carbonate reservoirs and systems: AAPG Memoir 81, p. 11-41.

Matteucci, G., 1996, Seismic attribute analysis and calibration: A general procedure and a case study: 66th Annual International Meeting, SEG, Expanded Abstracts, p. 373-376.

Mavko, G., Mukerji, T., and Dvorkin, J., 2009, The Rock Physics Handbook: Tools for Seismic Analysis in Porous Media: Cambridge University Press, New York, United States of America, p. 446.

May, J. A., and Eyles, D. R., 1985, Well log and seismic character of Tertiary Terumbu carbonate, South China Sea, Indonesia: AAPG Bulletin, v. 69, p. 1339-1358.

Neuhaus, D., Borgomano, J., Jauffred, J. -C., Mercadier, C., Olotu, S., and Grötsch, J., 2004, Quantitative seismic reservoir characterization of an Oligocene-Miocene carbonate buildup: Malampaya field, Philippines, *in* Eberli, G. P., Masaferro, J. L., and Sarg, J. F. (Eds.), Seismic imaging of carbonate reservoirs and systems: AAPG Memoir 81, p. 169-183.

Payton, C. E. (Ed.), 1977, Seismic stratigraphy – Applications to hydrocarbon exploration: AAPG Memoir 26.

Rankey, E. C., and Mitchell, J. C., 2003, That's why it's called interpretation: Impact of horizon uncertainty on seismic attribute analysis: The Leading Edge, v. 22, p. 820-828.

Rankey, E. C., 2016, On facies belts and facies mosaics: Holocene isolated platforms, South China Sea: Sedimentology, v. 63, p. 2190-2216.

Ricker, N., 1953, The form and laws of propagation of seismic wavelets: Geophysics, v. 18, p. 10-40.

Rijks, E. J. H., and Jauffred, J. C. E. M., 1991, Attribute extraction: An important application in any 3-D interpretation study: The Leading Edge, v. 29, p. 11-19.

Rudolph, K.W., and Lehmann, P.J., 1989, Platform evolution and sequence stratigraphy of the Natuna Platform, South China Sea, *in* Crevello, P. D., Wilson, J. L., Sarg, J. F., and Read, J. F. (Eds.), Controls on carbonate and basin development: SEPM Special Publication, v. 44, p. 353-361.

Rudolph, K. W., Schlager, W., and Biddle, K. T., 1989, Seismic models of a carbonate foreslope-to-basin transition, Picco di Vallandro, Dolomite Alps, northern Italy: Geology, v. 17, p. 453-456.

Sarg, J. F., 1988, Carbonate sequence stratigraphy, *in* Wilgus, C. K., Hastings, B. S., Kendall, C. G. St. C., Posamentier, H. W., Ross, C. A., and Van Wagoner, J. C. (Eds.), Sea-level changes: An integrated approach: SEPM Special Publication, v. 42, p. 155-181.

Sarg, J. F., and Schuelke, J. S., 2003, Integrated seismic analysis of carbonate reservoirs: From the framework to the volume attributes, The Leading Edge, v. 22, p. 640-645.

Stafleu, J., and Schlager, W., 1993, Pseudo-toplap in seismic models of the Schlern-Raibl contact (Sella platform, northern Italy): Basin Research, v. 5, p. 55-65.

Stafleu, J. and Sonnenfeld, M., 1995, Seismic models of a shelf-margin depositional sequence: Upper San Andres Formation, Last Chance Canyon, New Mexico: Journal of Sedimentary Research, v. B64, p. 481-499.

Schwab, A., Van Buchem, F. S. P., and Ebeli, G. P., 2004, Integration of high-resolution outcrop and subsurface data to enhance interpretation of low-resolution seismic data in the Upper Devonian (Frasnian) carbonate system in western Canada, *in* Grammer, G. M., Harris, P. M., and Eberli, G. P. (Eds.), Integration of outcrop and modern analogs in reservoir modeling: AAPG Memoir 80, p. 261-278.

Taner, M. T., 2001, Seismic attributes: Canadian Society of Exploration Geophysicists Recorder, v. 26, p. 48-56.

Tebo, J., and Hart, B. S., 2005, Use of volume-based 3-D seismic attribute analysis to characterize physical-property distribution: A case study to delineate sedimentologic heterogeneity at the Appleton Field, Southwestern Alabama, U.S.A.: Journal of Sedimentary Research, v. 75, p. 723-735.

Ting, K. K., AlJaaidi, O., and Hague, P., 2011, Effects of syn-depositional tectonics on platform geometry and reservoir characters in Miocene carbonate platforms of Central Luconia, Sarawak: International Petroleum Technology Conference (IPTC), #14247, p. 1-17.

Vahrenkamp, V. C., David, F., Duijndam, P., Newall, M., and Crevello, P., 2004, Growth architecture, faulting, and karstification of a middle Miocene carbonate platform, Luconia Province, offshore Sarawak, Malaysia, *in* Eberli, G. P., Masaferro, J. L., and Sarg, J. F. (Eds.), Seismic imaging of carbonate reservoirs and systems: AAPG Memoir 81, p. 329-350.

Van Wagoner, J. C., Posamentier, H. W., Mitchum, R. M., Vail, P. R., Sarg, J. F., Loutit, T. S., and Hardenbol, J., 1988, An overview of the fundamentals of sequence stratigraphy and key definitions, *in* Wilgus, C. K., Hastings, B. S., Kendall, C. G. S. C., Posamentier, H. W., Ross, C. A., and Van Wagoner, J. C. (Eds.), Sea-Level changes: An integrated approach: SEPM Special Publications, v. 42, p. 39-45.

Wang, Z., 1997, Seismic properties of carbonate rocks, *in* Palaz, I. and Marfurt, K. J. (Eds.), Carbonate Seismology: Society of Exploration Geophysicists, Geophysical Developments Series, v. 6, p. 29-52.

Warrlich, G., Bosence, D., Waltham, D., Wood, C., Boylan, A., and Badenas, B., 2008, 3D stratigraphic forward modeling for analysis and prediction of carbonate platform stratigraphies in exploration and production: Marine and Petroleum Geology, v. 25, p. 35-58.

Watts, N. R., 1987, Carbonate sedimentology and depositional history of the Nisku Formation (within the western Canadian sedimentary basin) in south central Alberta: Devonian Lithofacies and Reservoir Styles in Alberta: 13th CSPG Core Conference and Display, p. 87-152.

Watts, N. R., Coppold, M. P., and Douglas, J. L., 1994, Application of reservoir geology to enhanced oil recovery from Upper Devonian Nisku Reefs, Alberta, Canada: AAPG Bulletin, v. 78, p. 78-101.

Widess, M. B., 1973, How thin is a thin bed?: Geophysics, v. 38, p. 1176-1180.

Wright, V. P. and Burgess, P. M., 2005, The carbonate factory continuum, facies mosaics and microfacies: An appraisal of some of the key concepts underpinning carbonate sedimentology: Facies, v. 15, p. 17-23.

Yose, L. A., Brown, S., Davis, T. L., Eiben, T., Kompanik, G. S., and Maxwell, S. R., 2001, 3-D geological model of a fractured carbonate reservoir, Norman Wells Field, NWT, Canada: Bulletin of Canadian Petroleum Geology, v. 49, p. 86-116.

Zampetti, V., Schlager, W., van Konijnenburg, J. -H., and Everts, A.-J., 2003, Depositional history and origin of porosity in a Miocene carbonate platform of central Luconia, offshore Sarawak: Bulletin Geological Society of Malaysia, v. 47, p. 139-152.

Zampetti, V., Schlager, W., van Konijnenburg, J. -H., and Everts, A. -J., 2004, Architecture and growth history of a Miocene carbonate platform from 3D seismic reflection data; Luconia province, offshore Sarawak, Malaysia: Marine and Petroleum Geology, v. 21, p. 517-534.

Zampetti, V., Sattler, U., and Braaksma, H., 2005, Well log and seismic character of Liuhua 11-1 Field, South China Sea: Relationship between diagenesis and seismic reflections: Sedimentary Geology, v. 175, p. 217-236.

Zeller, M., Eberli, G. P., Weger, R. J., Giunta, D. L., and Massaferro, J. L., 2014, Seismic expressions of the Quintuco – Vaca Muerta system based on outcrop facies and geometry: IX Congreso de Exploración y Desarrollo de Hidrocarburos, p. 209-224.

FIGURES

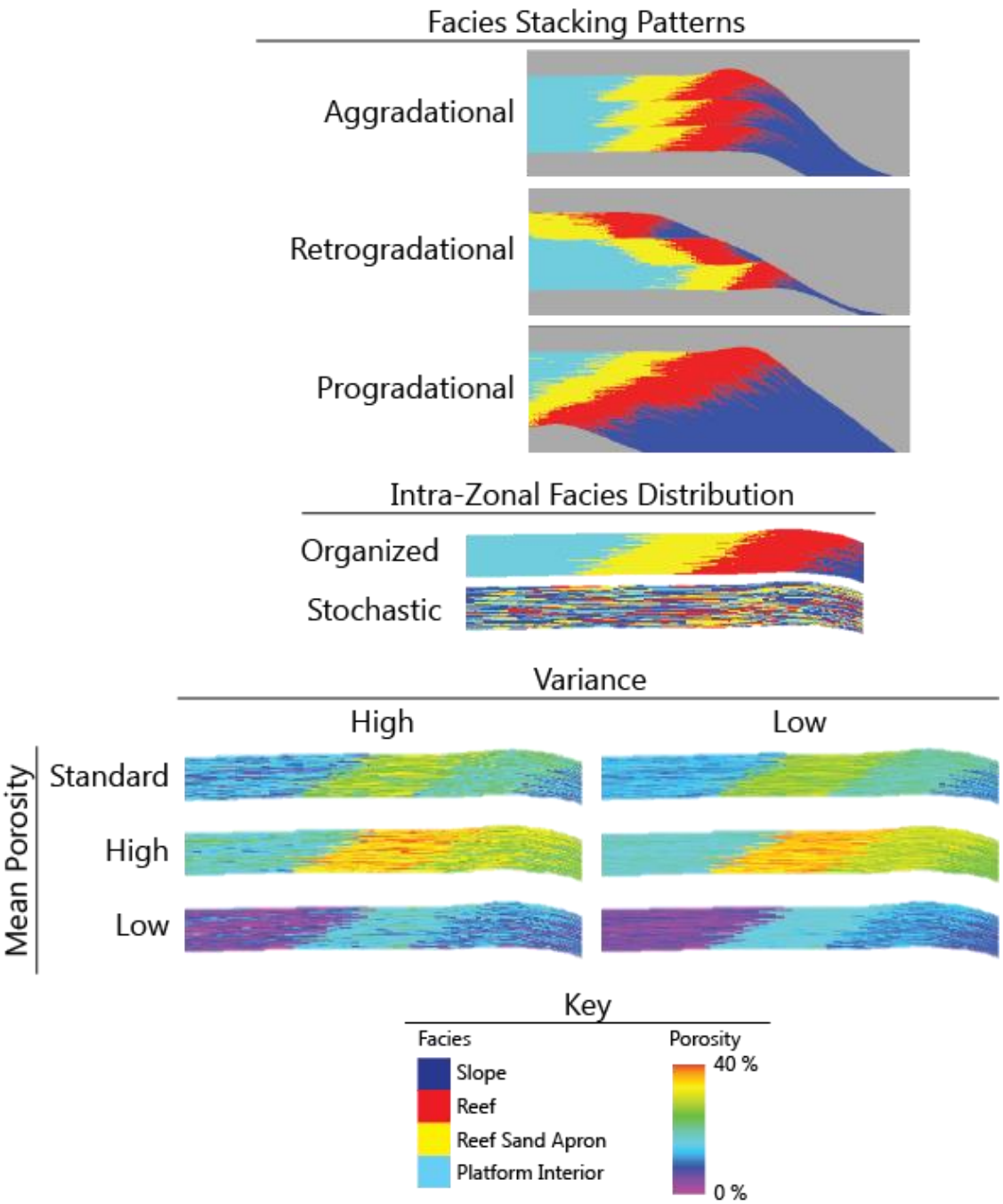

Figure 1: Schematic illustrating variable geological modeling parameters, including facies stacking patterns, intra-zonal facies stacking patterns, and mean porosity. The standard mean porosity = 17%, high mean porosity = 26%, and low mean porosity = 9%. High variance models have a range of porosity of +/- 10 p.u. and low variance models include a range of porosity of +/- 5 p.u. Each cell is 20 x 20 x 1m thick and ach zone is 100 m thick (see text for details).

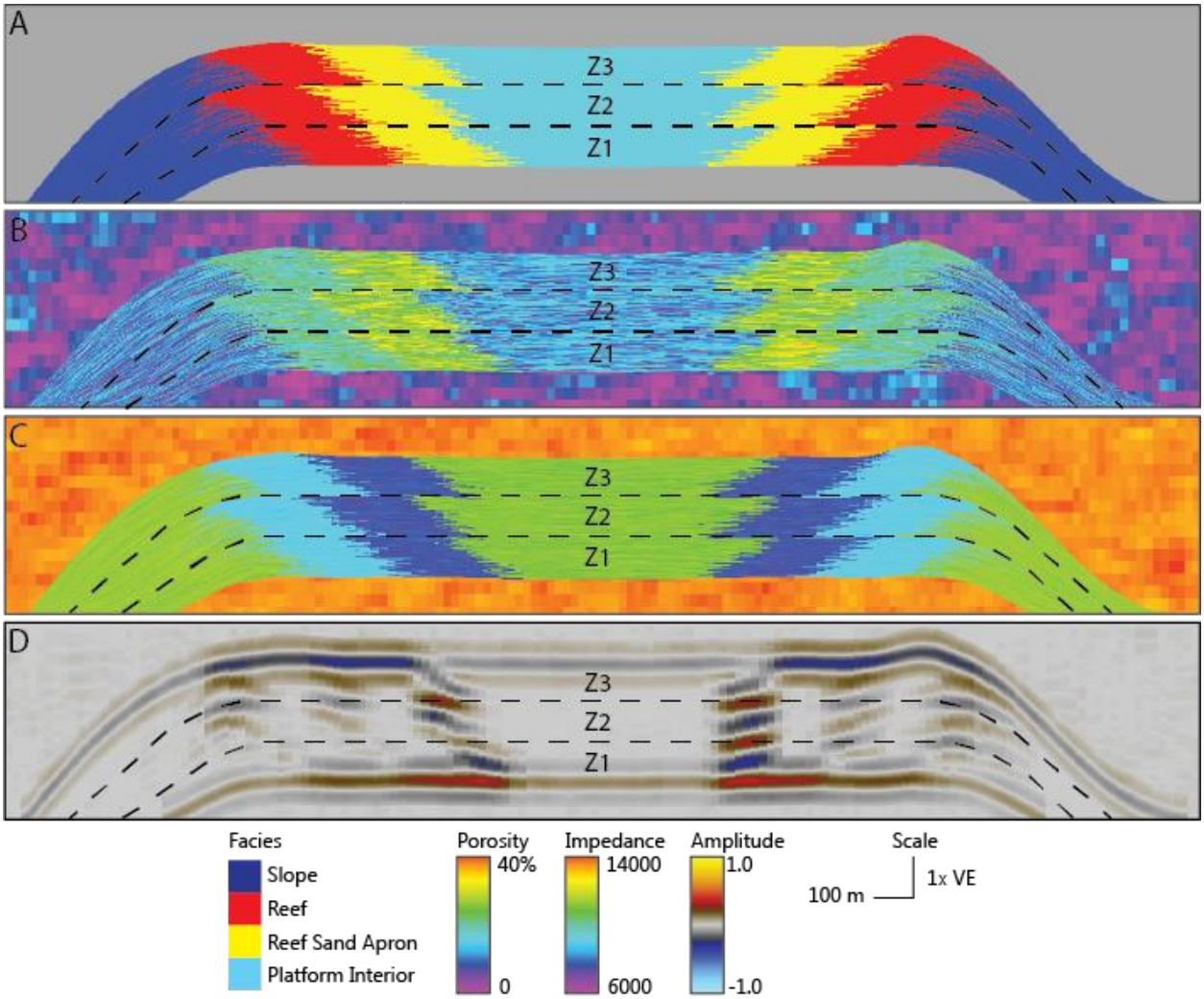

Figure 2: Base case scenario, A) facies volume, B) porosity volume, C) acoustic impedance volume, and D) synthetic seismic volume. Black dashed lines separate stratigraphic zones; Zone 2 (Z2) is the interval in which heterogeneity of interest is isolated. In this scenario, the left margin has basinward-prograding facies (Z1 and Z2) with a backstep to prograding facies between Zone 2 and Zone 3. The right margin has basinward-prograding facies with minor breaks between each zone (Z1, Z2, and Z3).

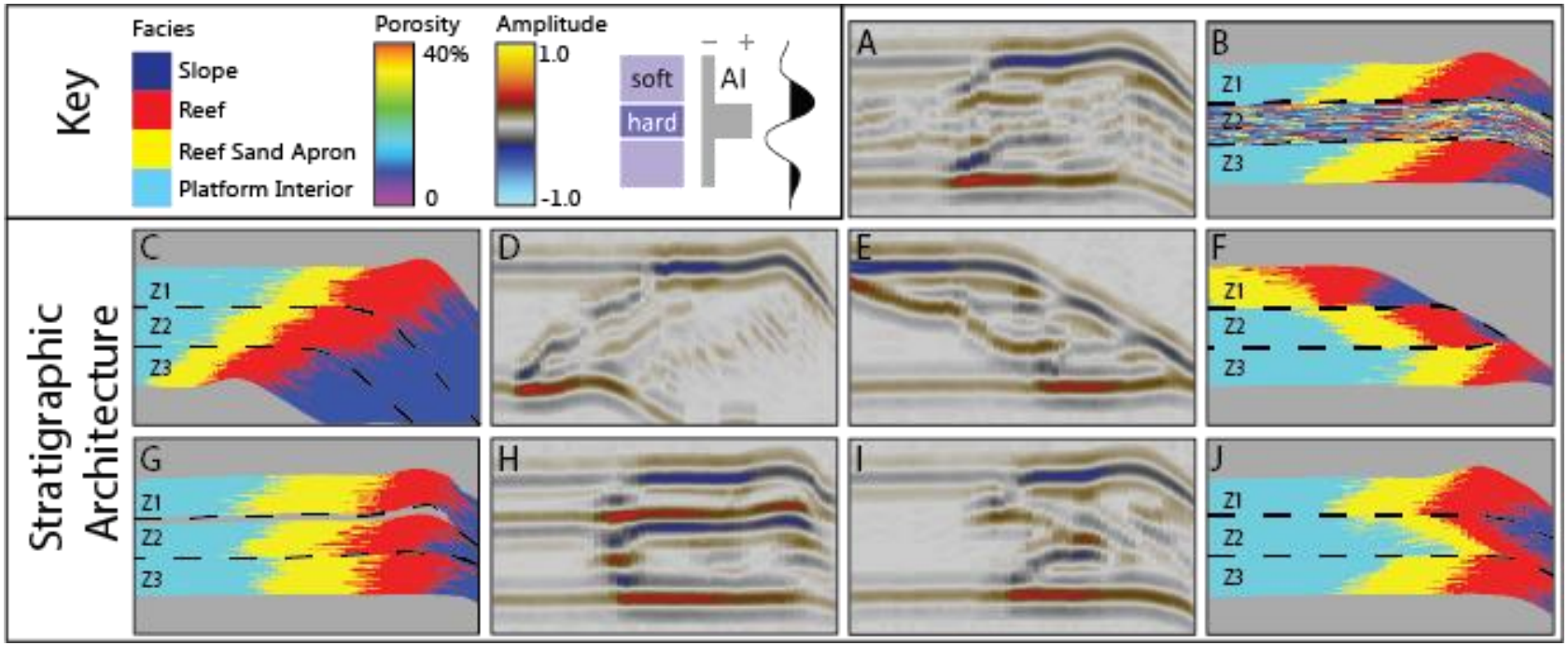
Key
Facies
Slope
Reef
Reef Sand Apron
Platform Interior
Porosity
40%
0
Amplitude
1.0
-1.0
soft
hard
AI
Stratigraphic Architecture
A
B
C
D
E
F
G
H
I
J
Z1
Z2
Z3

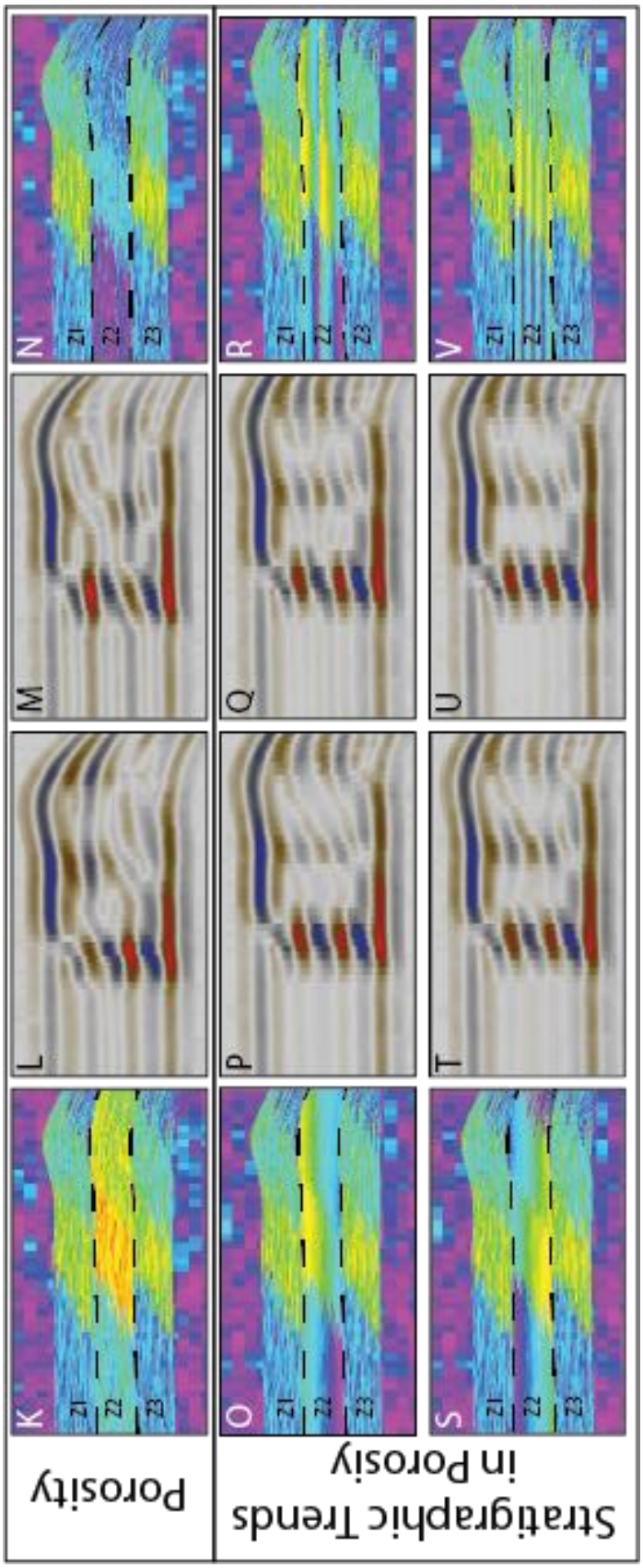

Figure 3: Paired geological models and generated synthetic seismograms from a representative suite of scenarios. (A) and (B) Null hypothesis (colors represent facies stochastically distributed - i.e., absence of any stratigraphic organization); (C) and (D) progradational zonal stacking pattern; (E) and (F) retrogradational zonal stacking pattern; (G) and (H) high impedance cap added to the base model; (I) and (J) depositional clinoform geometries; (K) and (L) high average porosity; (M) and (N) low average porosity; (O) and (P) 100-m thick upward increase in porosity; (Q) and (R) two 50-m thick intervals of upward-increase in porosity; (S) and (T) 100- m thick upward-decrease in porosity; (U) and (V) four 25-m thick intervals of upward-decrease in porosity. Stratigraphic architecture scenarios (A-J) show different facies models, whereas porosity scenarios (K-N) and stratigraphic trends in porosity scenarios (O-V) show different values and distributions of average porosity. The frequency of each geological model has dashed lines that separate stratigraphic zones; Zone 2 (Z2) is the focus. Each synthetic seismogram is at the resolvable limit of the thickness of Z2, approximately 100m. Tables 3 and 4 lay out each geologic parameters for each scenario.

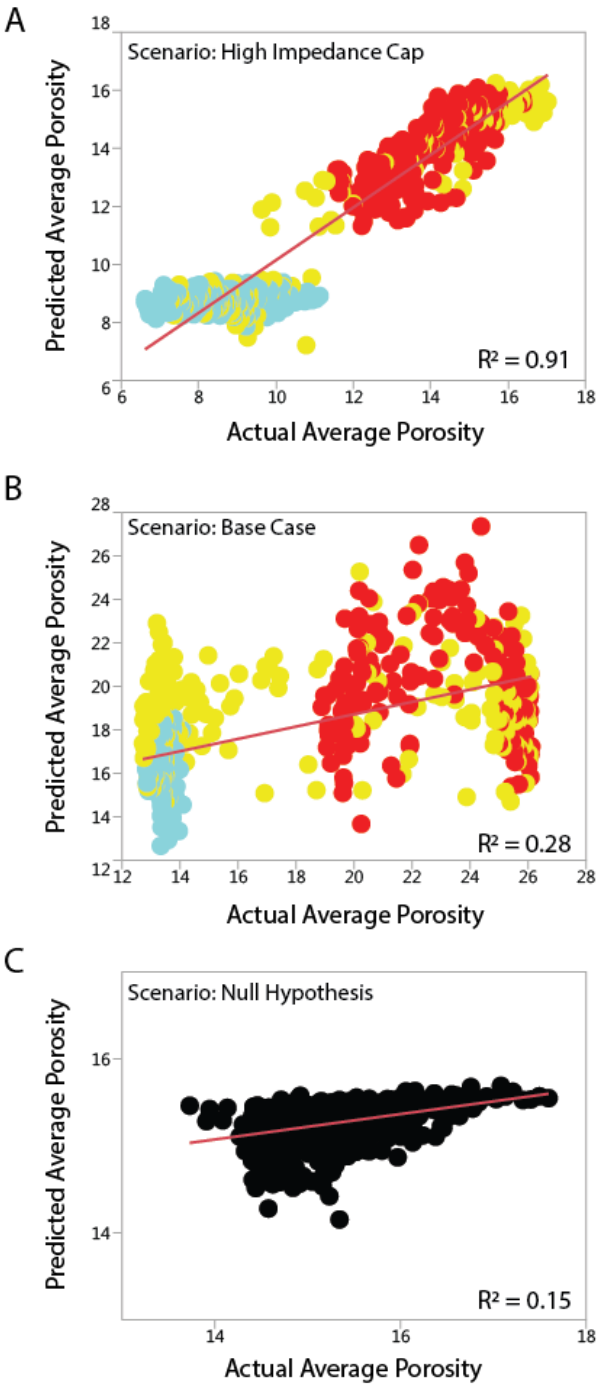

Figure 4: Examples of linear regression results. Best fit line is illustrated for each, as is the R^2 for the best fit correlation between nine attributes and average porosity. A) Scenario with a high impedance cap (shale drape; Figure 3G, H); B) Base case scenario (aggradational zonal stacking pattern; Figure 2). Data points predicted and observed values at each trace, and are colored by most common facies, red = reef, yellow = reef sand apron, and blue = platform interior. C) Null hypothesis scenario (i.e., absence of stratigraphic organization; Figure 3A, B). As facies are randomly distributed, they are roughly equiprobable, so data are all the same color.

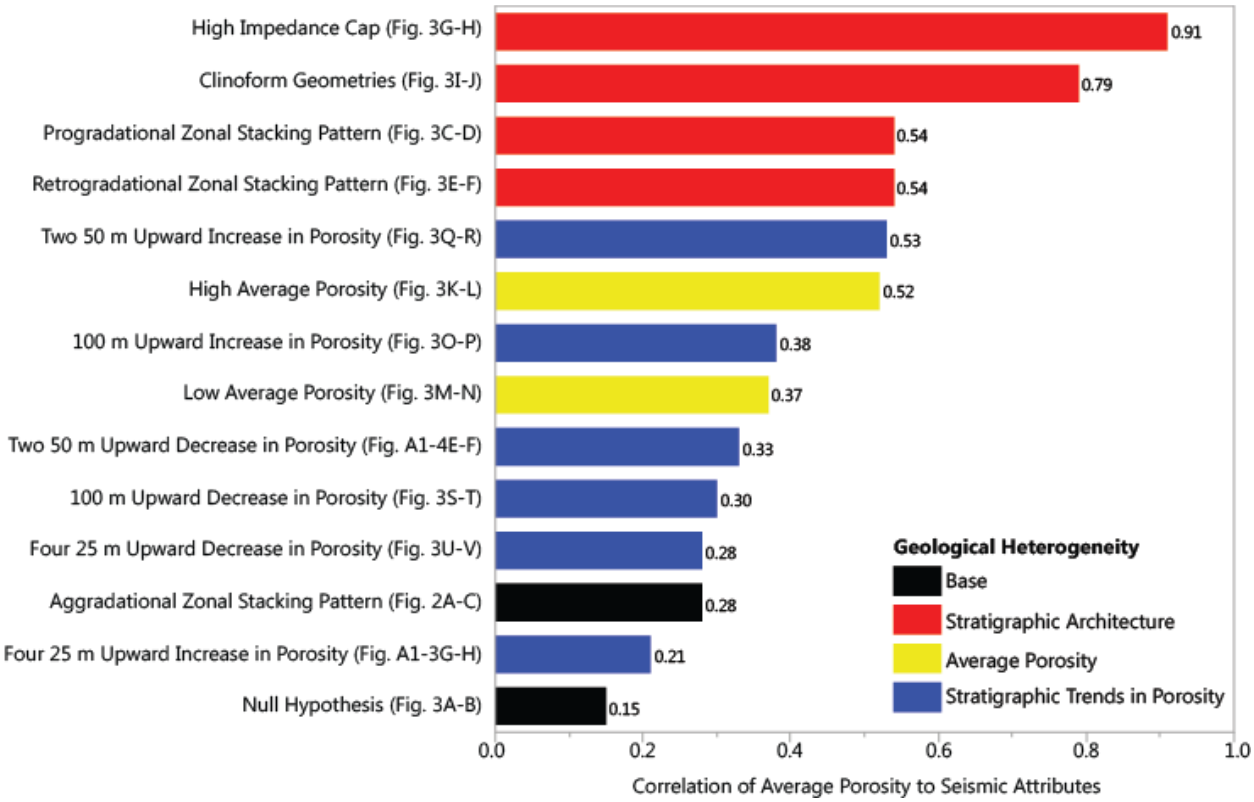

Figure 5: Plot summarizing results of regressions using all nine attributes to predict average porosity. Organized in ascending order of R^2 value, from base to top, each bar represents the correlation coefficient (R^2) for a distinct scenario (labeled to the left with reference to its geological model and synthetic seismic line), and colors represent classes of geological heterogeneity. Note that the ability of attributes to predict porosity varies considerably among scenarios and heterogeneity classes. See text for discussion.

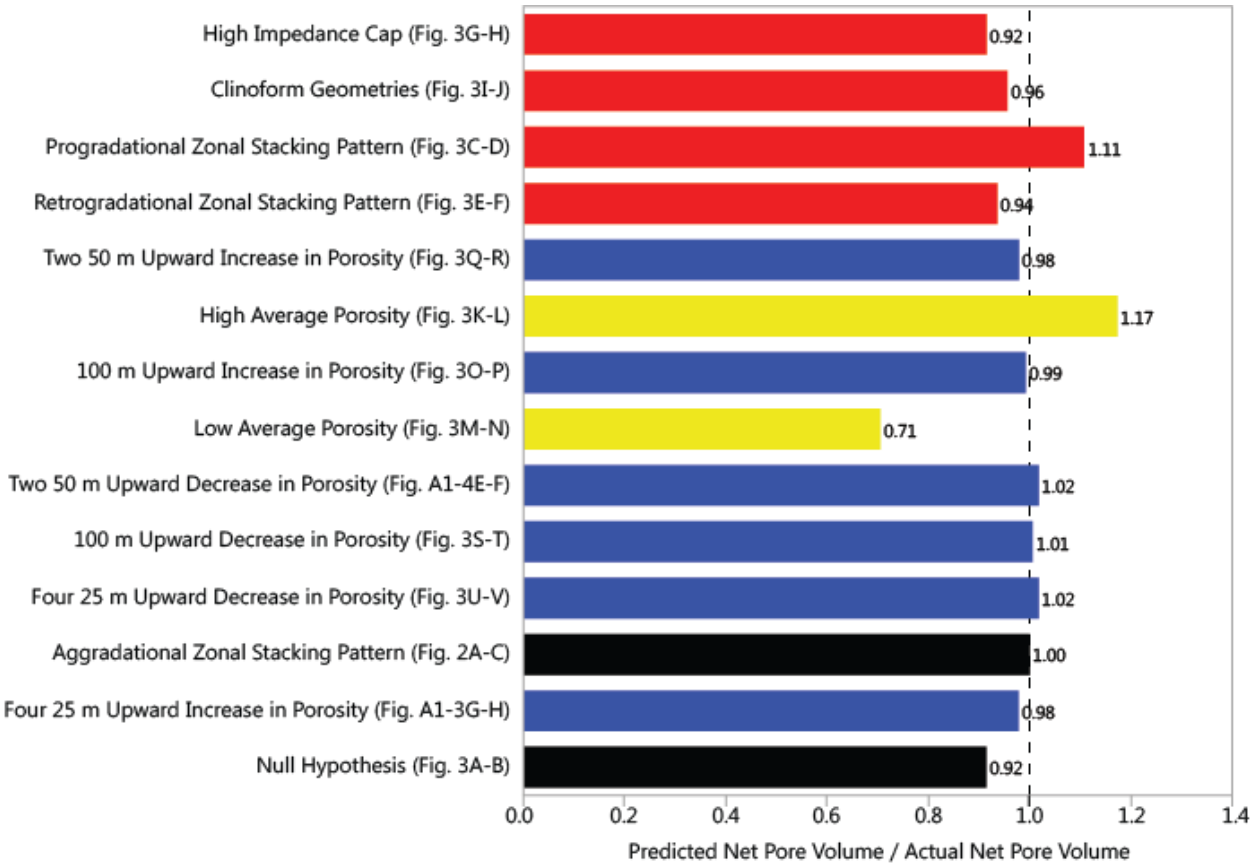

Figure 6: Plot summarizing results for predictability of net pore volume from attributes. Illustrated in the same order as data in Figure 5, each bar represents the ratio of predicted net pore volume to actual net pore volume for a distinct scenario (labeled to the left with reference to its geological model and synthetic seismic line), and colors represent classes of geological heterogeneity (key in Figure 5). A value of less than one documents under prediction, a value of greater than one means over – prediction.

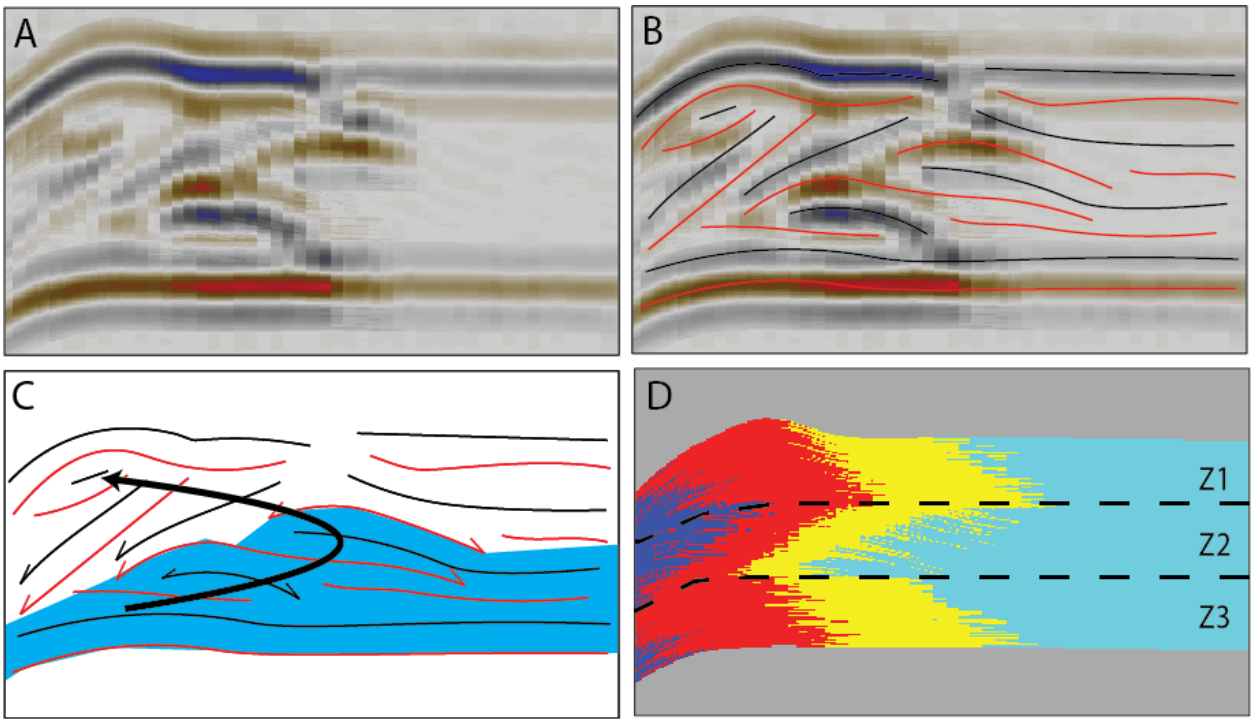

Figure 7: Uninterpreted (A), interpreted (B), and plausible, but incorrect (C) interpretation for the synthetic seismic line of the clinoform scenario. The plausible interpretation does not match geological model (D) used to generate this synthetic. The mounded geometries (colored blue in part C) appear to backstep, overlain by inclined reflectors that downlap onto the mounded geometries. The geological model, however, shows basinward progradation (to the left) in Z1 and Z3 and platformward progradation in Z2 (to the right).

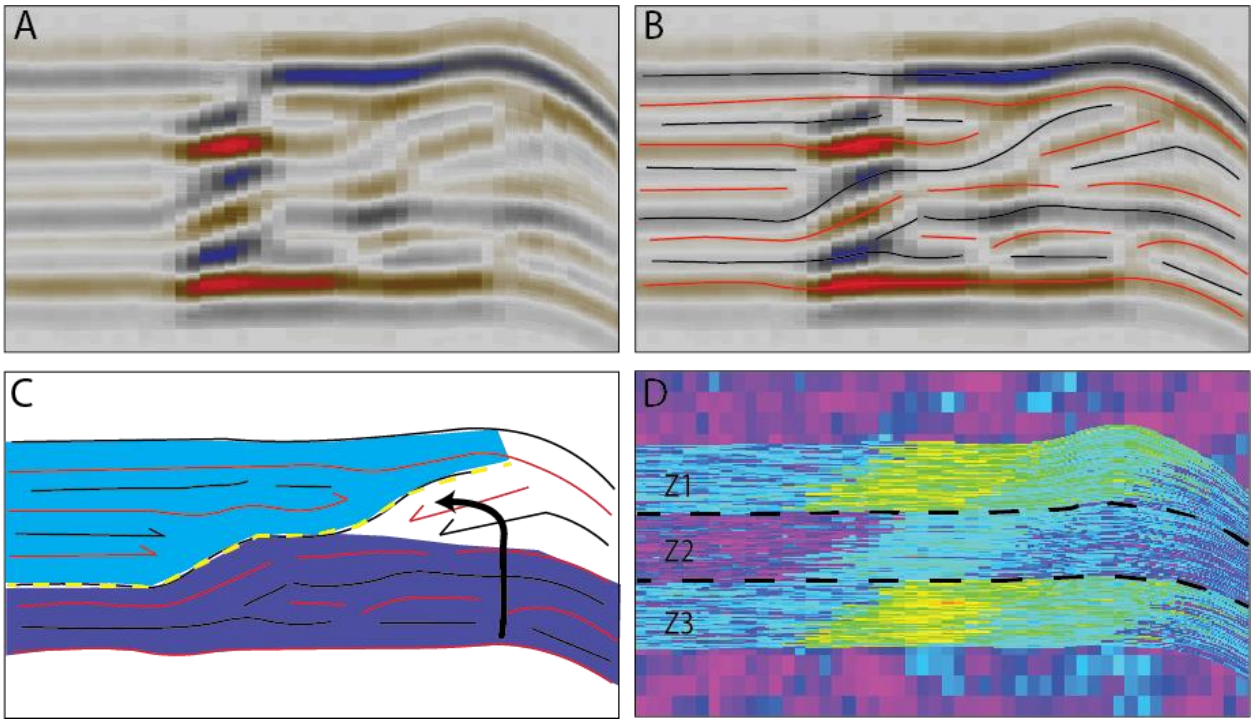

Figure 8: Uninterpreted (A), interpreted (B), and plausible, but incorrect (C) interpretation for the synthetic seismic line of the scenario of low average porosity. The geological model (D) used to generate this synthetic does not have facies prograding towards the platform interior (to the left, black arrow), rather, the geological model has all three zones include facies prograding basinwards (to the right). The trough (yellow dashed line in part C) that appears to be onlapped by parallel reflectors (light blue) follows the impedance contrast between Zone 2, with lower average porosity, and Zone 1.

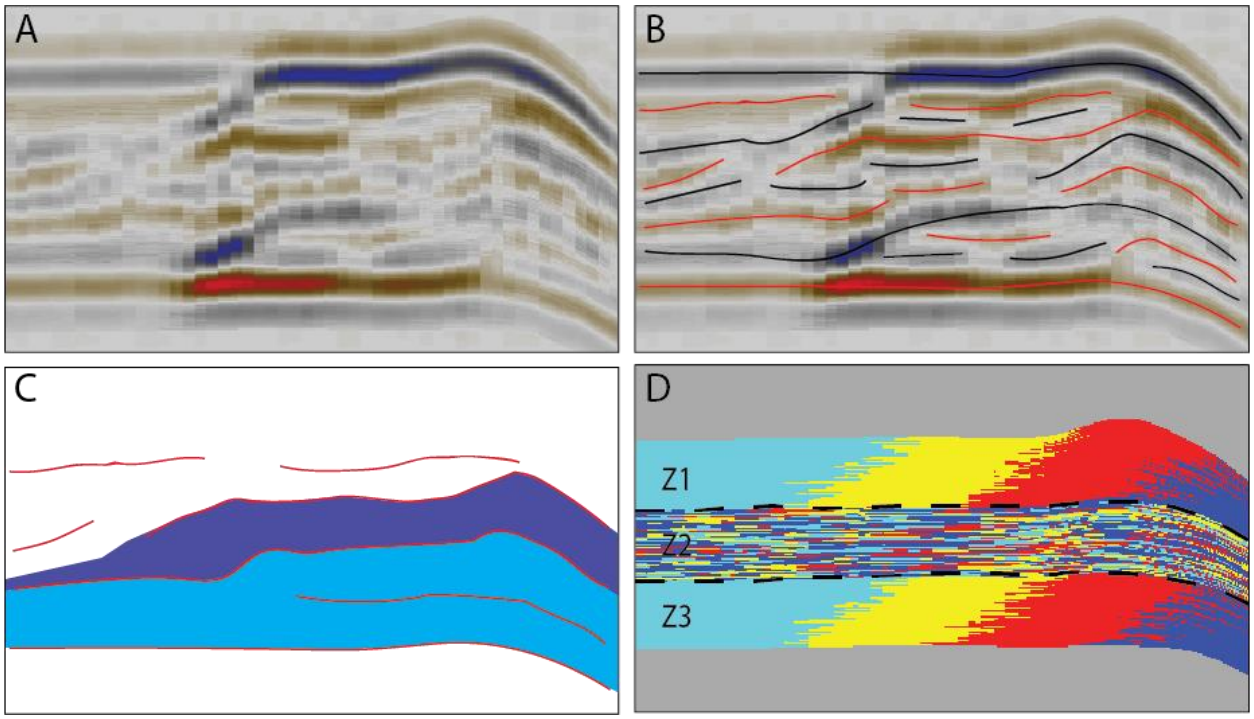

Figure 9: Uninterpreted (A), interpreted (B), and plausible, but incorrect (C) interpretation for the synthetic seismic line of the scenario that has non-geological heterogeneity. Lacking geological organization in Zone 2, facies are distributed randomly (D). The discontinuous reflectors with varying amplitudes contrast with the sheet-like geometry in the geological model.

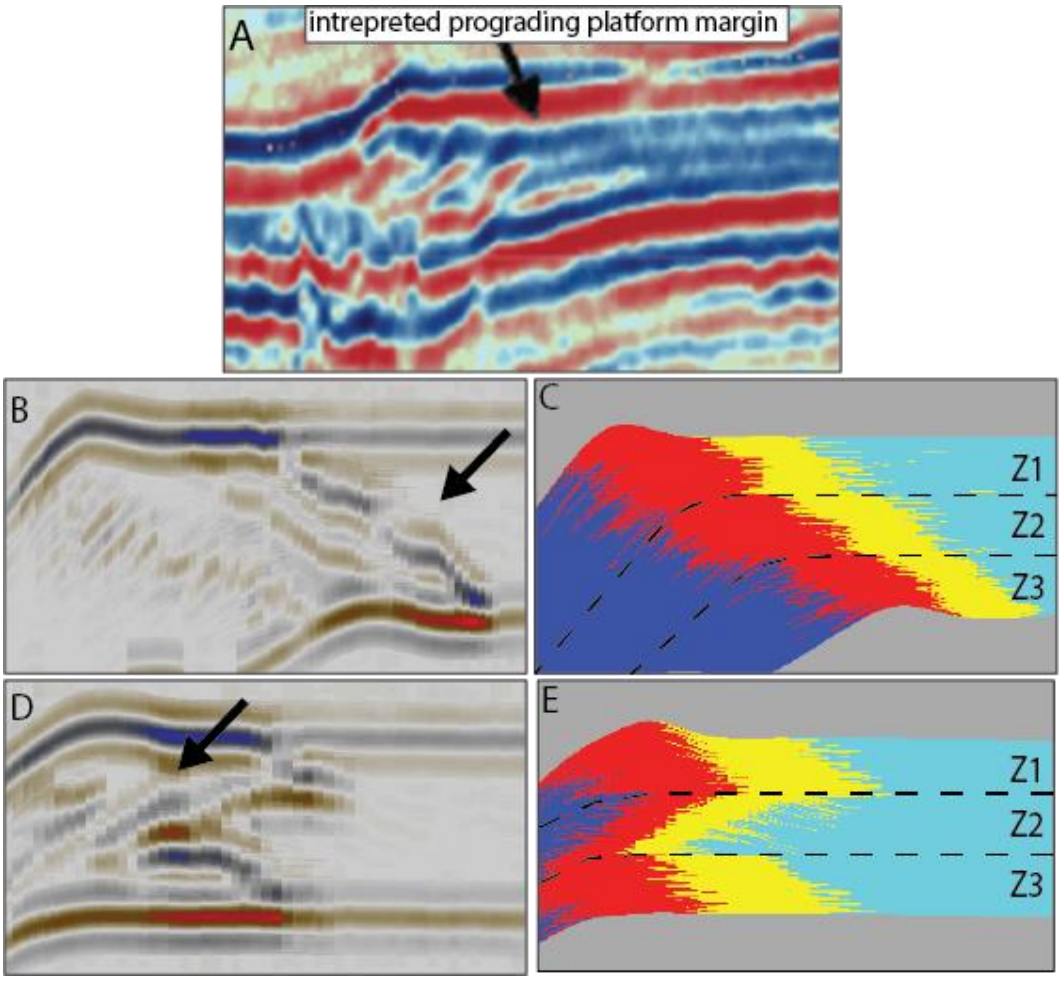

Figure 10: Comparison of Jintan platform seismic data with selected synthetic volumes. A) Seismic line of Jintan's smaller, backstepped platform (modified from Vahrenkamp et al., 2004). Interpreted synthetic line of a scenario with prograding margin (B) and geological model (C). D) Interpreted synthetic line generated from a scenario with depositional clinoform geometries and geological model (D). Note how inclined reflectors such as those in Jintan can be generated by a range of geological parameters.

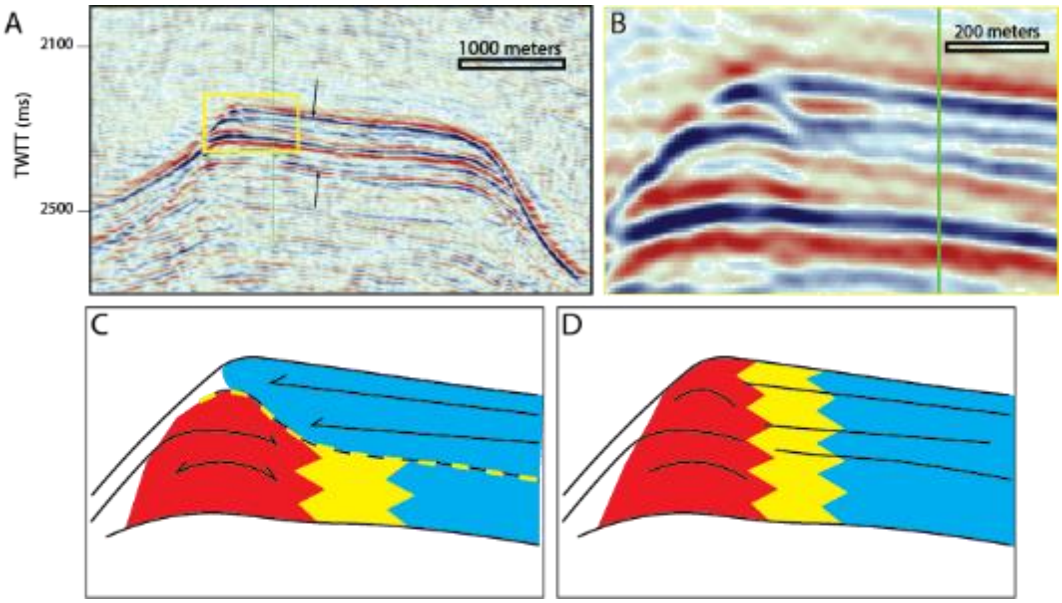

Figure 11: Comparison of Central Luconia Buildup, to the scenario with low average porosity's synthetic volume. A) Seismic line through central Luconia buildup (modified from Masaferro et al., 2003). B) Seismic line focusing on margin of buildup (modified from Masaferro et al., 2003). C and D) Plausible interpretations of platform margin (B). C) Interpretation suggests onlapping reflectors (light blue) from the interior of the platform (to the right) onto marginal mounded reflectors (red) (to the left). (D) Interpretation that suggests a facies transition between marginal units (red and yellow) and interior units (light blue). Models (e.g., Figure 3I, J) illustrate how facies changes (as in D) can create mounded geometries that appear to be onlapped. See text for discussion.

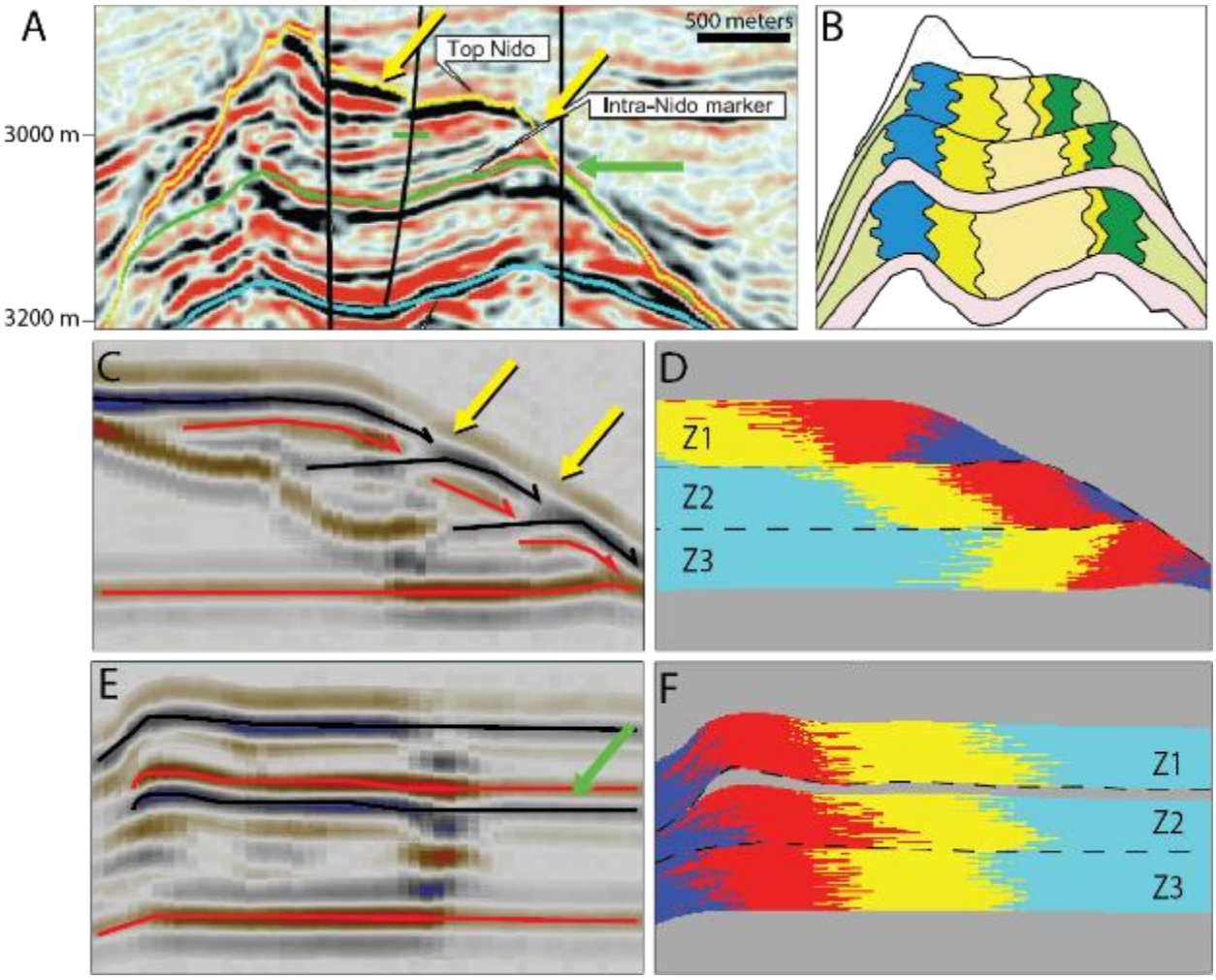

Figure 12: Comparison of Malampaya Field, Philippines, with selected scenarios. Seismic line through Malampaya Field (A, modified from Neuhaus et al., 2004) and conceptual model (B, modified from Grötsch and Mercadier, 1999). The seismic character of Malampaya has several qualitative similarities to scenarios that model a retrogradation margin. Note that the synthetic seismic line (C) includes backstepping (D), like the seismic, as emphasized by the yellow arrows in A and C. E-F) A high impedance layer (e.g., a cemented surface) produces a high-amplitude reflector in the middle of the platform (green arrow), similar to that interpreted for Malampaya. See text for discussion.

TABLES

Geological Parameter	References
Range of Average Porosity	
Devonian	Watts, 1987
Miocene	Bachtel et al., 2004; Fournier et al., 2004; Masaferro et al., 2004; and Neuhaus et al., 2004
Vertical Trends in Porosity	
Devonian	Watts, 1987
Miocene	Bachtel et al., 2004; Fournier et al., 2004; and Neuhaus et al., 2004
Stratigraphic Architecture	
Modern	Rankey, 2016
Ancient	Epting 1980, 1989; May and Eyles 1985; Rudolph and Lehmann 1989; Grötsch and Mercadier, 1999; Zampetti et al., 2003, 2004; Bachtel et al., 2004; Fournier et al., 2004, 2005; Neuhaus et al., 2004; Fournier and Borgomano, 2007

Table 1: Geological inspirations for the suite of models of this study. The idealized, conceptual, and fully constrained models constructed here utilize inputs of reservoir properties from two geologic end-member time periods (greenhouse Devonian; icehouse Miocene), and data on facies and architecture from both modern and ancient systems. See text for discussion.

Facies	Porosity (%)	Velocity (m/s)	Density (g/cm^3)	Impedance ($kg/m^3 * m/s$)
Shale	5	5650	2.49	14068.5
Slope	10	4950	2.32	11484
Reef	20	4000	2.27	9080
Reef Sand Apron	26	3550	2.17	7703.5
Platform Interior	12	4700	2.41	11327

Table 2: Mean petrophysical properties, base case scenario. Properties are varied systematically from these base case values to assess their impact on seismic character.

Stratigraphic Architecture Complexities		
Scenario	Zonal Stacking Pattern	Facies Distribution
Aggradational Zonal Facies Stacking	**Aggradational**	Layer Cake
Retrogradation Zonal Stacking Pattern	**Retrogradational**	Layer Cake
Progradational Zonal Stacking Pattern	**Progradational**	Layer Cake
Depositional Clinoform Geometries	Aggradational	**Clinoform**
High Impedance Cap	Aggradational	**Layer Cake with Shale Cap**
Null Hypothesis	**None**	**Stochastic**

Table 3: Geological parameters for each scenario within the stratigraphic architecture group. All petrophysical properties are the same (see Table 2 for values). For geological models and synthetic seismic lines, see Figure 3A-J.

Petrophysical Complexities			
Scenario	Facies	Mean Porosity	Number of Cycles
Aggradational Zonal Stacking Pattern	Reef	**20**	-
	Reef Sand Apron	**26**	
	Platform Interior	**12**	
High Average Porosity	Reef	**28**	-
	Reef Sand Apron	**36**	
	Platform Interior	**18**	
Low Average Porosity	Reef	**11**	-
	Reef Sand Apron	**16**	
	Platform Interior	**5**	
100 m Thick Upward Increase in Porosity	Reef	20	**1**
	Reef Sand Apron	26	
	Platform Interior	12	
Two 50 m Thick Intervals of Upward-Increase in Porosity	Reef	20	**2**
	Reef Sand Apron	26	
	Platform Interior	12	
Four 25 m Thick Intervals of Upward-Increase in Porosity	Reef	20	**4**
	Reef Sand Apron	26	
	Platform Interior	12	
100 m Thick Upward Decrease in Porosity	Reef	20	**1**
	Reef Sand Apron	26	
	Platform Interior	12	
Two 50 m Thick Intervals of Upward-Decrease in Porosity	Reef	20	**2**
	Reef Sand Apron	26	
	Platform Interior	12	
Four 25 m Thick Intervals of Upward-Decrease in Porosity	Reef	20	**4**
	Reef Sand Apron	26	
	Platform Interior	12	

Table 4: Geological parameters for each scenario within the petrophysical complexities group. All scenarios have constant stratigraphic architecture, the scenario with aggradational zonal stacking patterns (i.e., base case scenario, Figure 2).

APPENDIX 1. GEOLOGIC MODELS AND SYNTHETIC SEISMIC VOLUMES

Boundary and Intra-facies Complexities

Boundary Effects. Scenarios within the "boundary effects" group evaluate heterogeneity above and below the platform (Zones 1-3 remain constant). One scenario added a small carbonate pinnacle on top of the 300 m of carbonate facies (Figure A1-1A). The facies in this pinnacle scenario include slope, reef, and inner-shelf environment undifferentiated (with mean porosity of 9%). Another scenario modified the over- and underlying shales to have low impedance (Figure A1-1C) rather than high impedance (e.g. the base case).

Seismic data reveal subtle differences from the base case for all scenarios. The addition of the pinnacle to the base case scenario had no impact to the seismic character of the middle zone. At the boundary of the pinnacle and zone three, new reflectors appear that are not present in other scenarios (Figure A1-1B). Within the low impedance shale scenario, the middle zone had little visible change with slightly lower amplitude reflections. Outside of Zone 2, the reflectors from the low impedance shale scenario have a phase reversal between the carbonate strata and the above and underlying shale (Figure A1-1D), not surprising given the reversed impedance contrast.

Platform Interior Heterogeneity. Scenarios within this group model realizations in which porous patch reefs occur within the platform interior. To simulate this possibility, reef bodies were distributed stochastically within the platform interior, at abundances of 1% (, A1-1E), 10% (Figure A1-1G), and 25% (Figure A1-1I), each as a separate scenario; reef and reef sand apron facies distribution and porosity were not changed. The patch reefs did not have relief above the surrounding platform-interior cells, but their average porosity was greater (20% vs 12%).

Since this group of models modified only the platform interior, the seismic reflectors caused by the reef and reef sand apron are essentially the same in all models. Within the interior, little to no visible difference is evident between the 1% patch reef model (Figure A1-1F) and the base case (Figure 2D). The 10% patch reef scenario (Figure A1-1H) includes discontinuous reflectors with horizontal and inclined orientations. The scenario with 25% patch reefs (Figure A1-1J) has the largest visible difference to the base case, and resembles the stochastic distribution scenario (Figure 3C) within the platform interior area of the volume but with lower amplitudes.

Stratigraphic Porosity Trends at Elevated Porosity

The suite of seismic volumes that had little difference to the high average porosity scenario (Figures A1-4 and A1-5) and to each other. Like other scenarios, the highest amplitude reflectors occur at the platform interior – reef sand apron boundary and the platform interior region's additions of continuous reflectors.

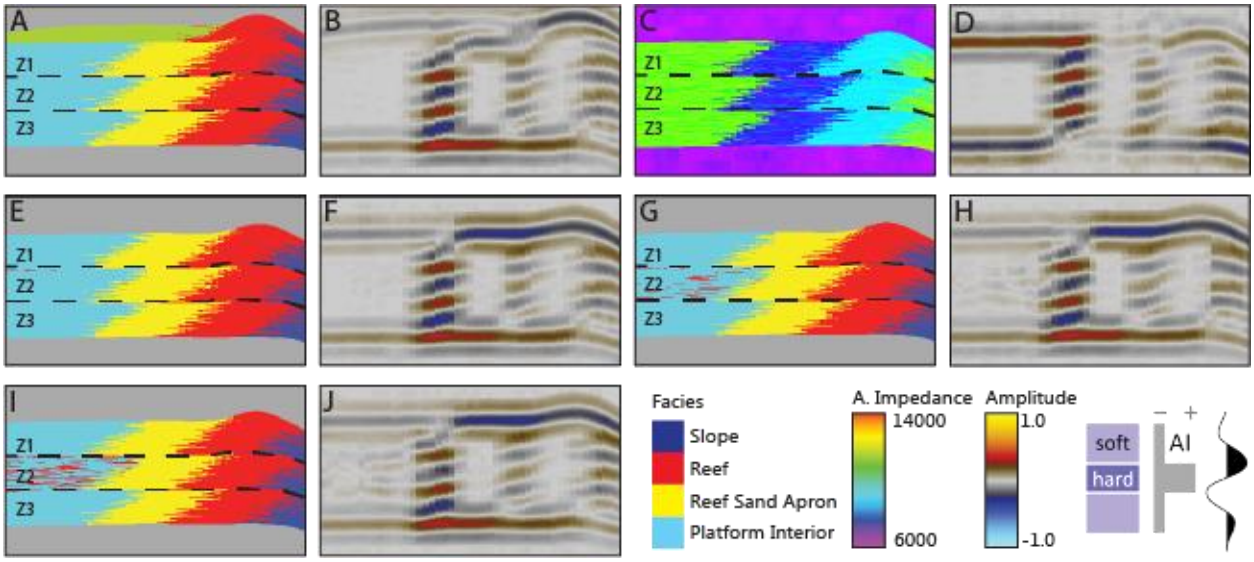

Figure A1-1: Model matrix of additional scenarios modeling boundary effects and platform interior heterogeneity. Addition of carbonate pinnacle's facies volume (A) and synthetic volume B). Base case scenario with low impedance shale's impedance volume (C) and synthetic volume (D). Presence of 1% patch reefs' facies volume (E) and synthetic volume (F). Presence of 10% patch reefs' facies volume (G) and synthetic volume (H). Presence of 25% patch reefs' facies volume (I) and synthetic volume (J).

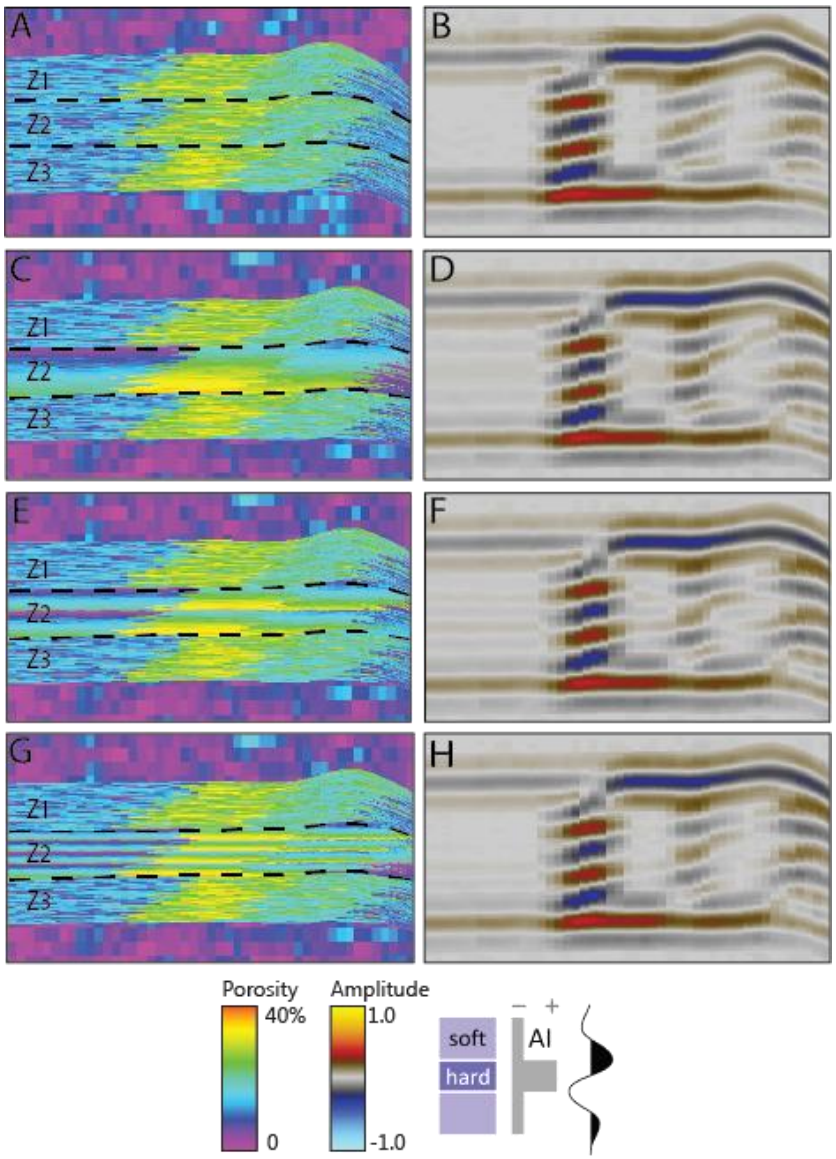

Figure A1-2: Comparison of base case scenario to dirtying-up scenarios within the cyclic porosity trends suite. Black dashed lines separate stratigraphic zones in the porosity models. Base case scenario's porosity volume (A) and synthetic volume (B), 100 m upward decrease in porosity (C) and synthetic volume (D); two 50 m upward decrease in porosity (E) and synthetic volume (F), and four 25 m upward decrease in porosity (G) and synthetic volume (H).

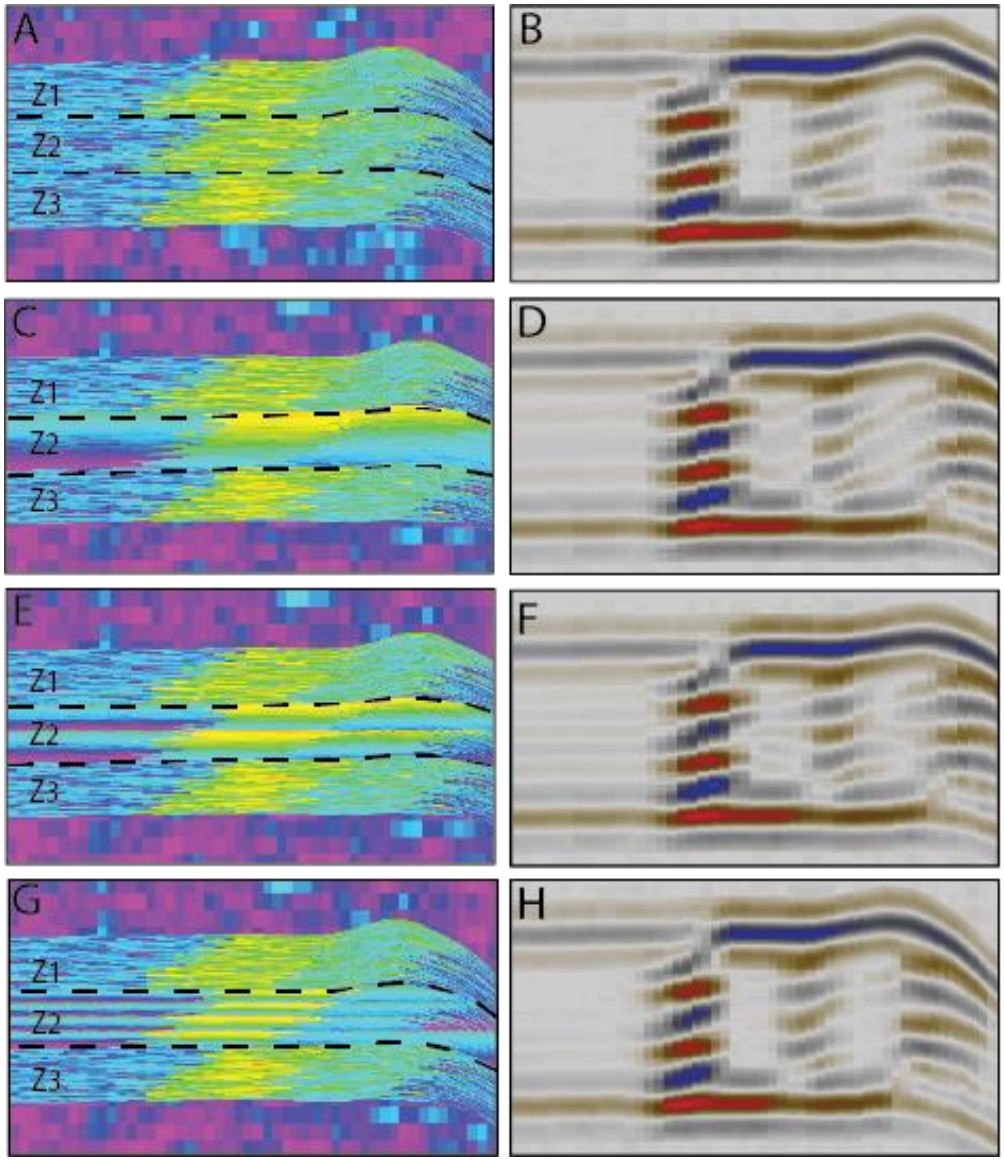

Figure A1-3: Comparison of base case scenario to cleaning-up scenarios within the cyclic porosity trends suite. Black dashed lines separate stratigraphic zones in the porosity models; zone Z2 is the focus. Base case scenario's porosity volume (A) and synthetic volume (B), 100 m upward increase in porosity (C) and synthetic volume (D); two 50 m upward increase in porosity (E) and synthetic volume (F), and four 25 m upward increase in porosity (G) and synthetic volume (H). Key in Appendix 1, Figure A1-2.

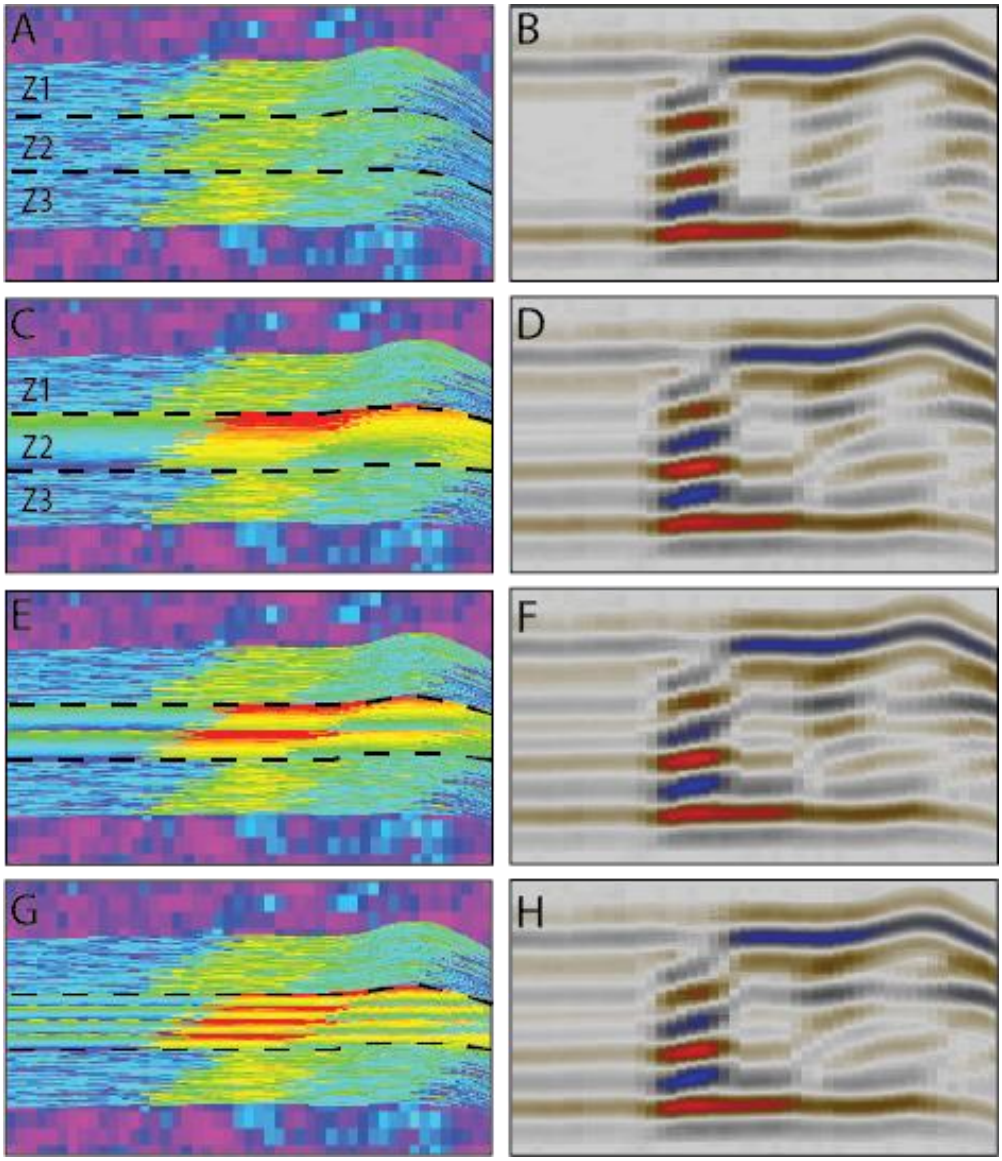

Figure A1-4: Comparison of base case scenario to cleaning-up scenarios within the cyclic porosity trends at elevated average porosity. Black dashed lines separate stratigraphic zones in the porosity models. Base case scenario's porosity volume (A) and synthetic volume (B). Elevated average porosity for models is 26%. C) 100 m upward increase in porosity and synthetic volume (D). (E) Two 50 m upward increase in porosity and synthetic volume (F). (G) Four 25 m upward increase in porosity and synthetic volume (H). Key in Appendix 1, Figure A1-2.

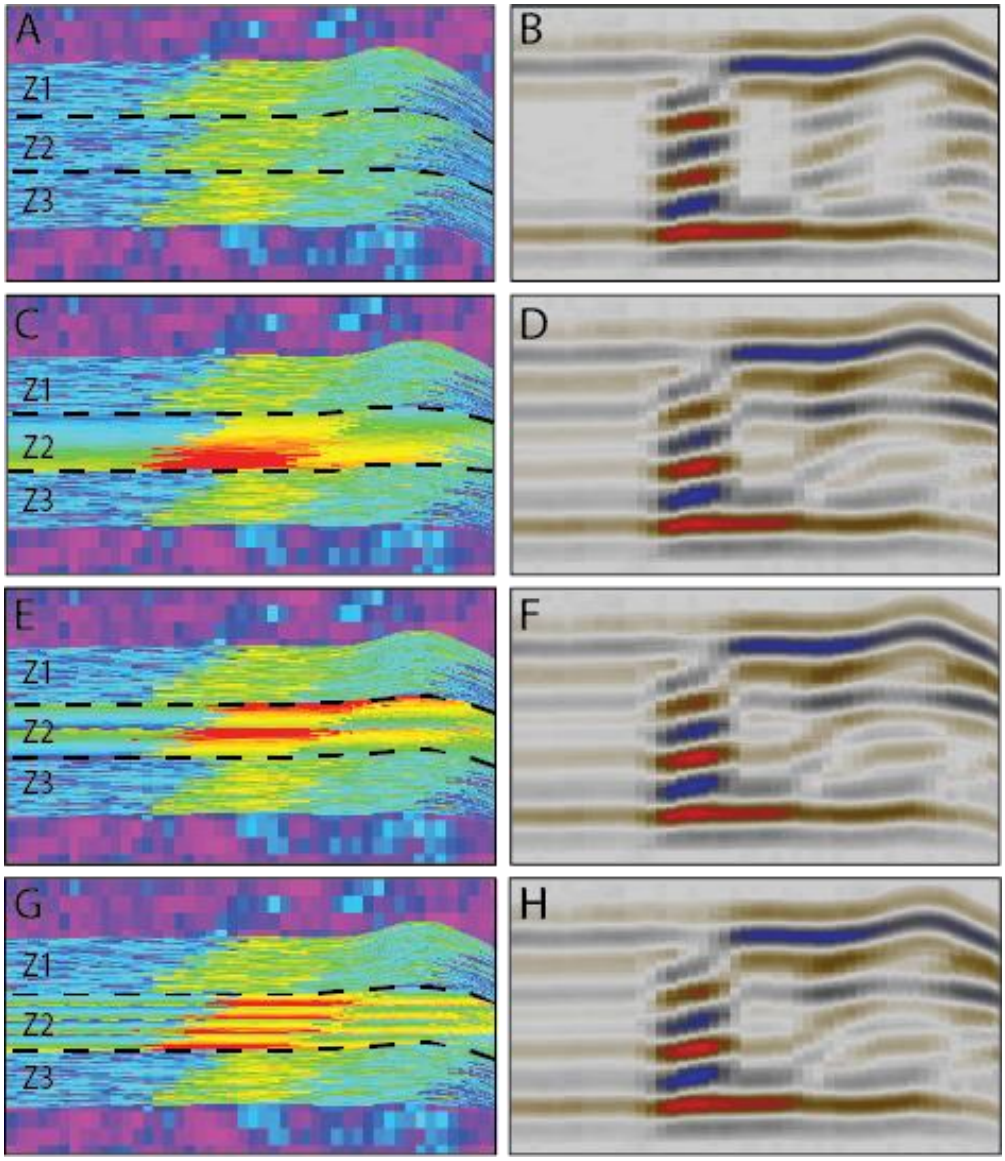

Figure A1-5: Comparison of base case scenario to dirtying-up scenarios within the cyclic porosity trends at elevated average porosity. Black dashed lines separate stratigraphic zones in the porosity models. Base case scenario's porosity volume (A) and synthetic volume (B). Elevated average porosity for models is 26%. C) 100 m upward decrease in porosity and synthetic volume (D). (E) Two 50 m upward decrease in porosity and synthetic volume (F). (G) Four 25 m upward decrease in porosity and synthetic volume (H). Key in Appendix 1, Figure A1-2.

APPENDIX 2. QUANTITATIVE CHARACTERIZATION OF SEISMIC CHARACTER

Base Case and Null Hypothesis Scenarios

Seismic attributes extracted from the base case scenario highlight how geology quantitatively influences seismic character (Figure A2-1). All attributes except for positive to negative ratio have increased values in the facies transitions between reef sand apron and platform interior (average facies colored green), and reef sand apron and reef (average facies colored orange). Interestingly, only one facies transition has a peak in both average duration of negative and positive loops attributes, but are not the same facies transition. Average duration of negative loops attribute has a high in the reef sand apron-platform interior transition but not in the reef-reef sand apron transition. Whereas, average duration of positive loops attribute has the reverse, a high in the reef-reef sand apron transition and not in the platform interior-reef sand apron transition.

Stratigraphic Architecture

The scenarios that isolate stratigraphic architecture all have the same facies-based average porosity. Seismic attributes extracted cannot be plotted on a single axis because the stratal architecture is different and therefore the location of each facies is different (Figure A2-2). The nine attributes do not show any substantial differences between scenarios in this group.

Petrophysical Complexities

Average porosity. Seismic attributes extracted from the high average porosity scenario are plotted on the red colored line (Figure A2-3). The high average porosity scenario's attributes have similar character to the base case scenario. For example, there are peaks in value in the two

facies transitions zones for all attributes. However, there is an additional peak in value for three attributes in the reef sand apron facies that is not present in the base case scenario (positive to negative ratio, and both average duration of negative and positive loops). Focusing more on the positive to negative ratio attribute, there isn't a large difference between the values within the platform interior facies, the line is more or less flat.

Seismic attributes extracted from the low porosity scenario are plotted on the green colored line (Figure A2-3). RMS amplitude, average energy, and average magnitude all have higher values in the facies transitions. In the average peak value attribute, there is an additional higher value in the reef sand apron facies that is not present in any other scenario in this group. The positive to negative ratio attribute does not have a large range of values except at each side of the reef facies, here, there is a spike in higher values.

To summarize, the scenarios that isolated average porosity (base model, high and low average porosity) have some attributes that have no difference among scenarios and other attributes that are different. For example, in all three scenarios, RMS amplitude average energy, average magnitude, and standard deviation of loop duration are all plotting almost on top of each other, even though there are differences in average porosity by facies (and therefore impedance) (Figure A2-3). There are peaks in the four attributes in the facies transition between reef sand apron and platform interior. Conversely, attributes that measure seismic loop the scenarios differ much more. Comparing the three scenarios, the platform interior region (average facies colored blue) lines plot top of each other leading one to believe despite the change in average porosity values there is no statistical difference in attributes (no whistle blower). This holds true except for three attributes. The most obvious contrast is evident in the positive to negative ratio attribute. Here the base case scenario differs greatly from the high and low average porosity

scenarios that plot on top of each other. Similarly in the other two contrasting attributes, average duration of negative loops and average loop duration, both high and low average porosity scenarios plot on top of each other but also have higher values than the base case scenario.

Stratigraphic porosity trends. The scenarios that isolate vertical porosity trends but have the same stratigraphic architecture and average porosity (Figure A2-4). The base case scenario is colored black. The cleaning-upward porosity distributions (100 m, two 50 m, and four 25 m) are colored red, green, and purple respectively; the dirtying-upward porosity distributions (100 m, two 50 m, and four 25 m) are colored orange, teal, and magenta respectively.

The cleaning-upward porosity distribution group have little to no differences in RMS amplitude, average energy, average magnitude, or average peak value, all the scenarios are plotting on top of each other. Positive to negative ratio attribute does not have marked differences among the cleaning-upward scenarios, however, between the base case scenario and the rest of the group there is a much greater difference, especially within the platform interior area. Average duration of negative loops have lower values across all scenarios in the reef and sand apron facies, however, the transition to platform interior has increased values. Within the platform interior there is a split in scenarios, with one 100 m cycle with the highest values, followed by the two 50 m cycles, and the lowest values are shared by the base case scenario and four 25 m cycle. Interestingly, there are reverse relationships seen in the average duration positive loops attribute. The values are higher in the reef and transition to reef sand apron and then split into the platform interior. The one 100 m cycle has the lowest values and the other scenarios are plotting on top of each other. The las two attributes, average loop duration and standard deviation of loop duration, have similar trends to the average duration of negative loops

attribute except for the addition of peaks in values in the facies transition between reef and reef sand apron.

Like the cleaning-upward scenarios, the dirtying-upward porosity distribution group also has little to no differences in RMS amplitude, average energy, average magnitude, or average peak value, all the scenarios are plotting on top of each other. The positive to negative ratio attribute is generally the same in all scenarios but within the platform interior there starts to be some variation among scenarios. The remaining attributes all have higher values in the facies transitions and have similar variations in the platform interior region.

To summarize, the attributes that measure characteristics of amplitude cannot differentiate the cyclicity in the vertical porosity distributions. The attributes that measure seismic loop characteristics better discern the vertical porosity trends. Although, the base case scenario and both four 25 m cleaning- and dirtying-upward cycles have most similar attributes except for positive to negative ratio and standard deviation of loop duration.

The second set of scenarios at higher average porosity (between 16-36%) with the same vertical porosity intervals show very similar trends in attribute character among all models (Figure A2-5). The higher average porosity scenario is colored blue. The higher average porosity with cleaning-upward porosity distributions (100 m, two 50 m, and four 25 m) are colored red, green, and purple respectively; the higher average porosity with dirtying-upward porosity distributions (100 m, two 50 m, and four 25 m) are colored orange, teal, and magenta respectively.

All six scenarios have similar trends when plotted with the high average porosity that used Gaussian distribution. The variation among scenarios is less pronounced in the facies

transitions, whereas the pure facies have more pronounced spread of values for the attributes that measure loop shape.

Expanded Search Window

All models used stratigraphic surfaces as interval constraints for calculating the attributes for the middle zone of interest. With the low frequency wavelet being almost one seismic loop for 100 m the stratigraphic surfaces did not allow the entire wave to measure the zone boundary. Therefore, a subset of scenarios (nine) had an expanded search window for calculating and extracting attributes (average porosity in Appendix 2, Figure A2-6 and stratigraphic architecture Appendix 2, Figure A2-7). These scenarios extend the search interval by 20 ms above and below interval range to allow the entire wavelet (that represents the interface) to be measured. Overall for both porosity and stratigraphic architecture scenario groups, the expanded search window's attributes display similar qualitative trends as the attributes calculated within the standard search window for attributes that measure amplitude. Alternatively, the shape attributes show more variation from the standard search window attributes.

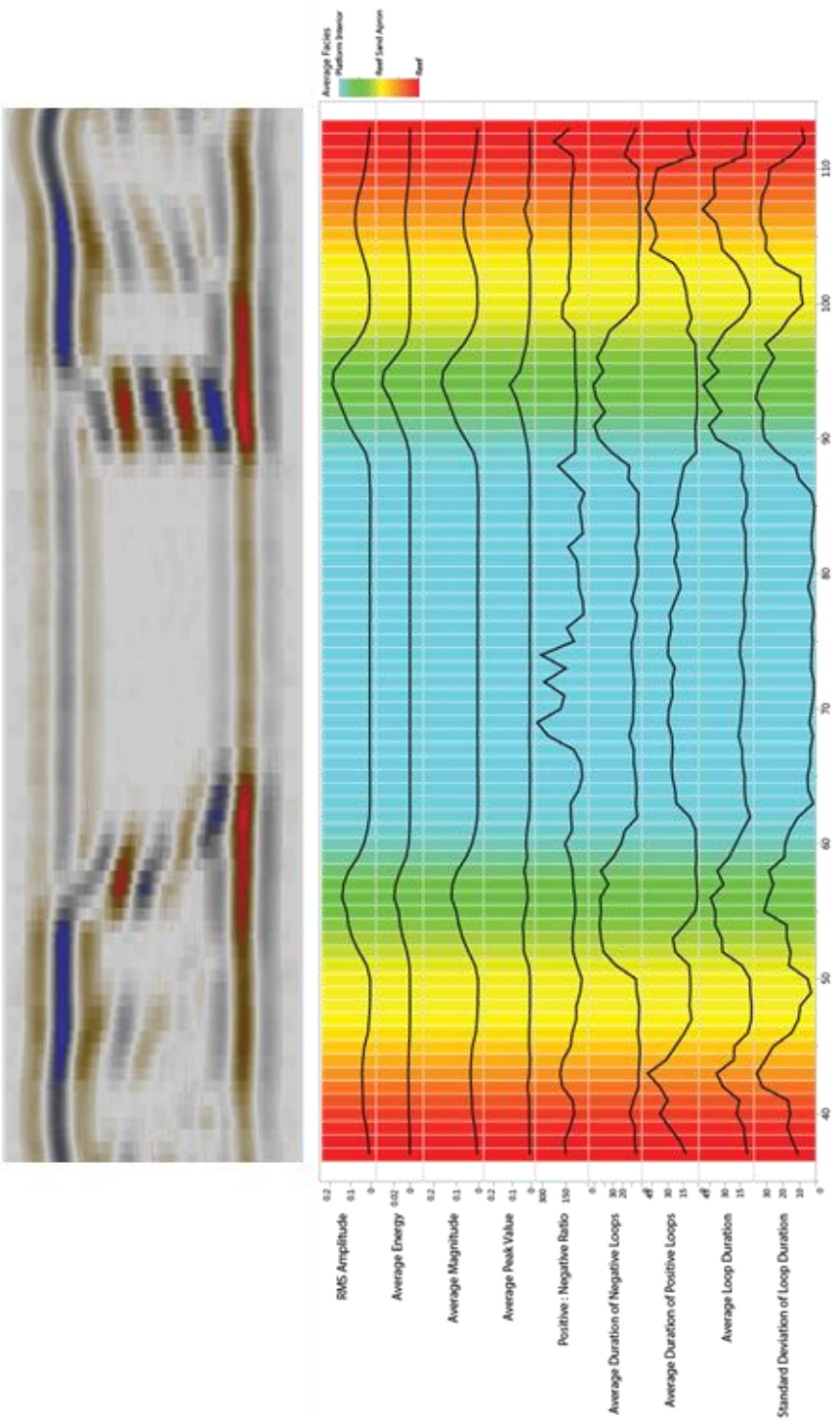

Figure A2-1: Base case scenario's nine attributes calculated at each trace. Color of plot background is the average facies at each trace. Red = reef, yellow = reef sand apron, and blue = platform interior. Transitional colors orange and green represent facies transitions between reef and reef sand apron and reef sand apron and platform interior, respectively.

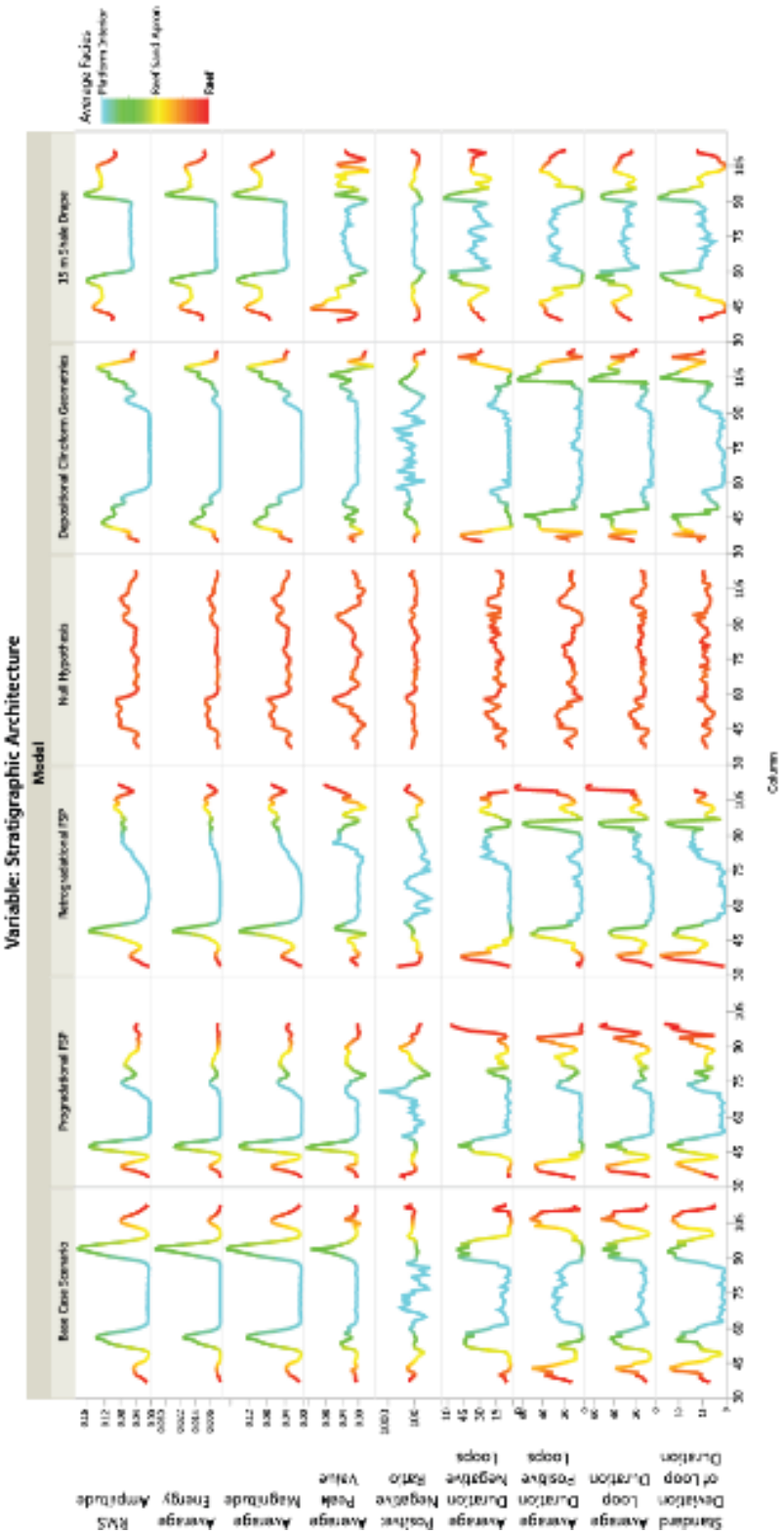

Figure A2-2: Comparison of attributes from the scenarios that varied stratigraphic architecture.

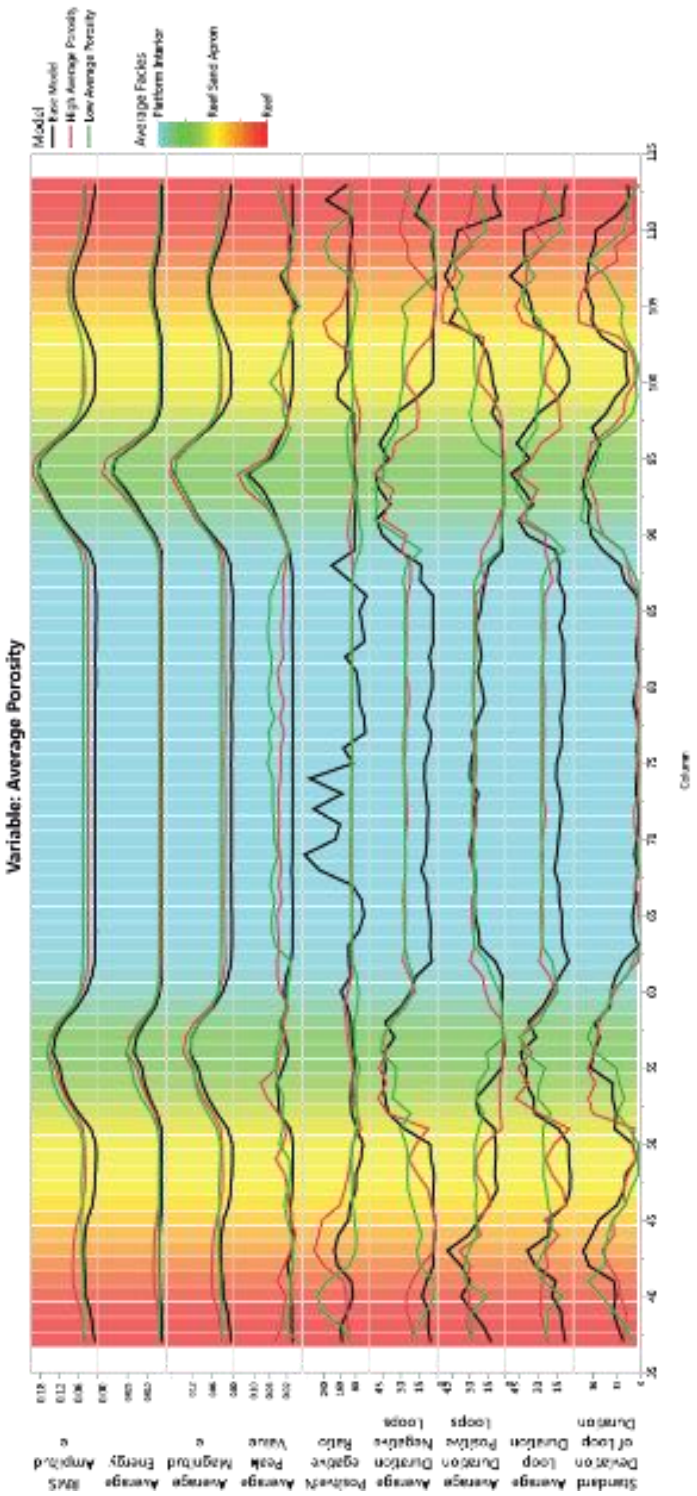

Figure A2-3: Comparison of attributes from the scenarios that varied average porosity. Color of plot background is the average facies at each trace. Red = reef, yellow = reef sand apron, and blue = platform interior. Transitional colors orange and green represent facies transitions between reef and reef sand apron and reef sand apron and platform interior, respectively.

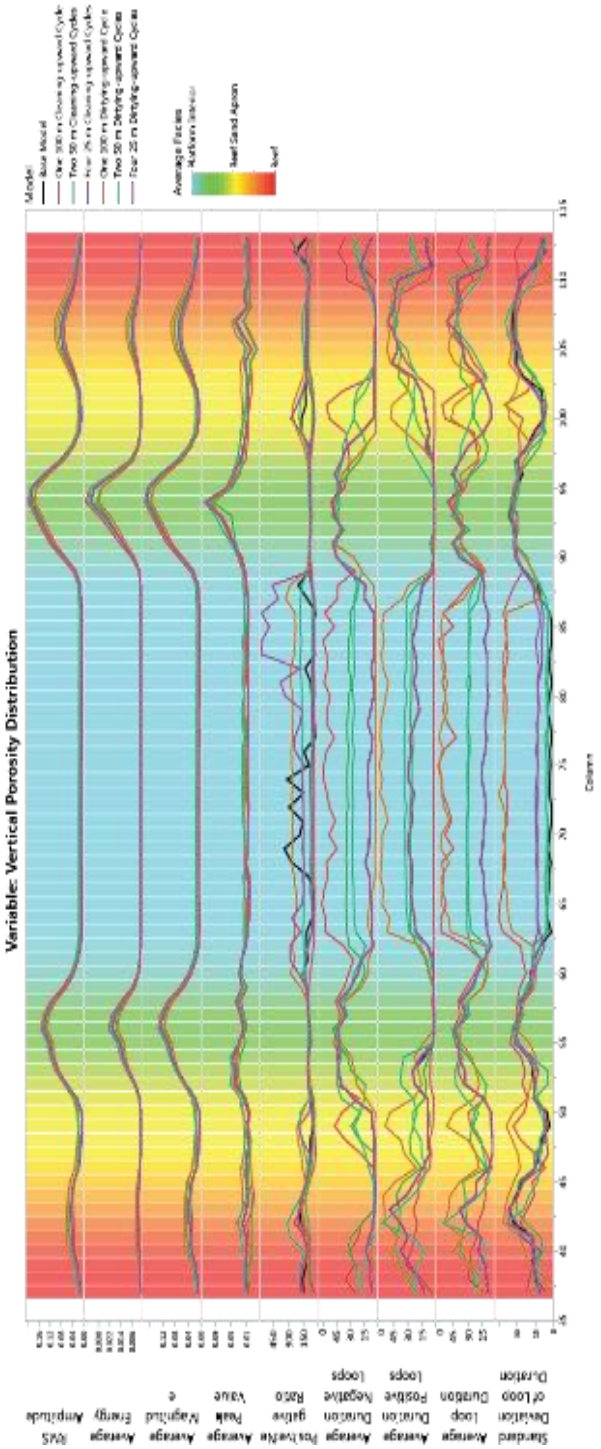

Figure A2-4: Comparison of attributes from the scenarios that modeled stratigraphic trends in porosity. Color of plot background is the average facies at each trace. Red = reef, yellow = reef sand apron, and blue = platform interior. Transitional colors orange and green represent facies transitions between reef and reef sand apron and reef sand apron and platform interior, respectively.

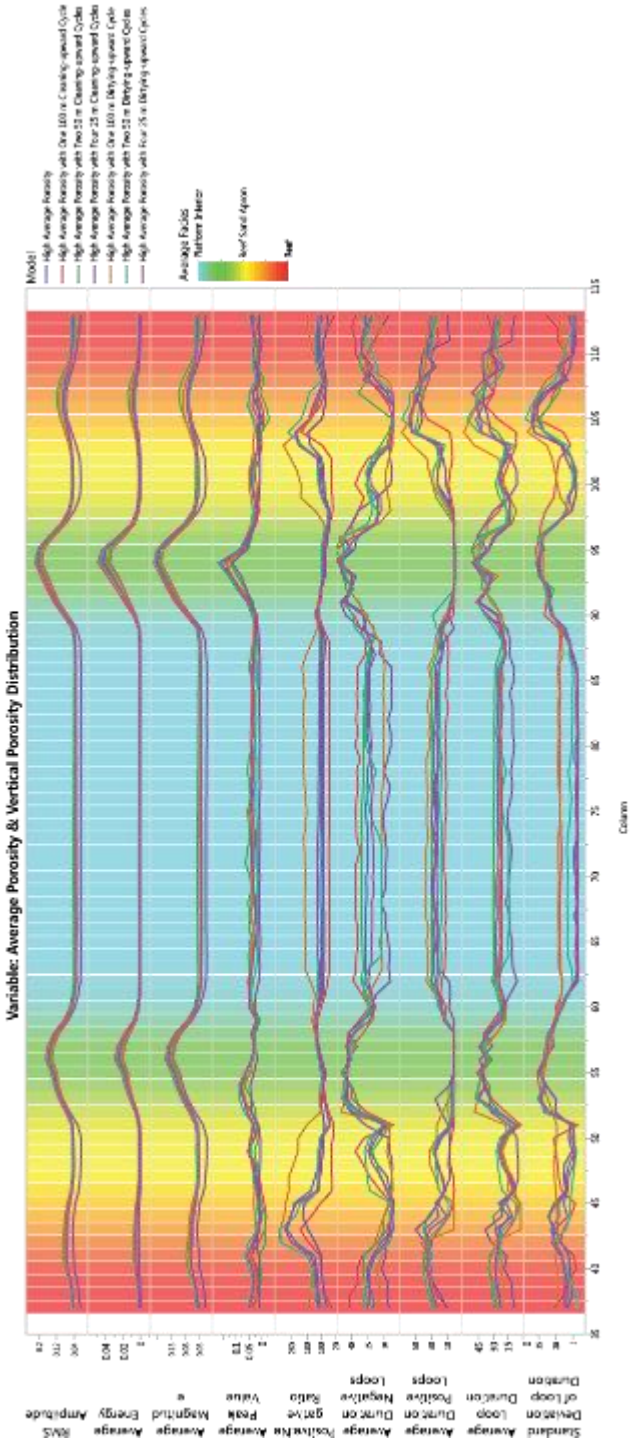

Figure A2-5: Comparison of attributes from scenarios that modeled stratigraphic trends in porosity at elevated mean porosity. Color of plot background is the average facies at each trace. Red = reef, yellow = reef sand apron, and blue = platform interior. Transitional colors orange and green represent facies transitions between reef and reef sand apron and reef sand apron and platform interior, respectively.

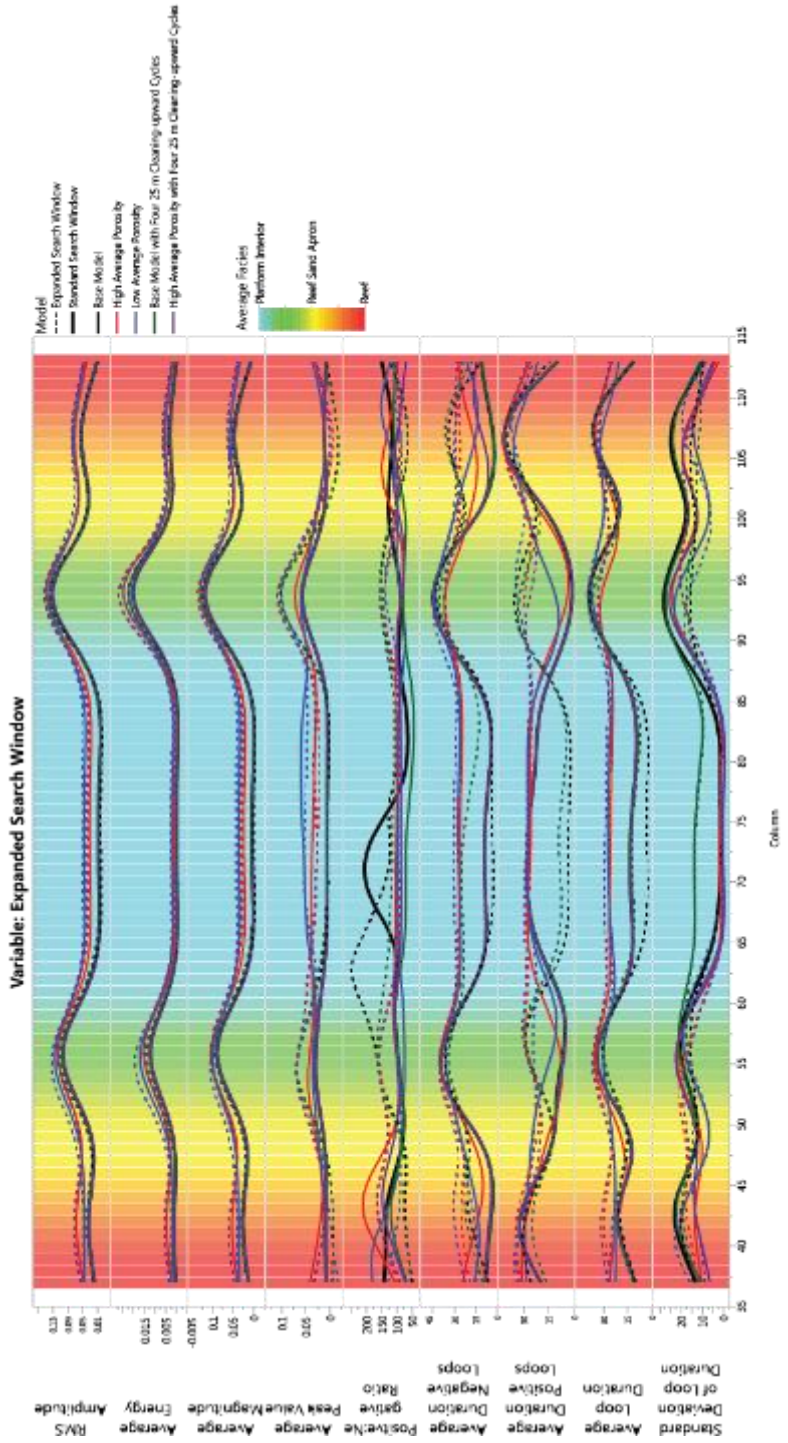

Figure A2-6: Comparison of attributes from scenarios that varied average porosity, calculated with an expanded search window. Color of plot background is the average facies at each trace. Red = reef, yellow = reef sand apron, and blue = platform interior. Transitional colors orange and green represent facies transitions between reef and reef sand apron and reef sand apron and platform interior, respectively.

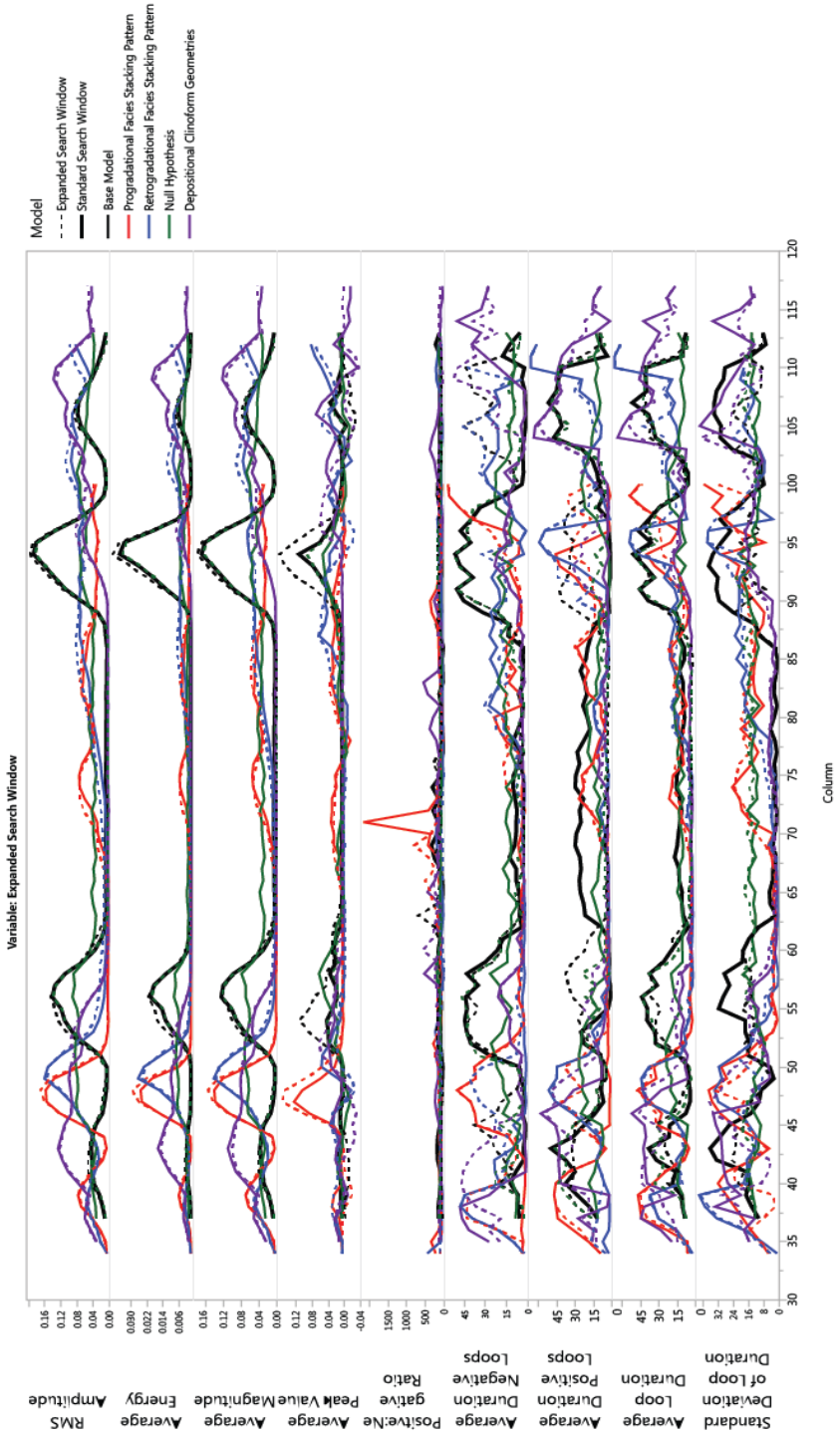

Figure A2-7: Comparison of attributes from scenarios that varied stratigraphic architecture, calculated with an expanded search window.

APPENDIX 3. PREDICTION OF ROCK PROPERTIES FROM SEISMIC DATA

To rank the relative importance of type of attribute for predictability of rock properties, each regression was queried for the most significant predictor (attribute) to the least significant. The nine attributes can be organized into three distinct groups (attribute families) amplitude, shape, and standard statistics. The result of this query is shown in pie chart form that illustrates each scenario group and the ranked attribute families (9 is most significant, 1 is least significant) (Figure A3-1). Stratigraphic architecture group (consists of six scenarios including the base case scenario) has a single attribute family that has the highest mean significance, amplitude. Average porosity group (consists of three scenarios including the base case scenario) has two attribute families that have almost equal mean significance for predicting average porosity, shape and amplitude. Stratigraphic trends in porosity group (consisting of seven scenarios including the base case scenario) doesn't have an attribute family that is the best predictor, rather all three families have similar mean significant values. While each scenario group is different, the scenarios within each group also differ for best attribute family predictors (Figure A3-2-4).

Eight scenarios (representing each scenario group) attempted to predict average porosity and net pore volume with each separate attribute family (Figure A3-5 and 6). The correlation coefficients for average porosity reflects the order of significance of attribute families (e.g., base case scenario), whereas others do not (e.g., four 25 m upward decrease in porosity).

Predicting with Limited Data

Three scenarios tested the robustness of the attributes to predict porosity with a limited dataset (e.g., few well logs and trying to predict rock properties). Scenarios for this exersice included the high impedance cap (highest correlation coefficient), base case scenario (intermediate

correlation coefficient), and the null model (lowest correlation coefficient). Two percent of the total number of traces were randomly selected and used their attributes as regression inputs to predict porosity, and ultimately apply the equation to the entire volume.

The null model and the scenario with a high impedance cap had p-values less than 0.05 and the aggradational facies stacking pattern did not, and therefore was not statistically significant. The null model's regression is statistically significant but the correlation coefficient was 0.0009. Alternatively, the high impedance cap had a regression that resulted statistically significant and the correlation coefficient of 0.88, which is close in value to the correlation coefficient when all traces were used (Figure A3-7). Interestingly, the residual porosity (actual – predicted porosity) for the high impedance cap is very similar, and therefore the trends of over- or under-predicting porosity remains consistent regardless of the number of traces. This suggests that the presence of the shale cap is enough impedance contrast to accurately predict porosity from attributes when all traces are used as well as when limited traces are used.

Frequency of Wavelet

Nine scenarios generated synthetic volumes that used a wavelet with a central frequency of 40 Hz (about three loops per 100 m). These synthetic volumes were more interpretable and highlighted the internal range of impedance contrasts that are not resolvable at lower frequencies.

Accuracy of porosity predictions did not always improve with the increased frequency. For example, although the average porosity correlation coefficient (R^2) increased from 0.28 to 0.58 for the base case scenario, the null model's correlation coefficient decreased 0.15 to 0.06 (Figure A3-8).

Expanded Search Window

All models used stratigraphic surfaces as interval constraints for calculating the attributes for the middle zone of interest. With the low frequency wavelet being almost one seismic loop for 100 m the stratigraphic surfaces did not allow the entire wave to measure the zone boundary. Therefore, a subset of scenarios (nine) had an expanded search window for calculating and extracting attributes. These scenarios extend the search interval by 20 ms above and below interval range to allow the entire wavelet (that represents the interface) to be measured. The extracted attributes were then used as model effects to predict average porosity and compared to the results from the normal search window (Figure A3-9). Majority of the scenarios saw increased correlation between average porosity and attributes, but the largest improvement was the aggradational facies stacking pattern at 6%. The scenarios that saw a decrease in correlation all had different isolated variables. The greatest decline was the scenario with four cleaning-upward cycles at -14%.

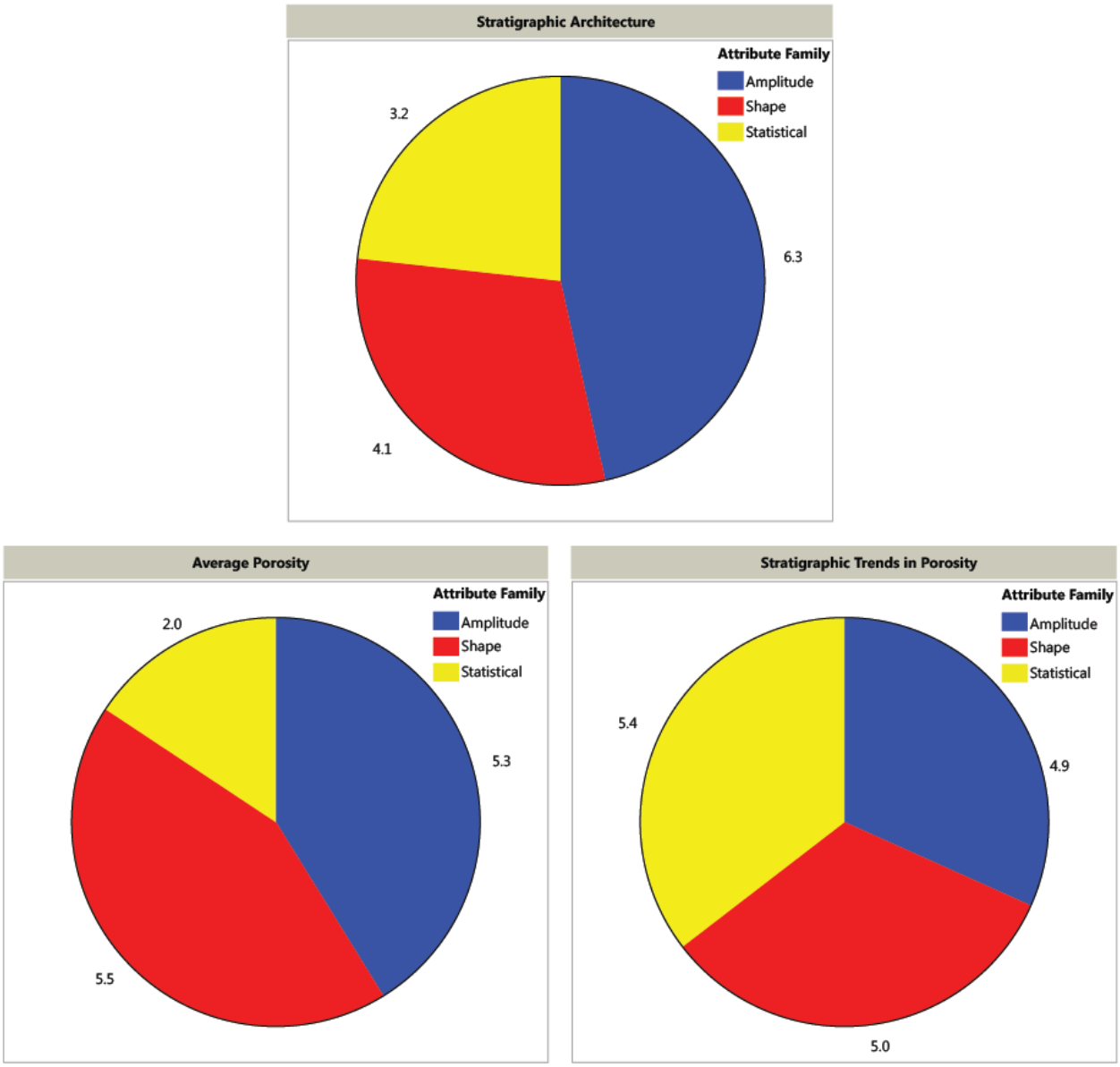

Figure A3-1: Comparison of each scenario groups' mean significance per attribute family. The value 9 is the most significant predictor and 1 being the least significant predictor for average porosity. Notice one attribute is markedly higher family for the stratigraphic architecture group, compared to two attributes that have almost equal significance for average porosity group, and the lack of a single most significant attribute family for the stratigraphic trends in porosity.

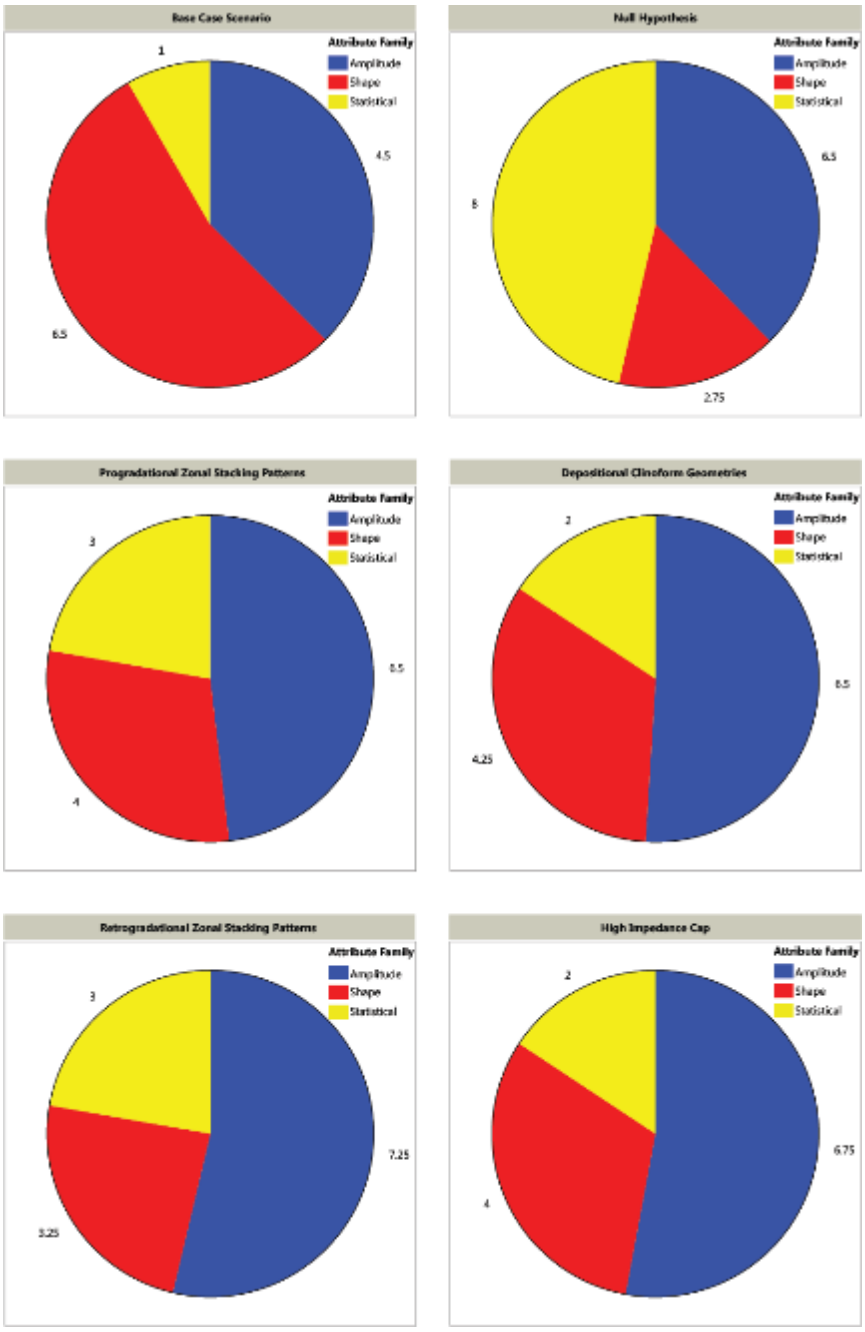

Figure A3-2: Comparison of significance attribute families within the stratigraphic architecture group. The value 9 is the most significant predictor and 1 being the least significant predictor for average porosity.

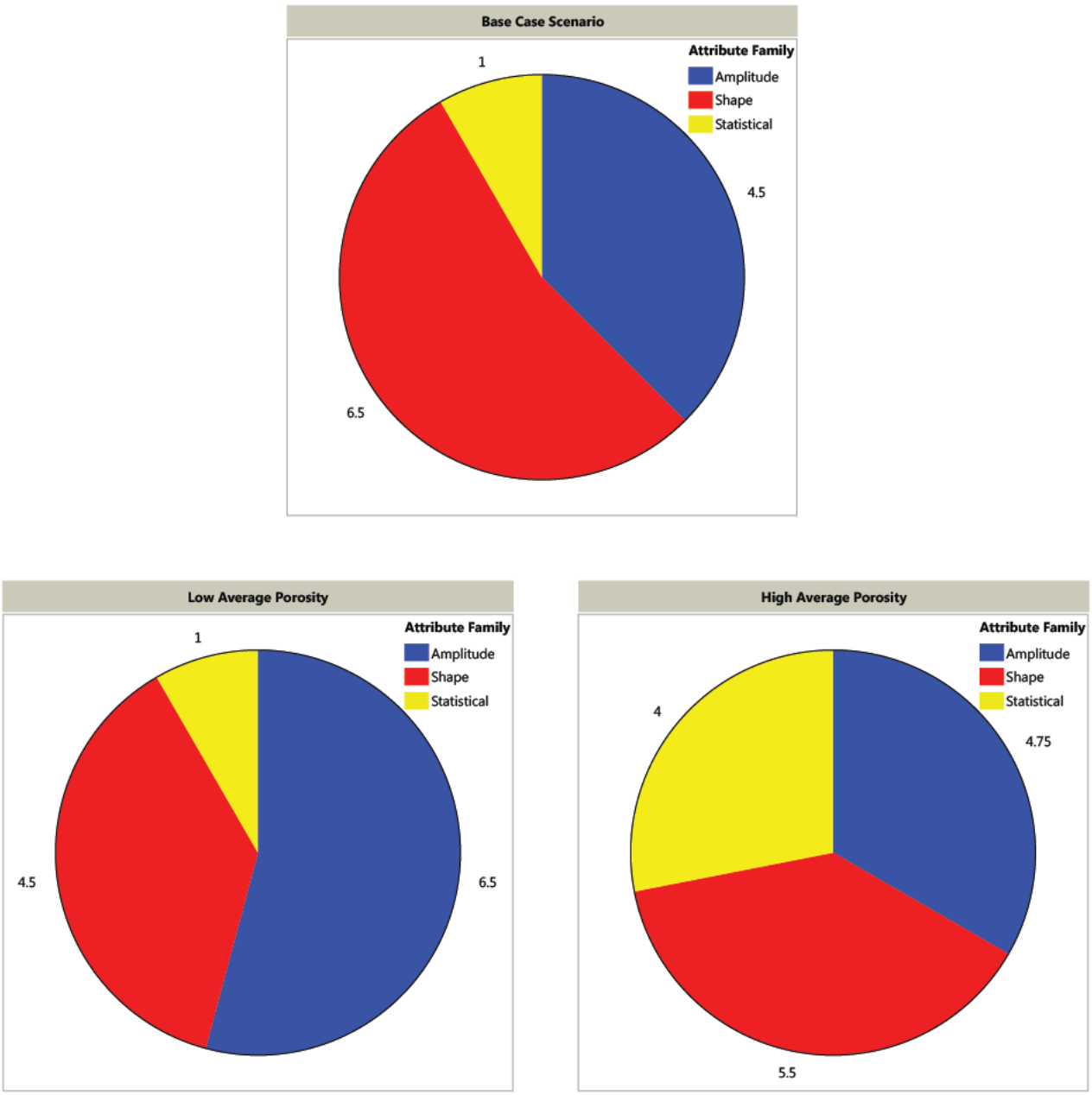

Figure A3-3: Comparison of significance attribute families within the average porosity group. The value 9 is the most significant predictor and 1 being the least significant predictor for average porosity.

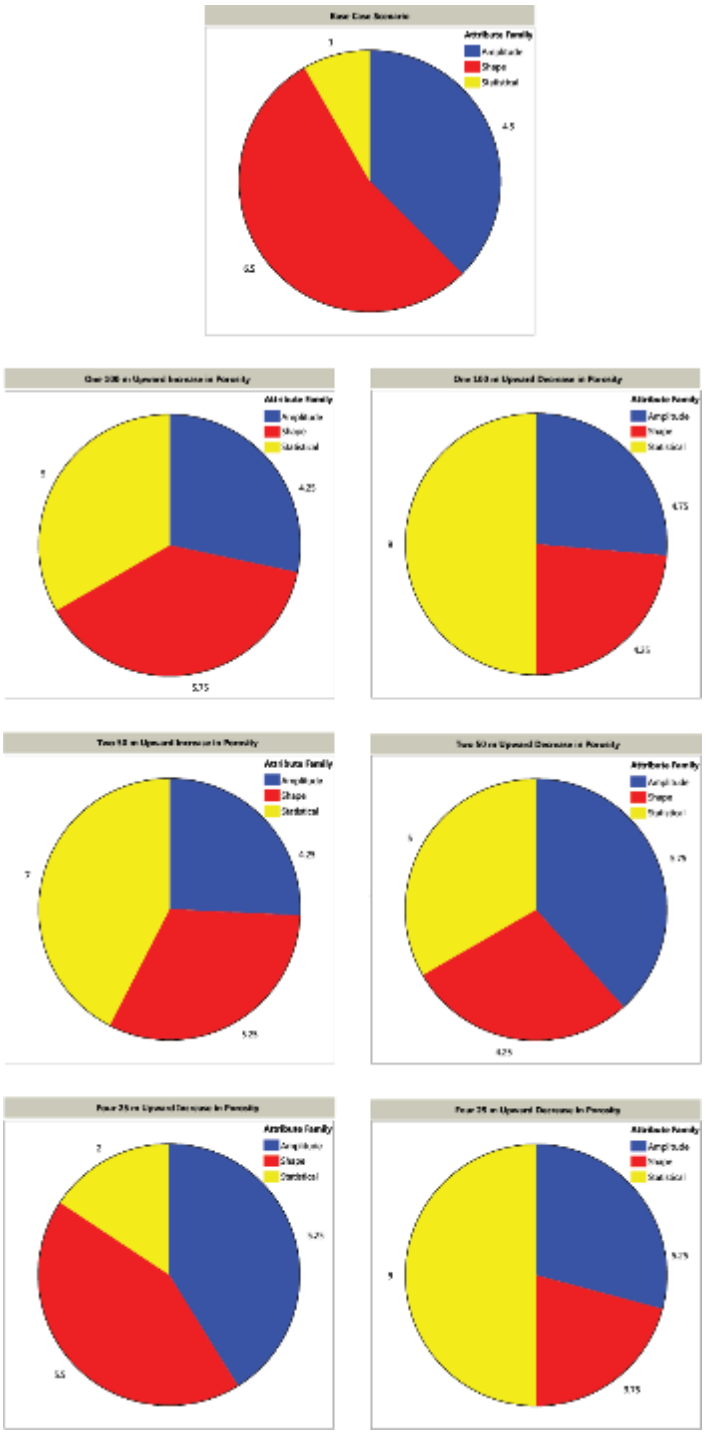

Figure A3-4: Comparison of significance attribute families within the stratigraphic trends in porosity. The value 9 is the most significant predictor and 1 being the least significant predictor for average porosity.

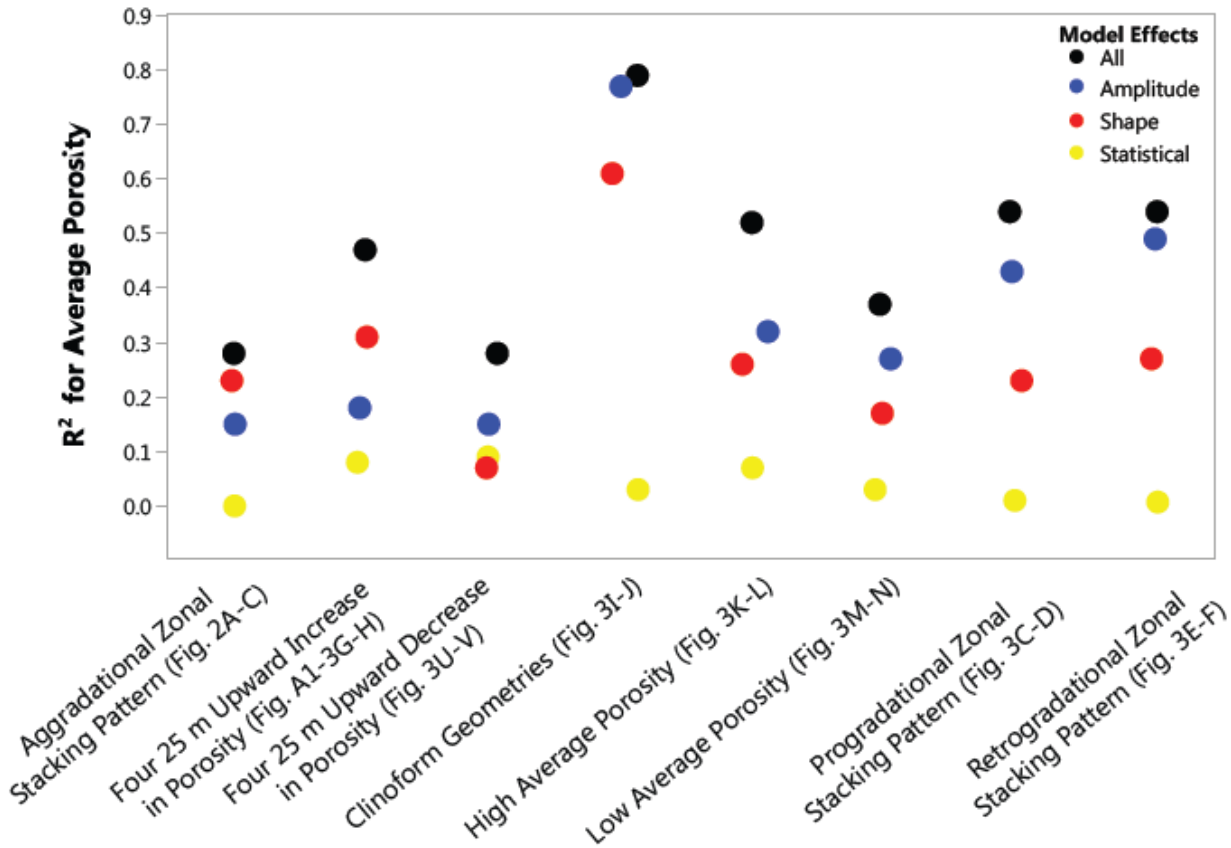

Figure A3-5: Comparison of correlation coefficients from predicting average porosity calculated using individual attribute families as predictors rather than all nine attributes.

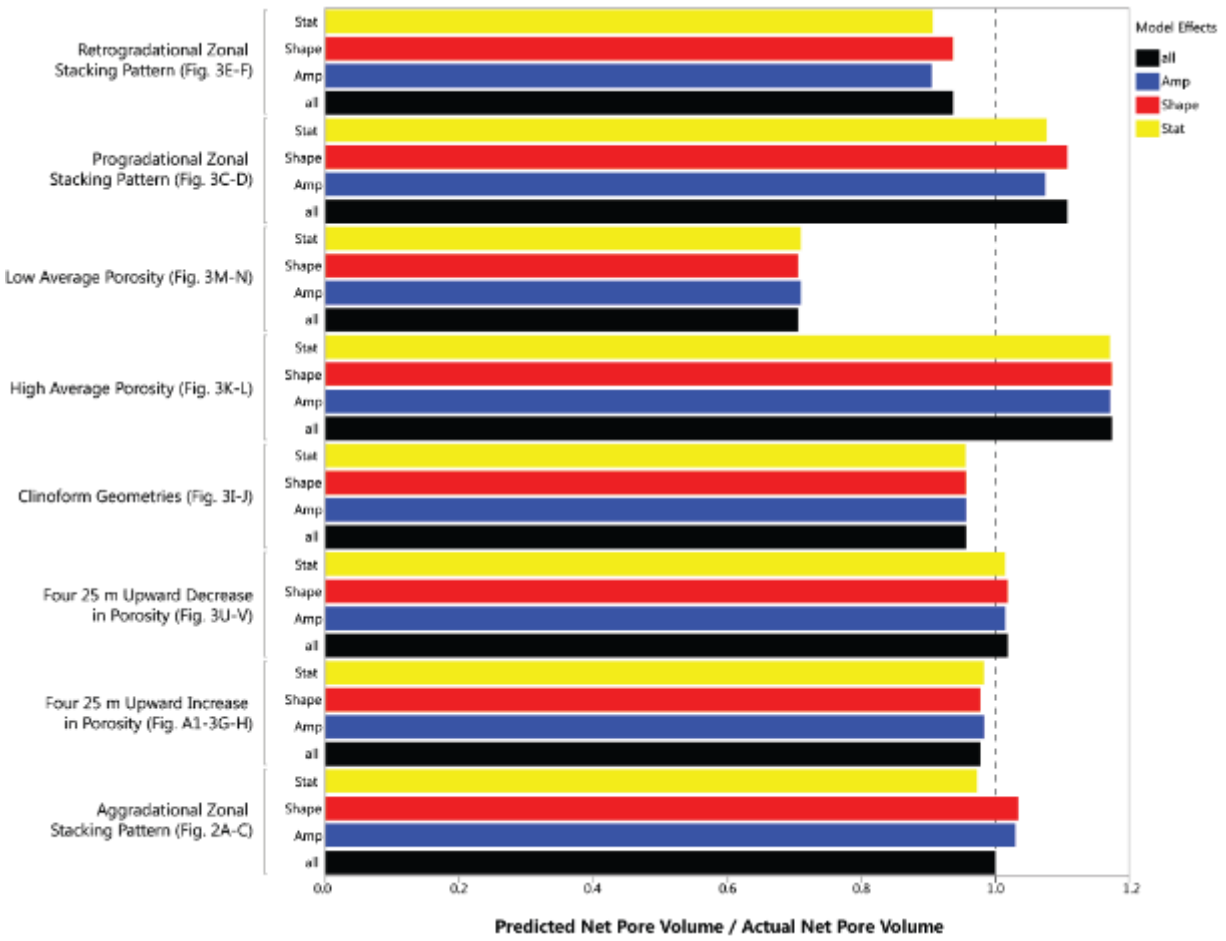

Appendix 3, Figure A3-6: Comparison of correlation coefficients from predicting net pore volume calculated using individual attribute families as predictors rather than all nine attributes.

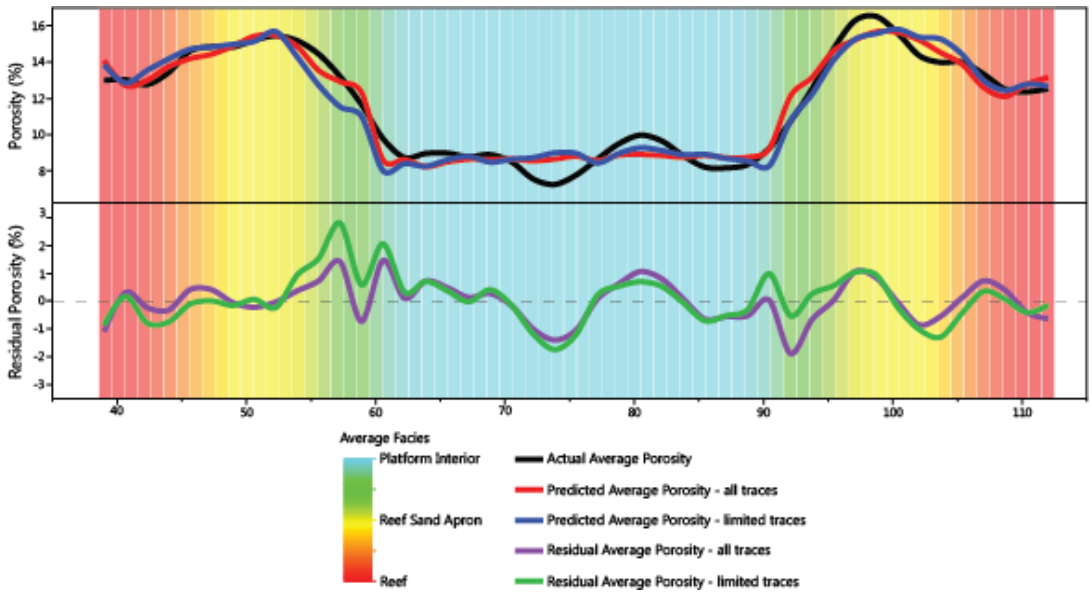

Figure A3-7: Comparison of the use of limited traces vs. all traces for predicted and residual porosity. The correlation value calculated when all traces were used = 0.91. The correlation value calculated when limited traces were used = 0.88. Residual porosity = actual porosity – predicted porosity. Positive values indicates under-estimation and negative values indicates over-estimation. The background is colored by average facies calculated at each trace.

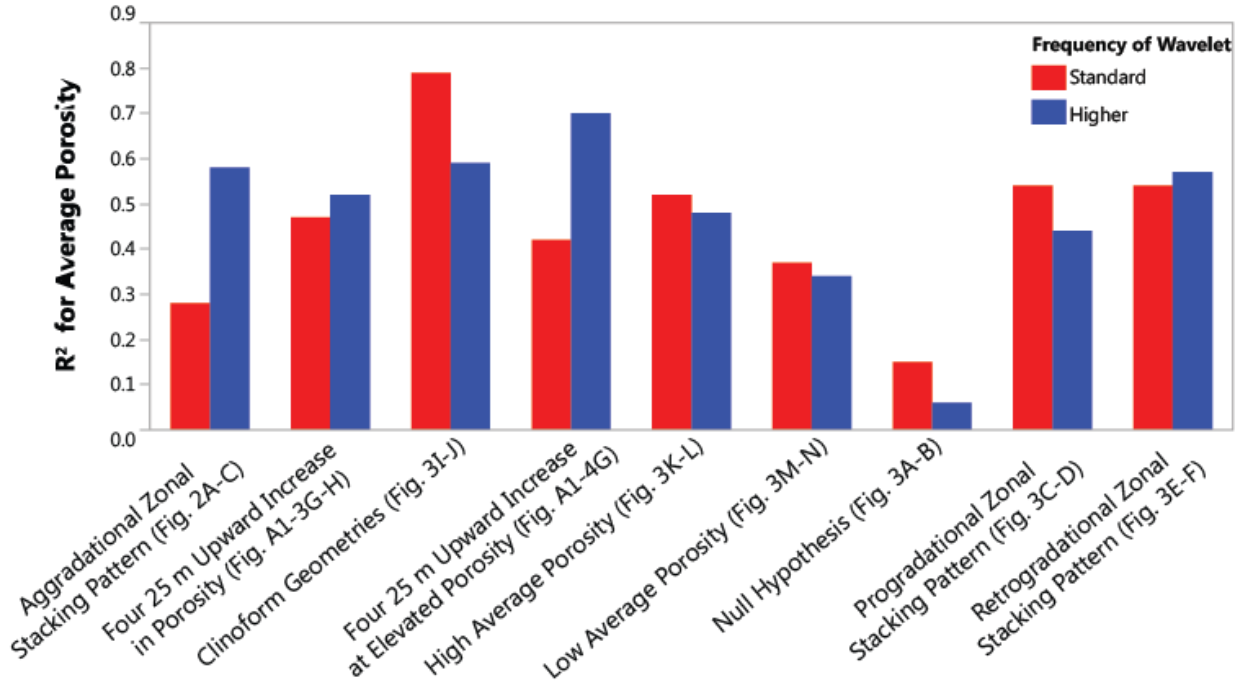

Figure A3-8: Comparison of varying wavelet frequencies and their effects on the correlation coefficient.

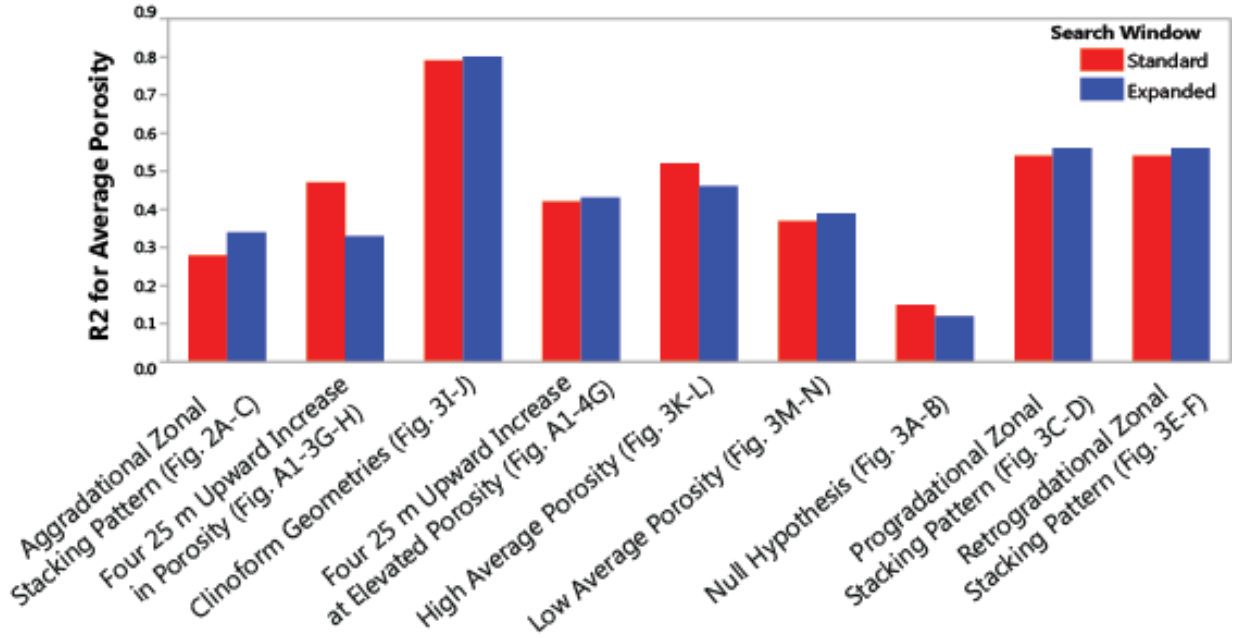

Figure A3-9: Comparison of expanded search window to standard search window correlation of average porosity to seismic attributes.

APPENDIX 4. TABLES

Petrophysical Property	Low Standard Deviation	High Standard Deviation
Porosity (%)	1.6	3.3
Velocity (m/s)	83.3	166.6
Impedance ($kg/m^3 * m/s$)	66.6	133.3

Appendix Table 1: Petrophysical properties and their standard deviation for cell population using Gaussian distribution.

APPENDIX 5. PLOTS OF MULTIVARIATE REGRESSIONS

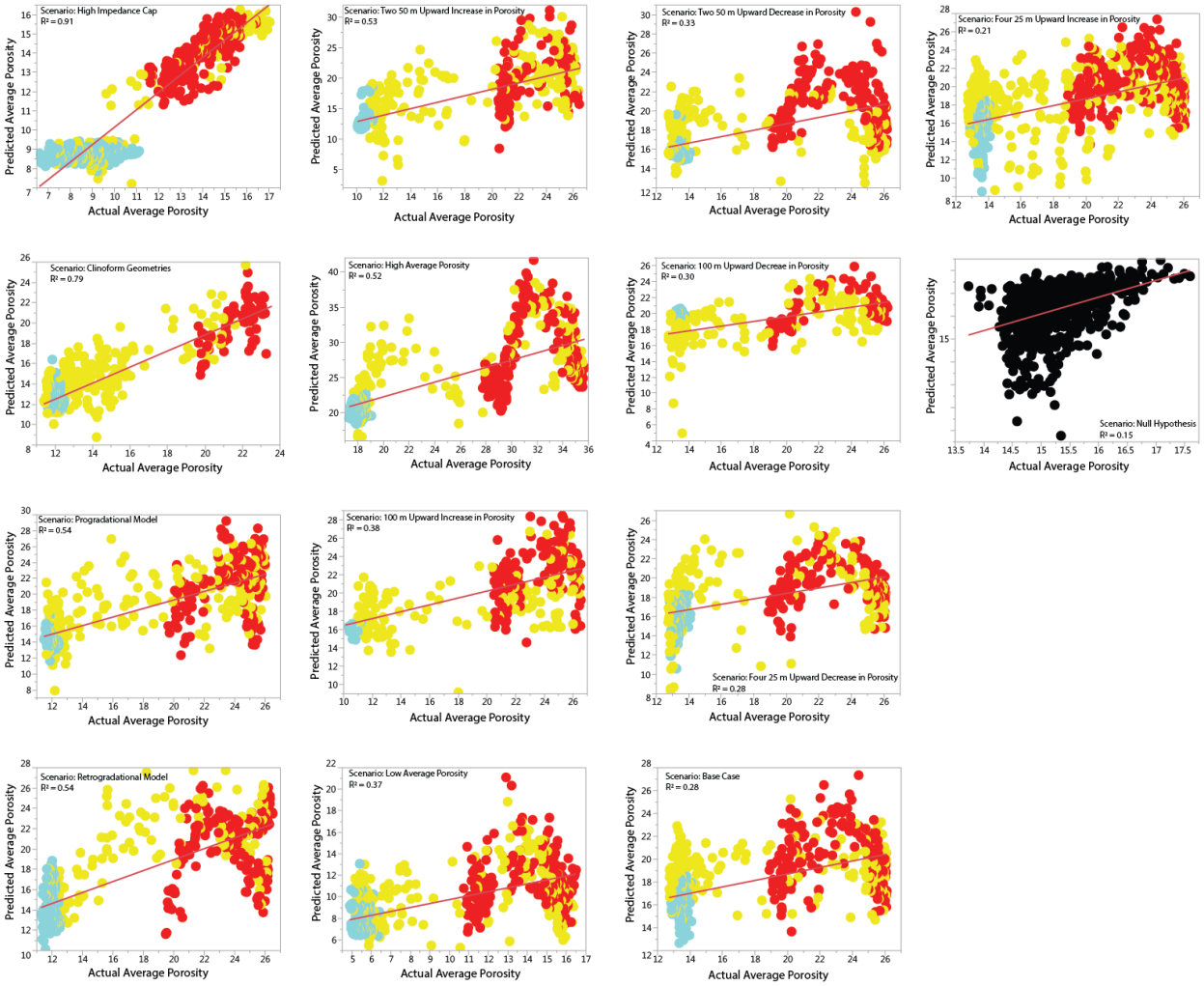

Figure A5-1: linear regression results for scenarios listed in Figures 5 and 6. Best fit line is illustrated for each, as is the R^2 for the best fit correlation between nine attributes and average porosity. Data points predicted and observed values at each trace, and are colored by most common facies, red = reef, yellow = reef sand apron, and blue = platform interior. Null hypothesis scenario (i.e., absence of stratigraphic organization; Figure 3A, B). As facies are randomly distributed, they are roughly equiprobable, so data are all the same color.

APPENDIX 6. PLOTS OF VARIABLE AMPLITUDE SEISMIC TRACES

Scenarios listed in Figure 5 and 6.

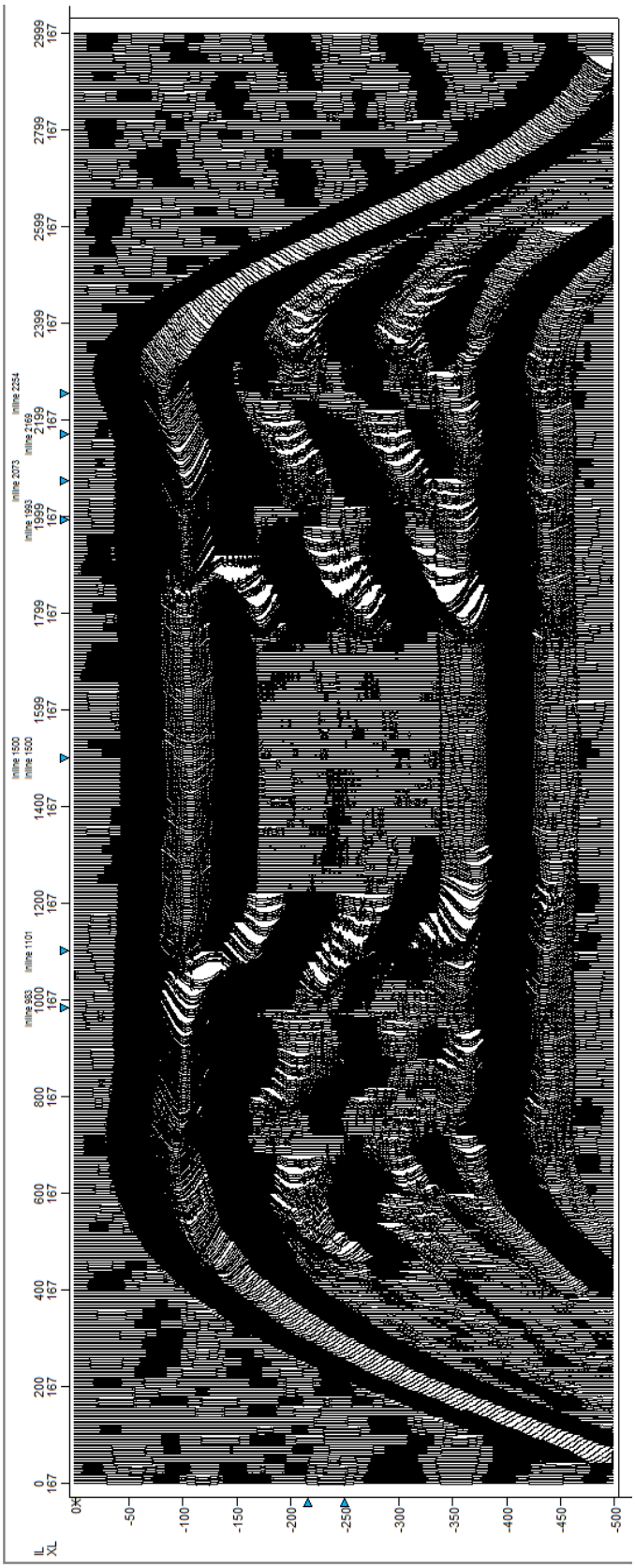

Aggradational Facies Stacking Pattern

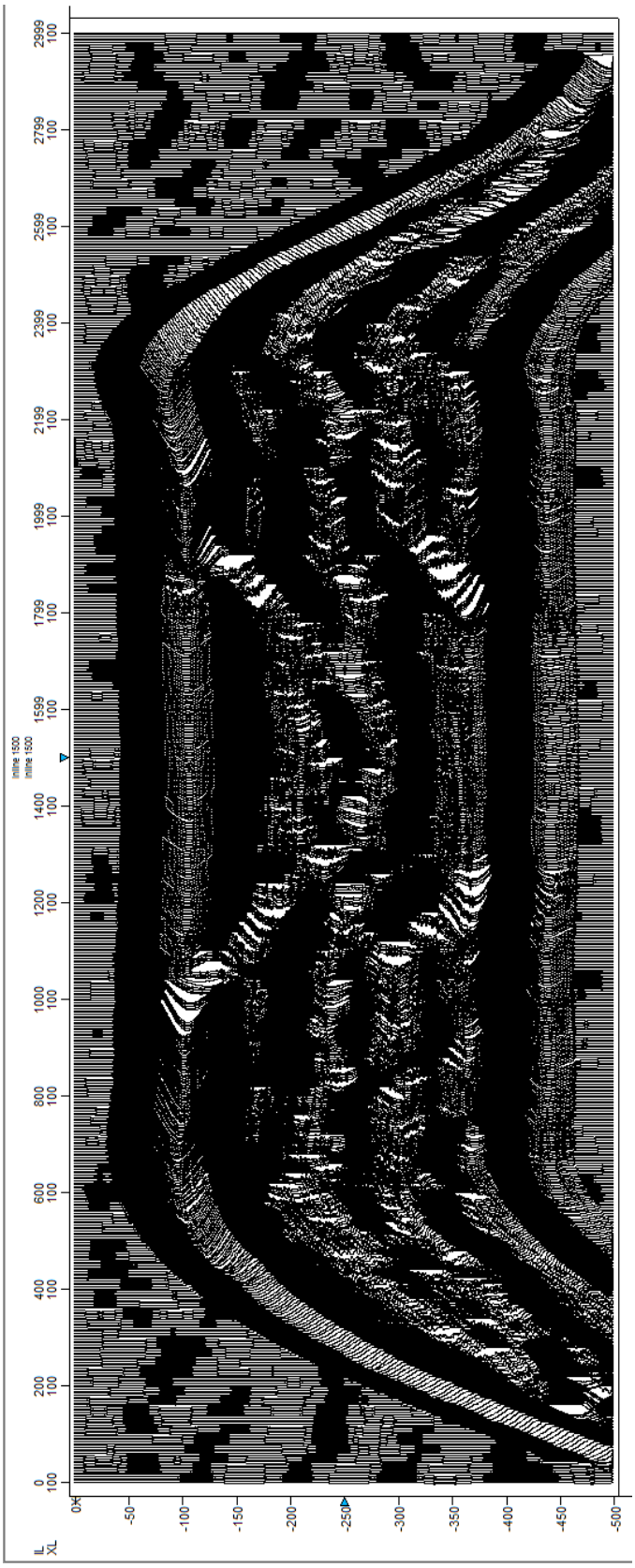

Null Hypothesis

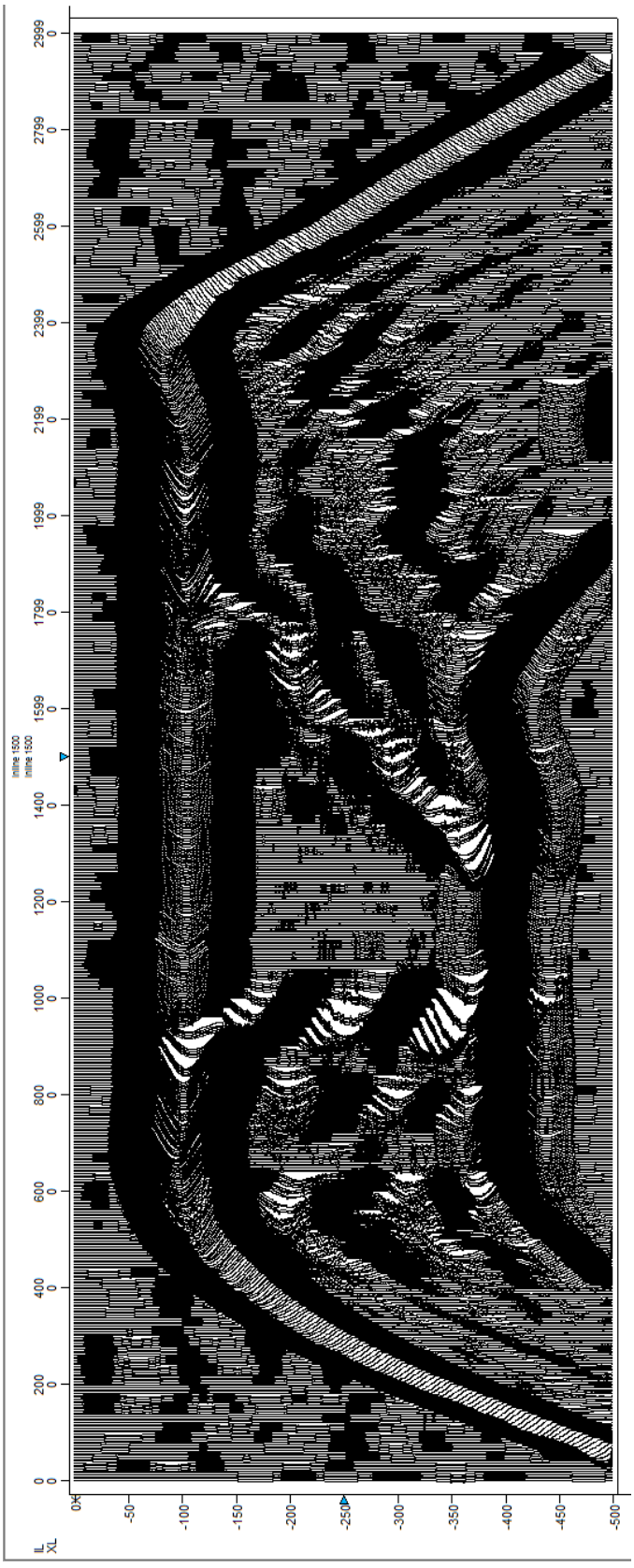

Progradational Zonal Stacking Pattern

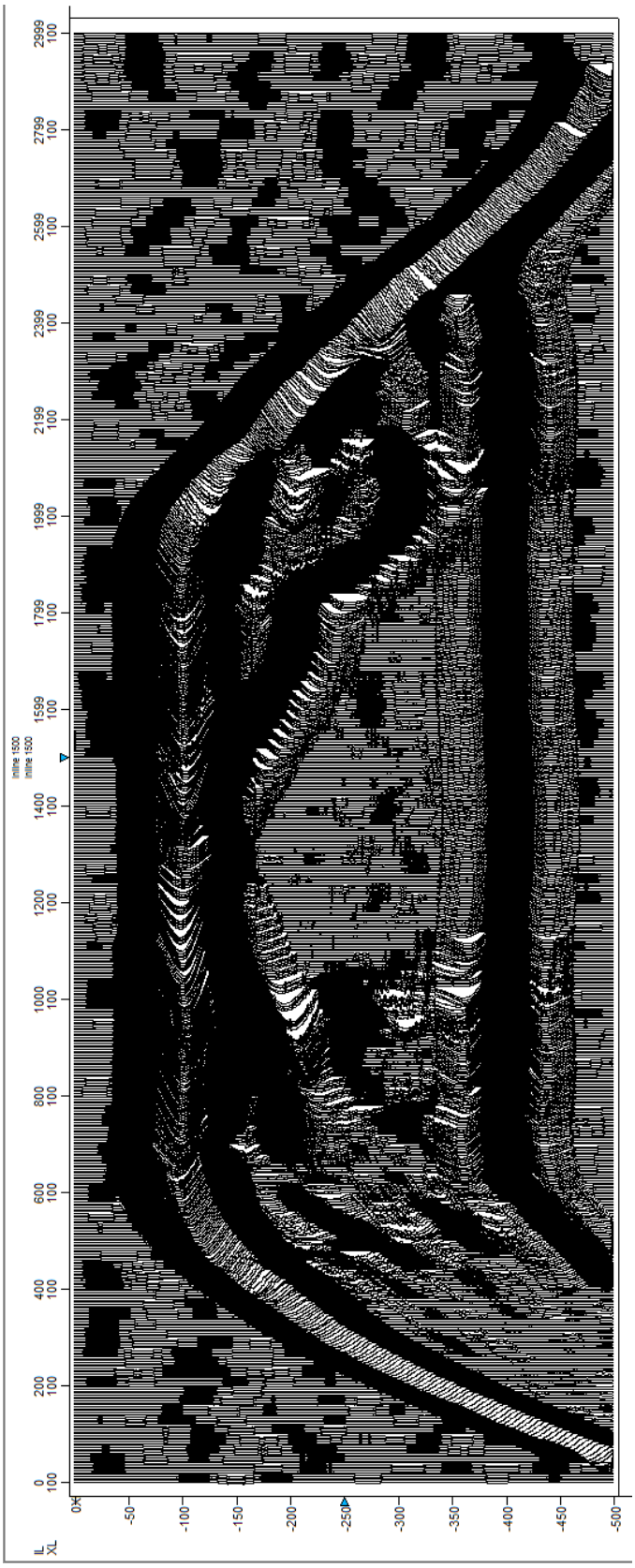

Retrogradational Zonal Stacking Pattern

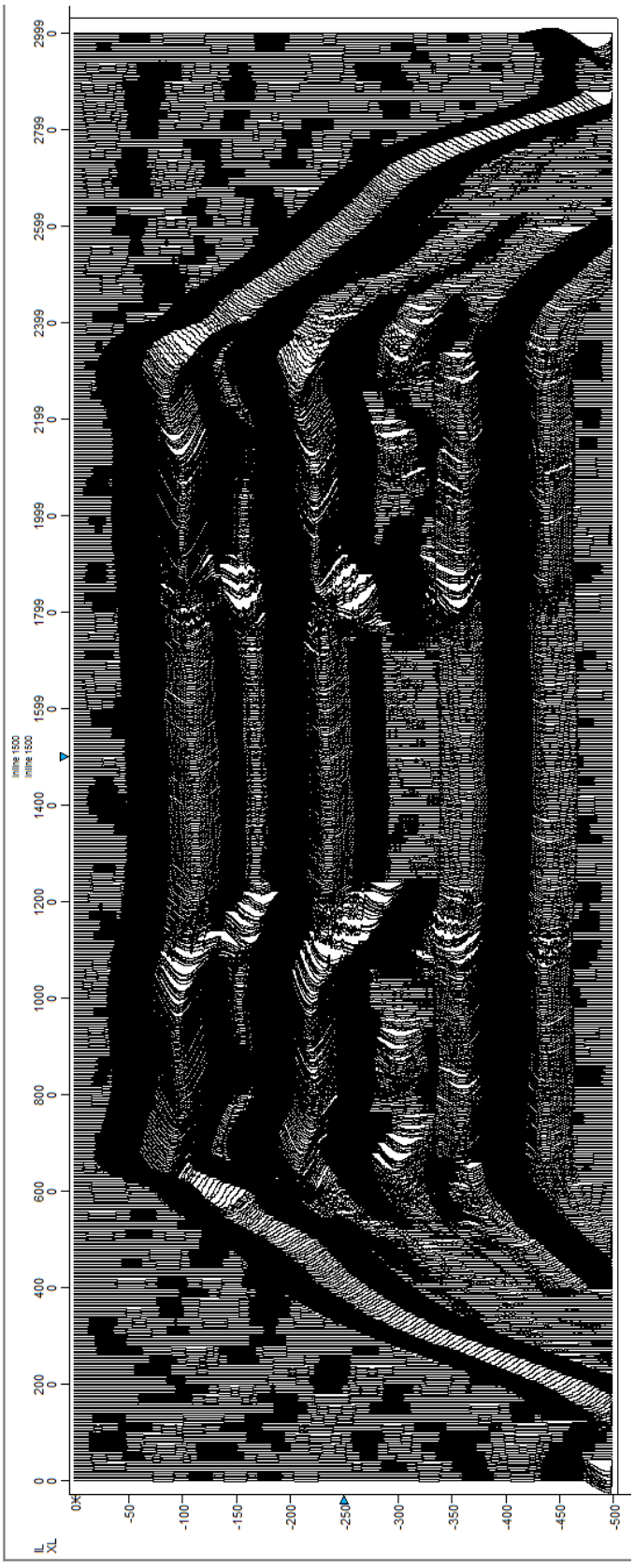

High Impedance Cap

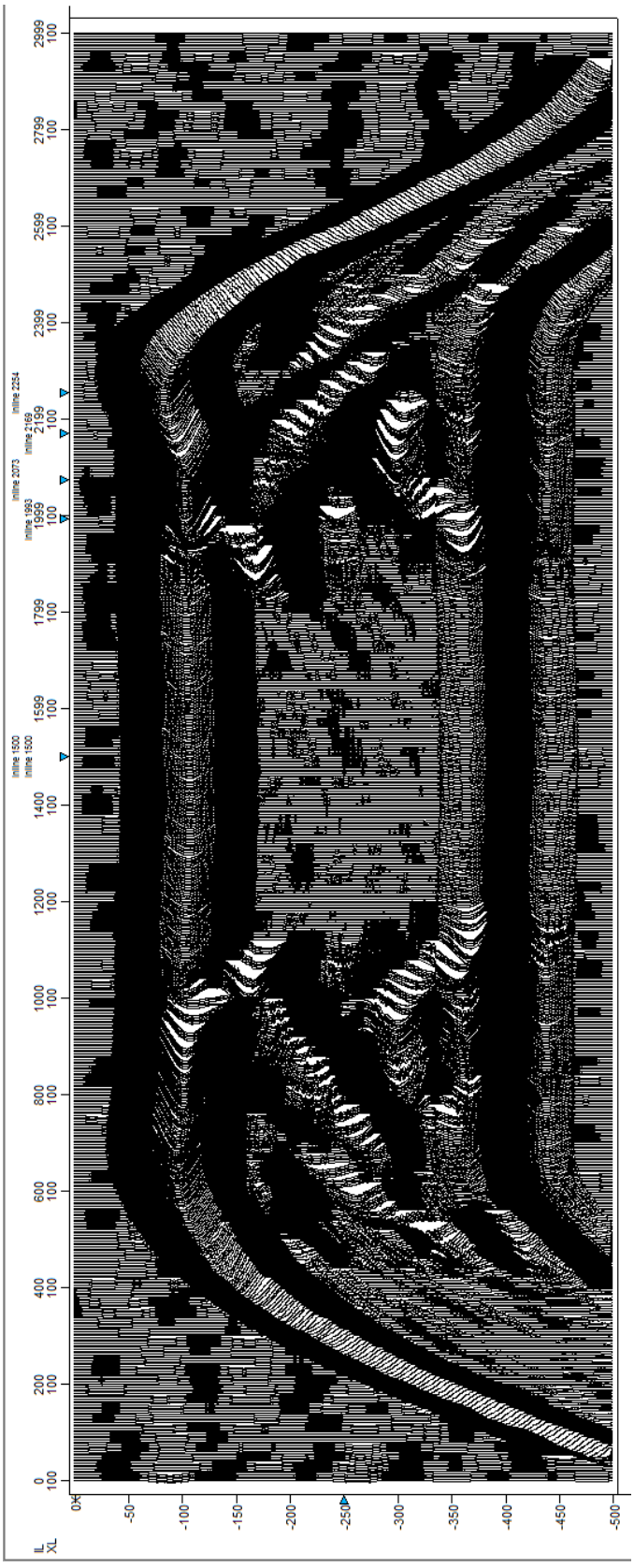

Clinoform Geometries

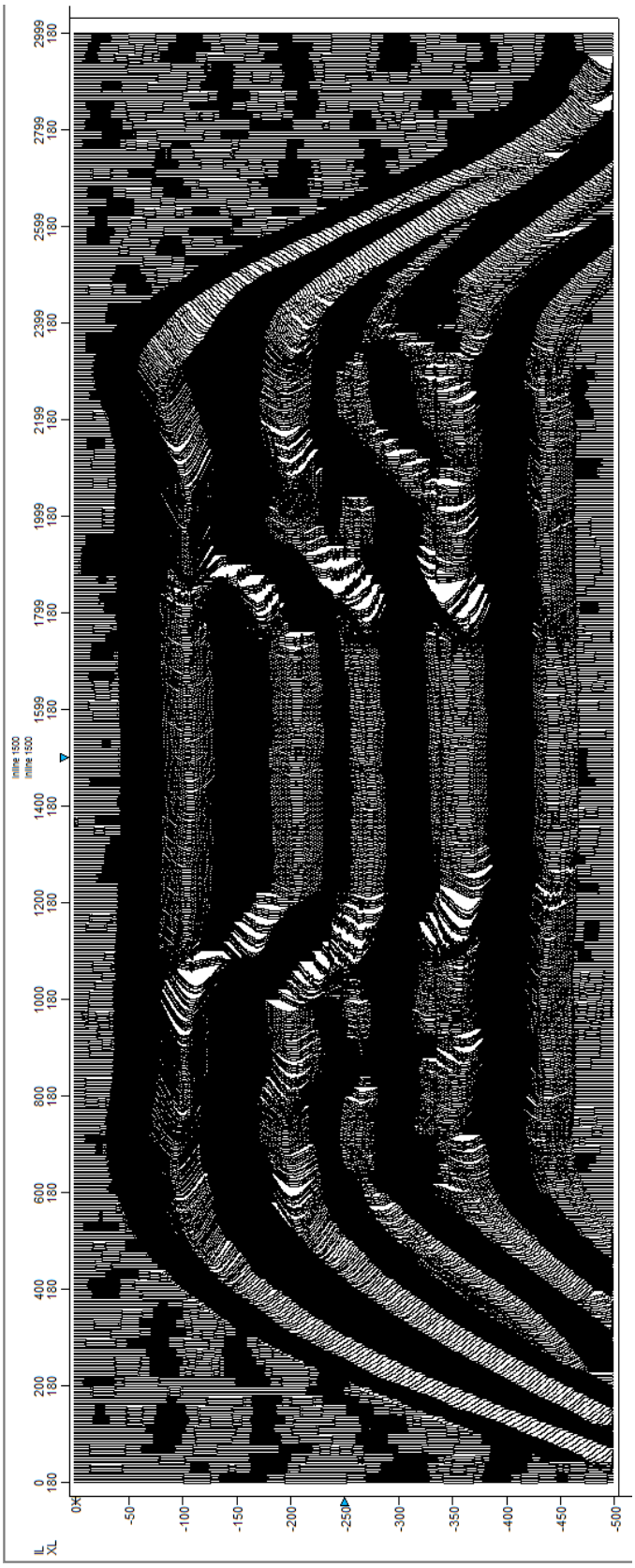

High Average Porosity

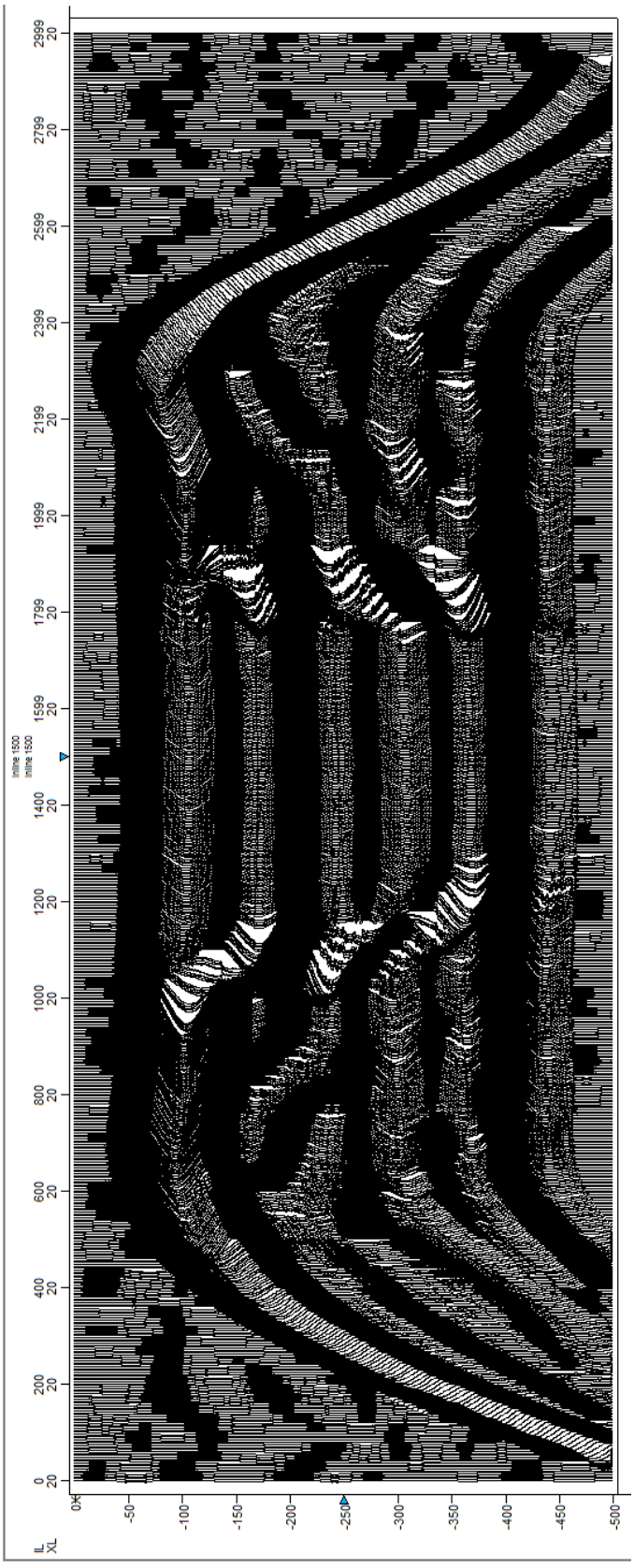

Low Average Porosity

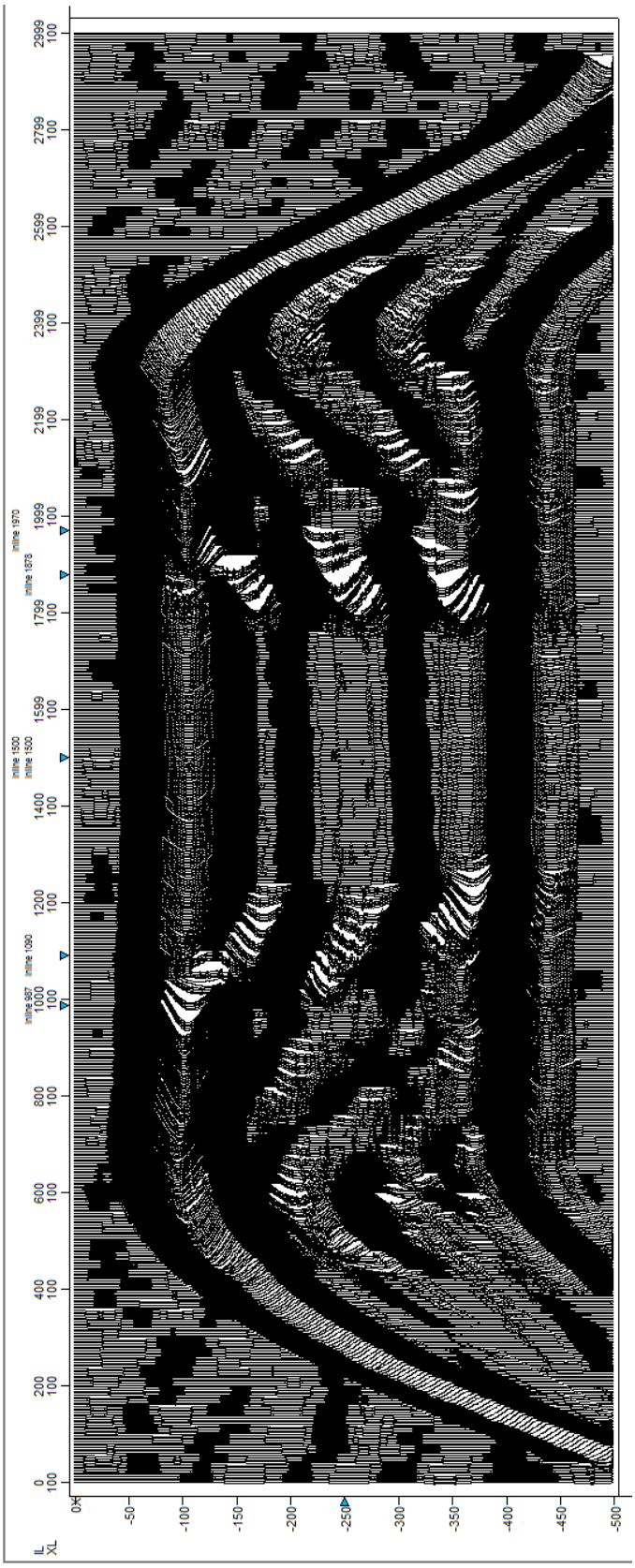

One Cleaning Upward Cycle of Porosity

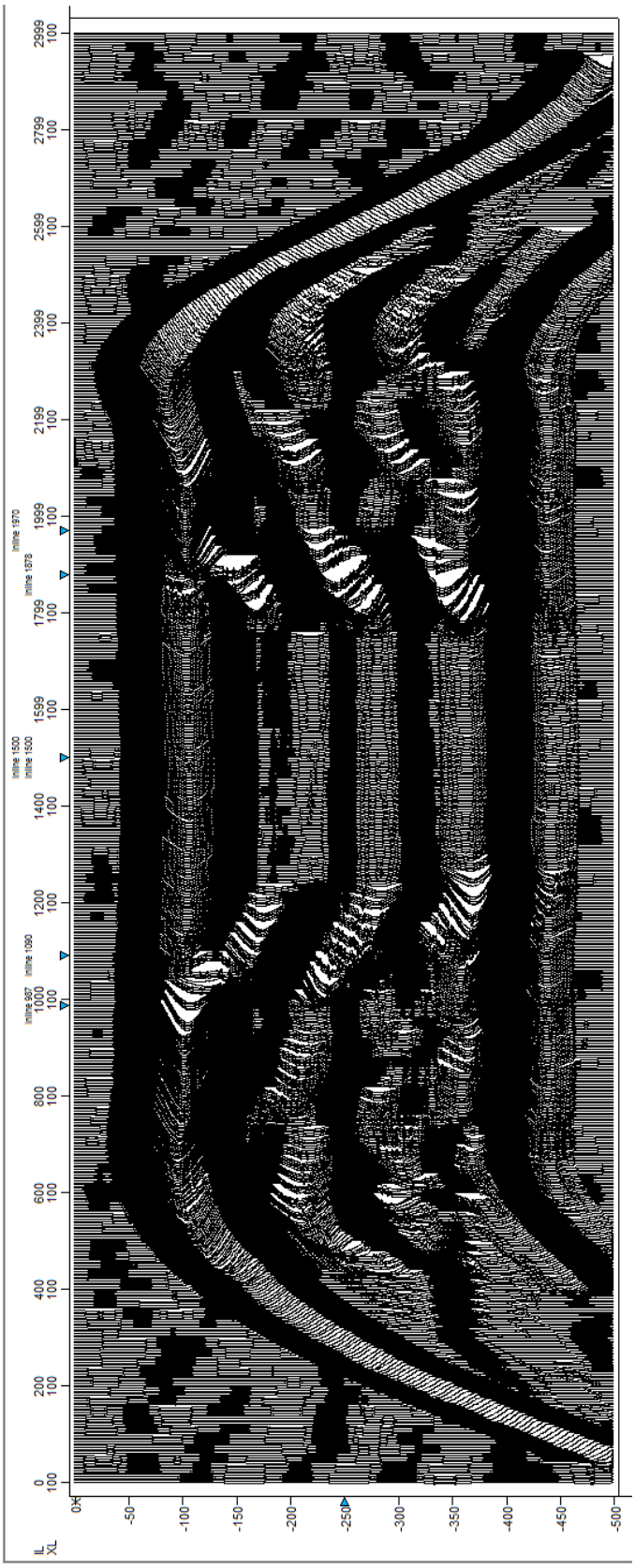

Two Cleaning Upward Cycles of Porosity

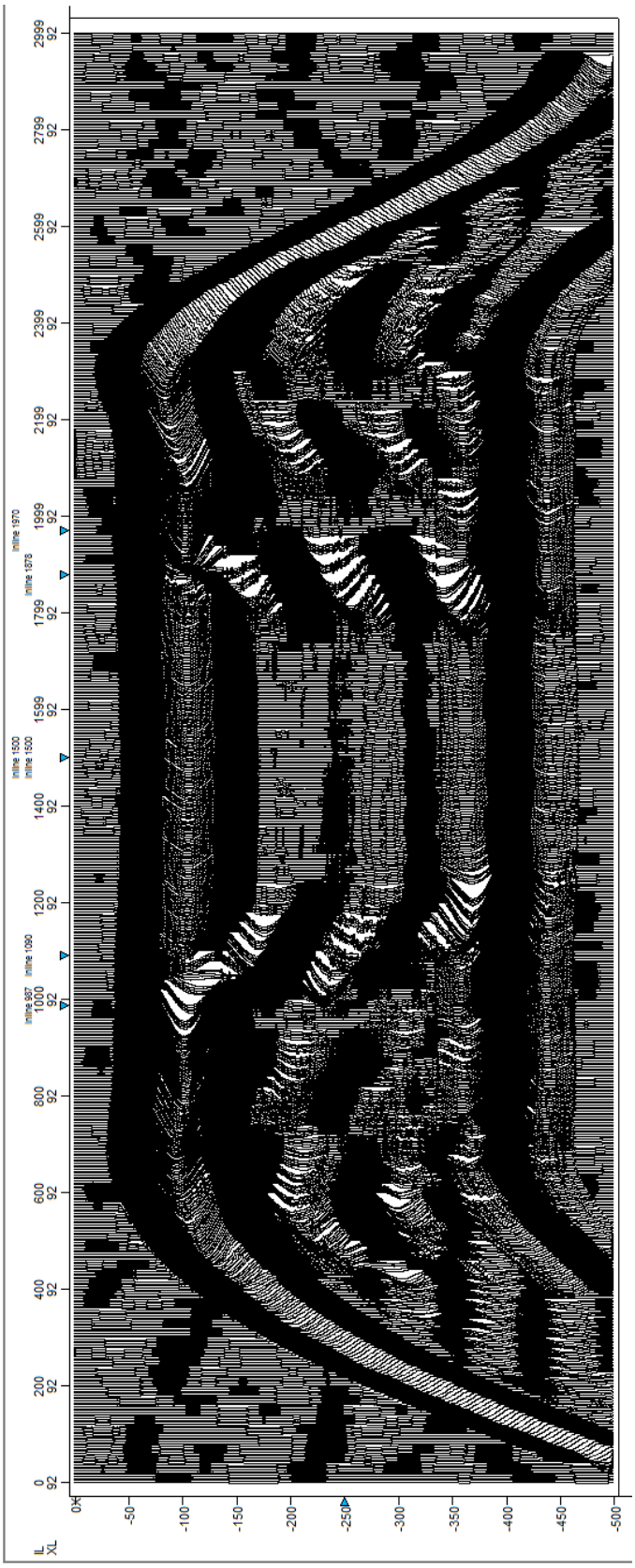

Four Cleaning Upward Cycles of Porosity

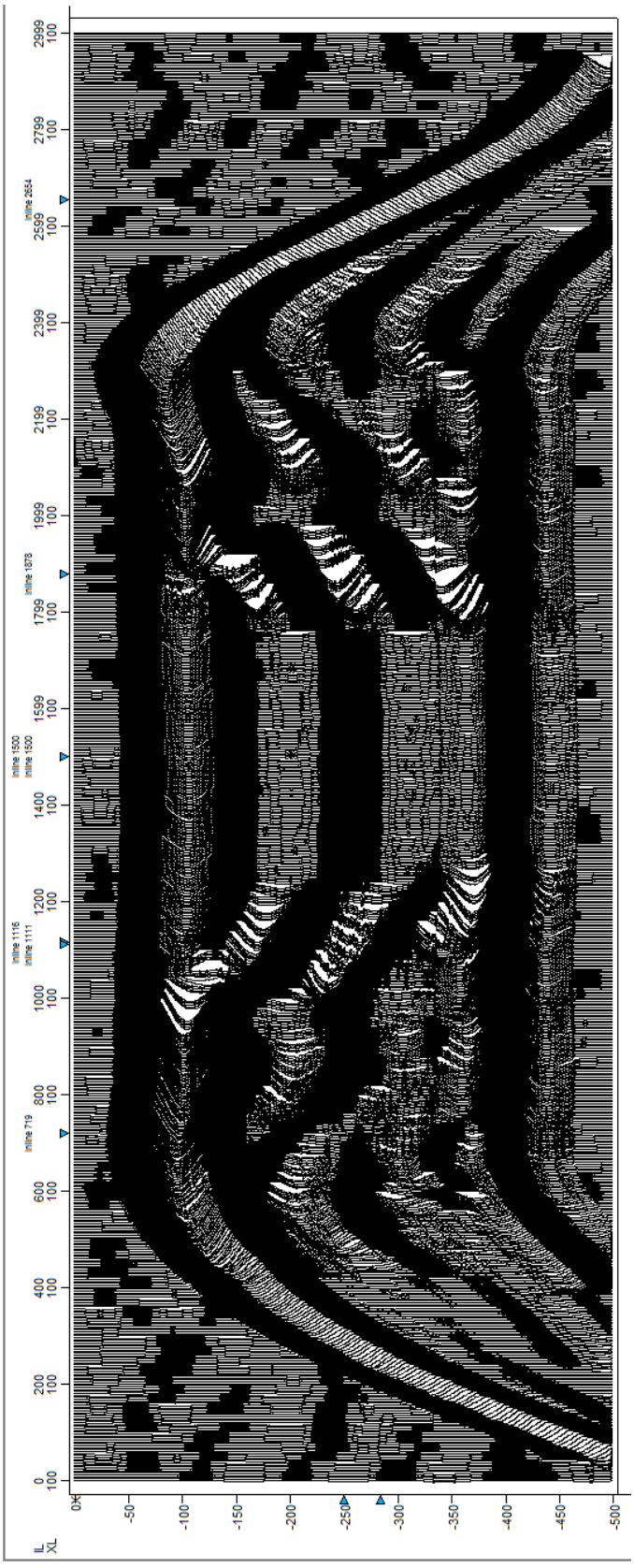

One Dirtying Upward Cycle of Porosity

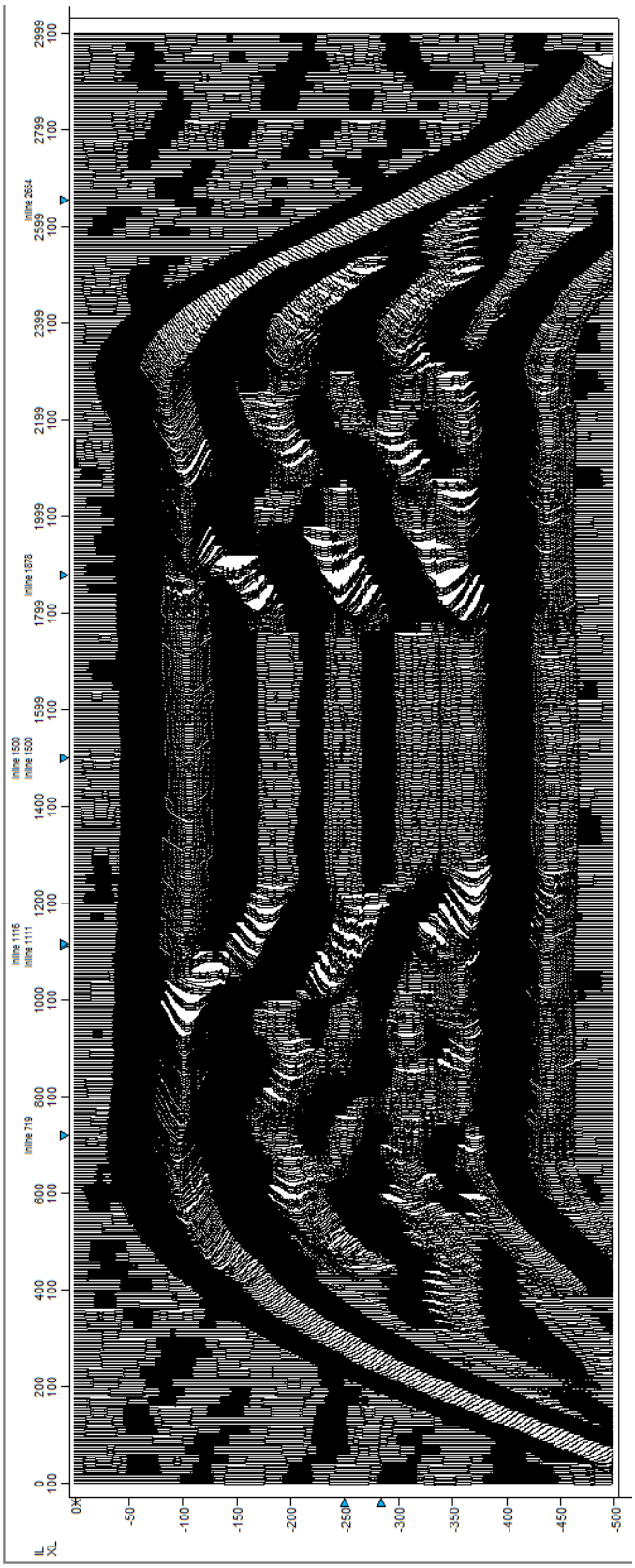

Two Dirtying Upward Cycles of Porosity

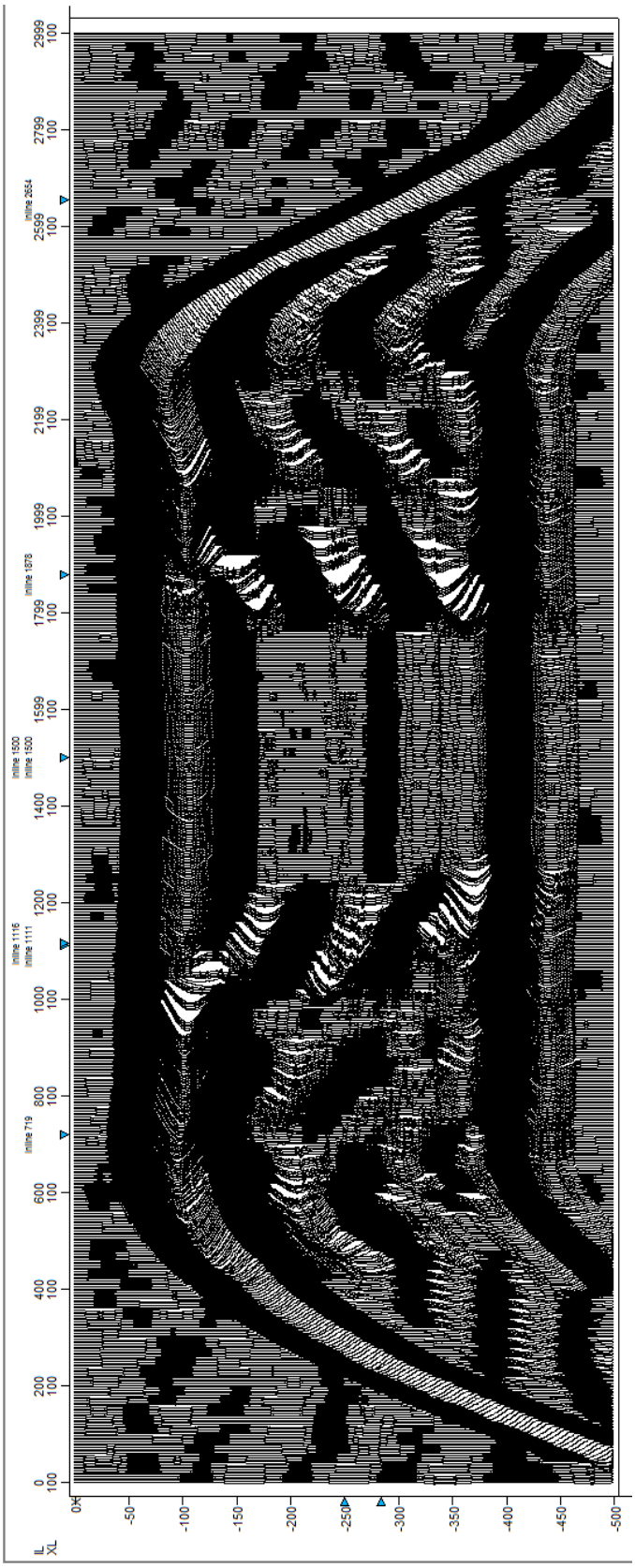

Four Dirtying Upward Cycles of Porosity

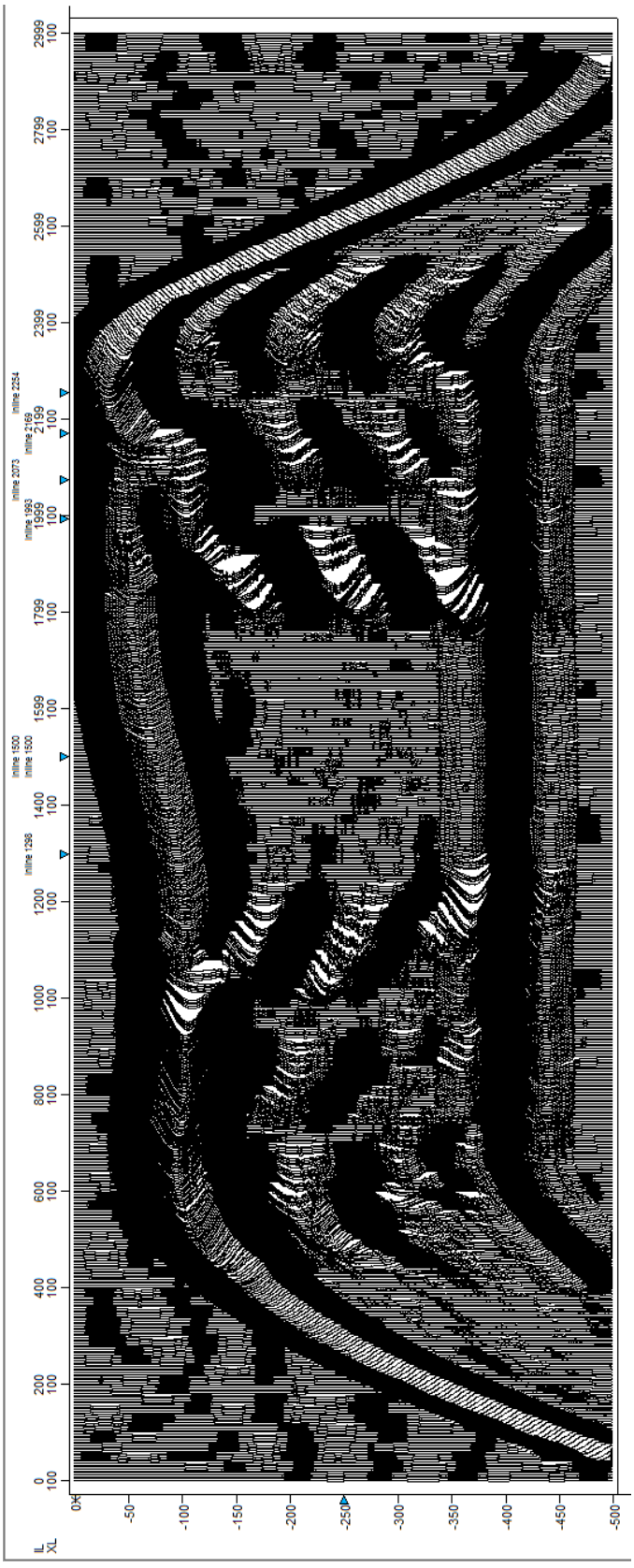

Carbonate Pinnacle

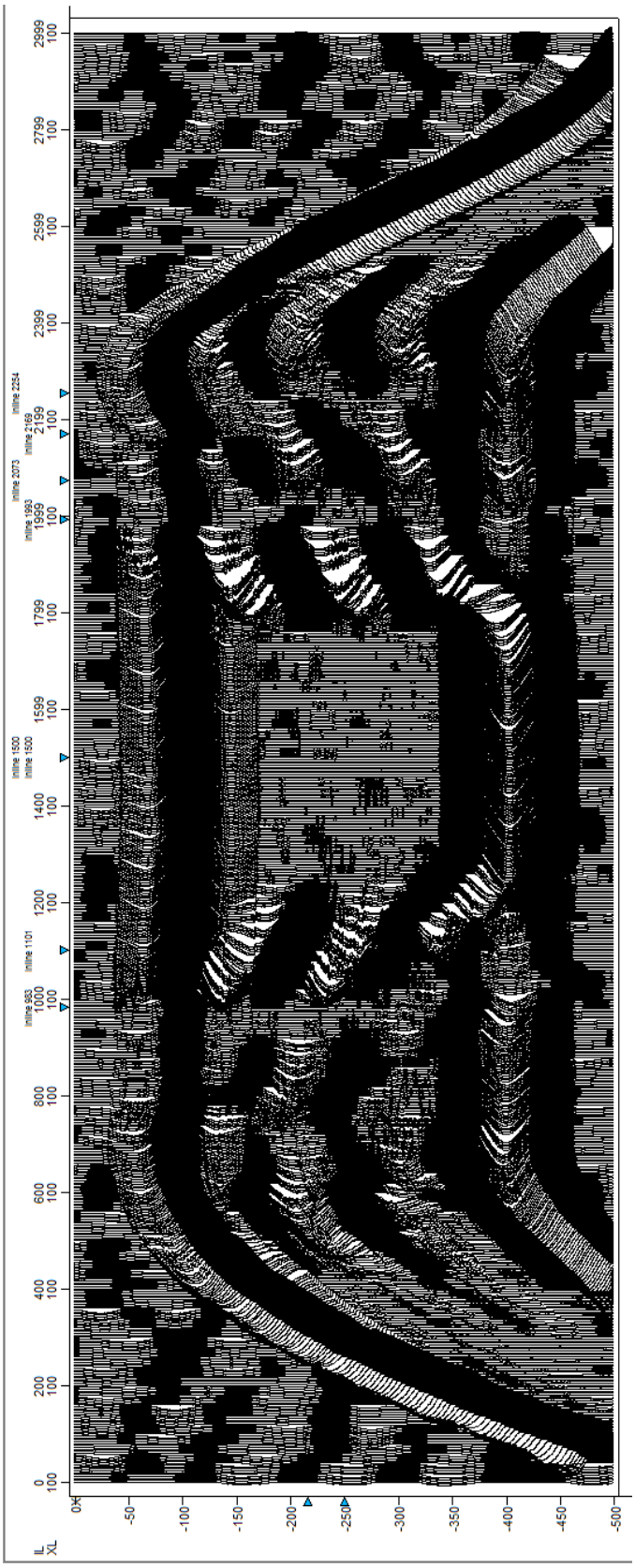

Low Impedance Shale

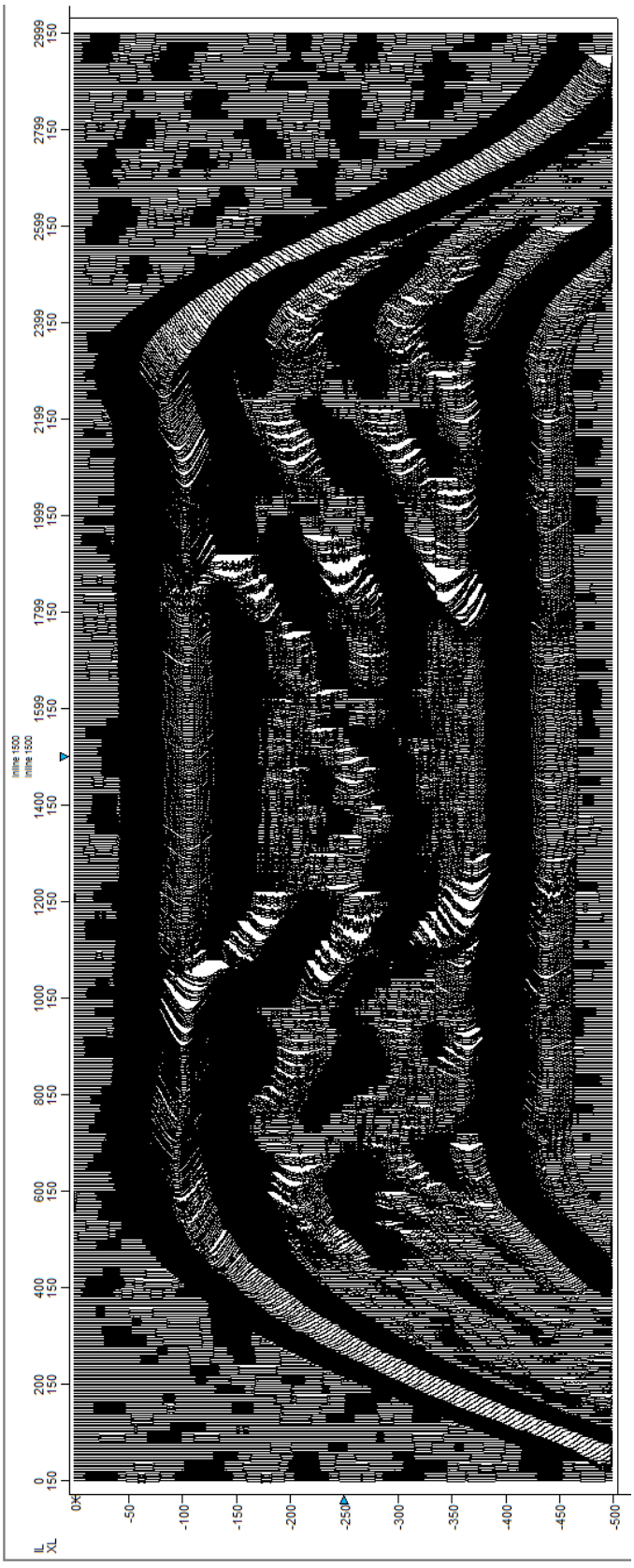

25% Patch Reefs

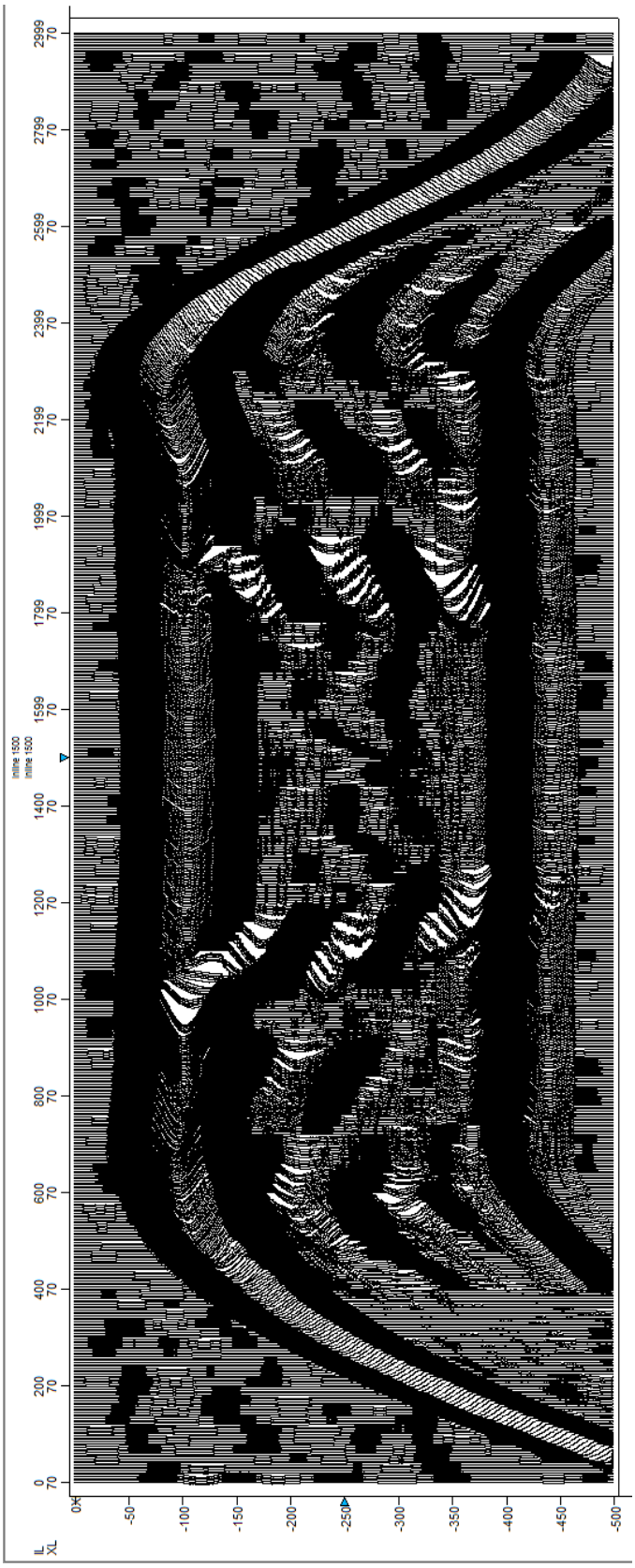

10% Patch Reefs

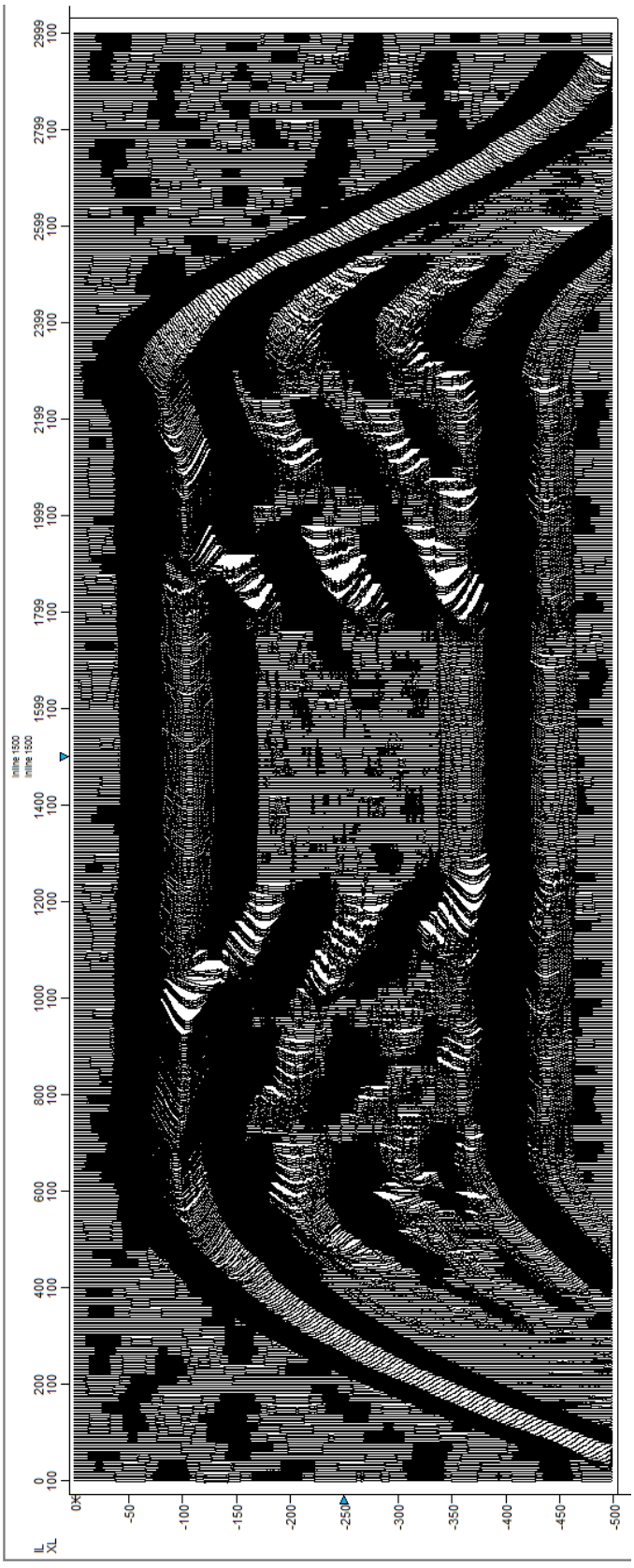

1% Patch Reefs

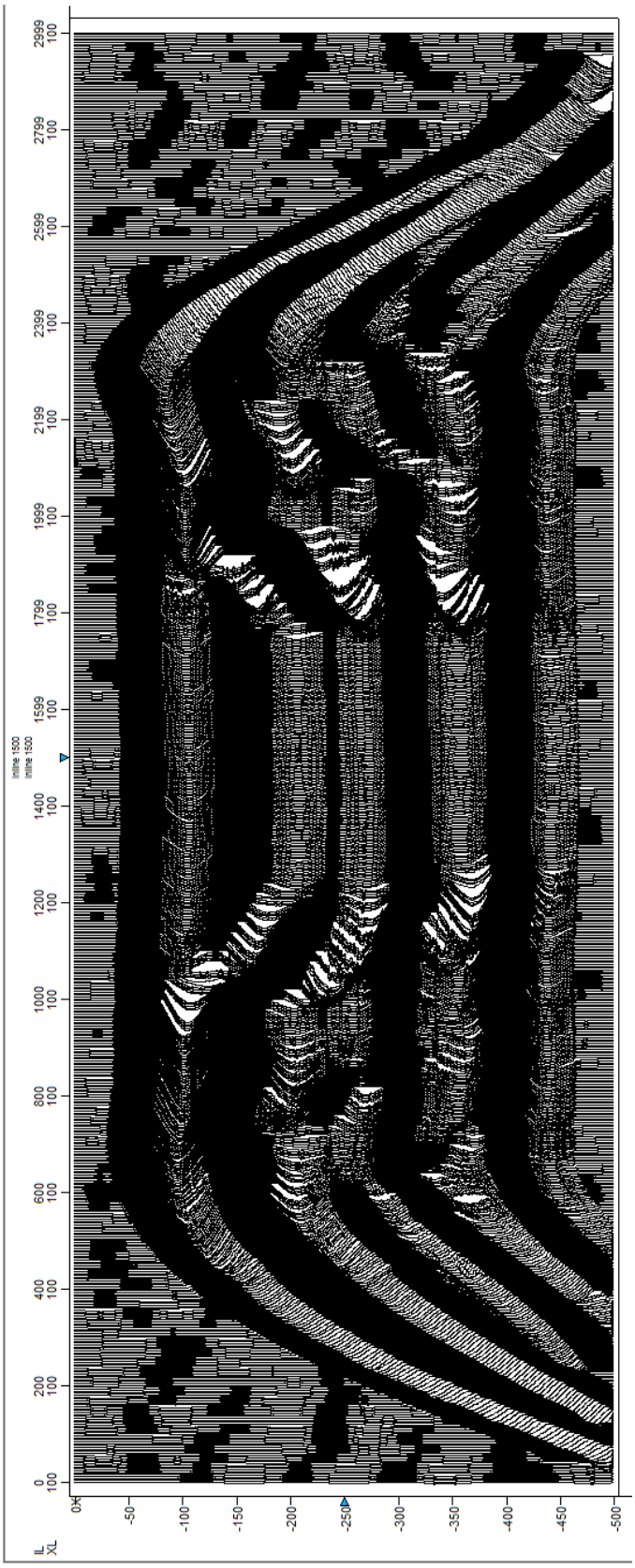

One Cleaning Upward Cycle at Elevated Porosity

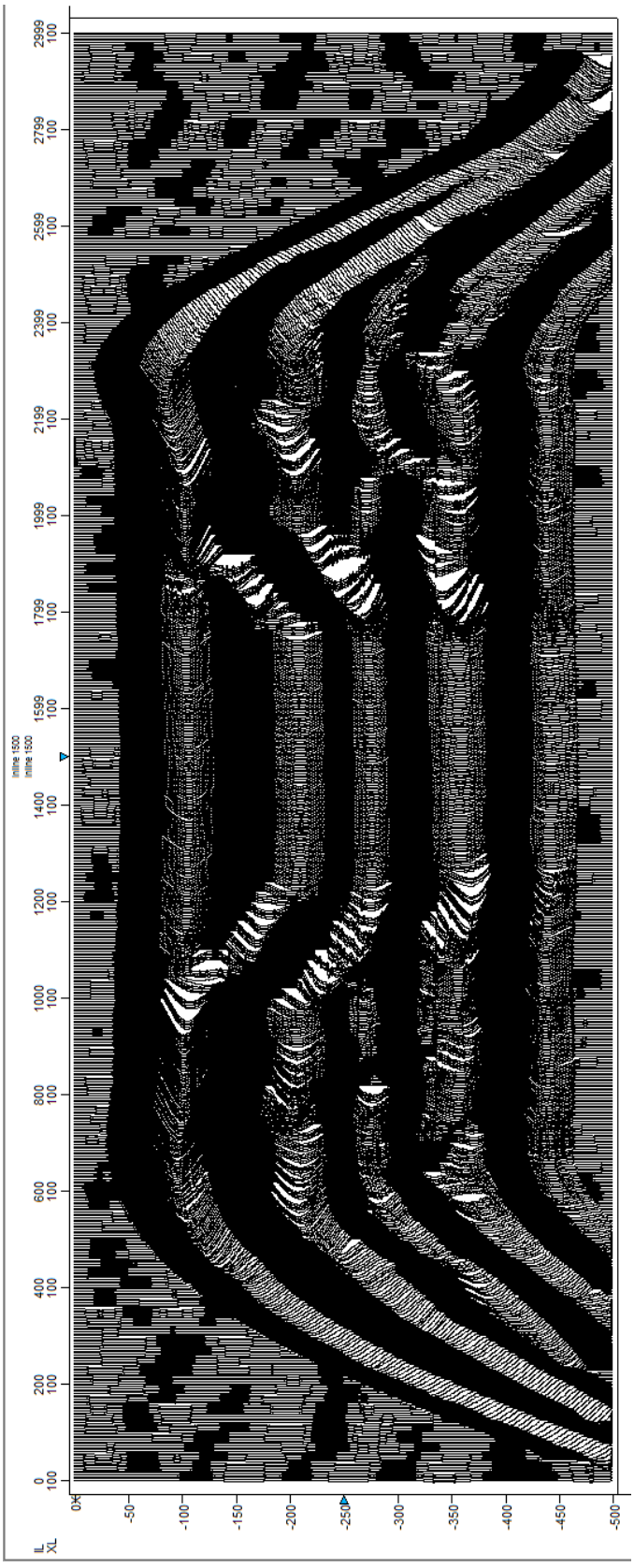

Two Cleaning Upward Cycles at Elevated Porosity

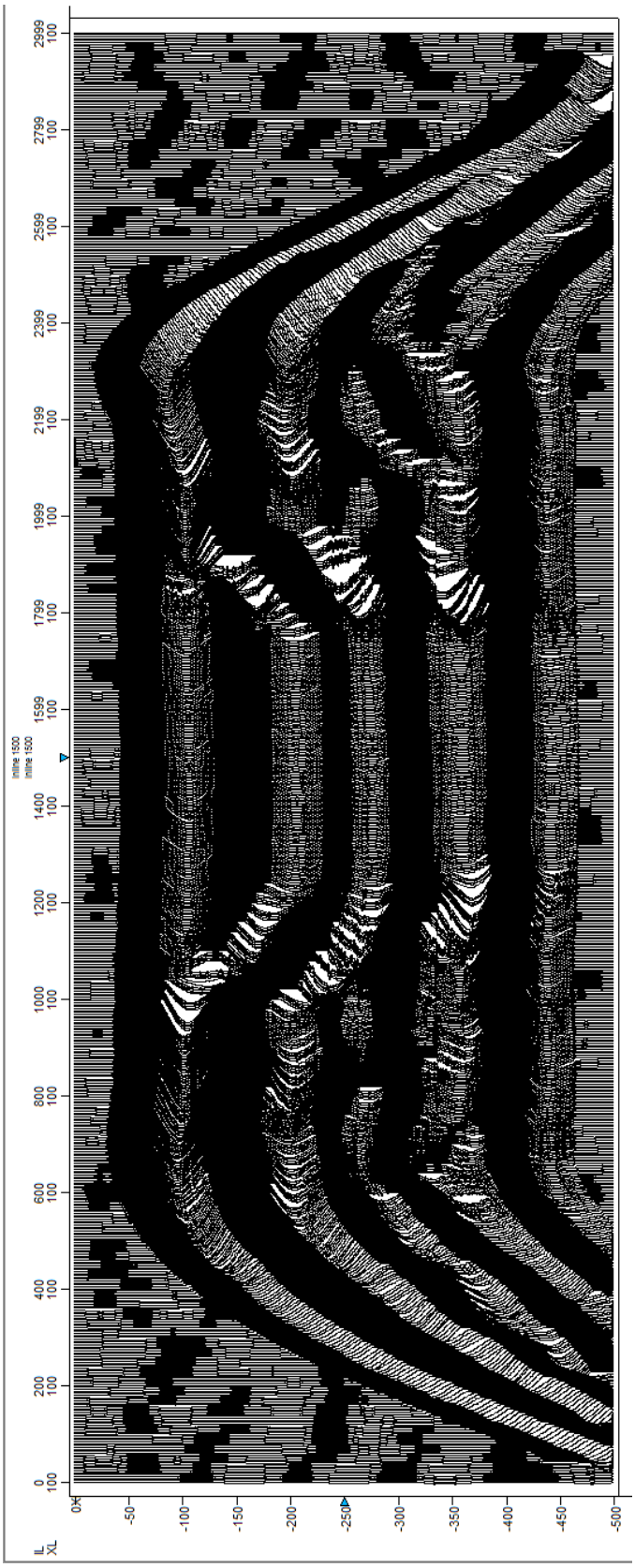

Four Cleaning Upward Cycles at Elevated Porosity

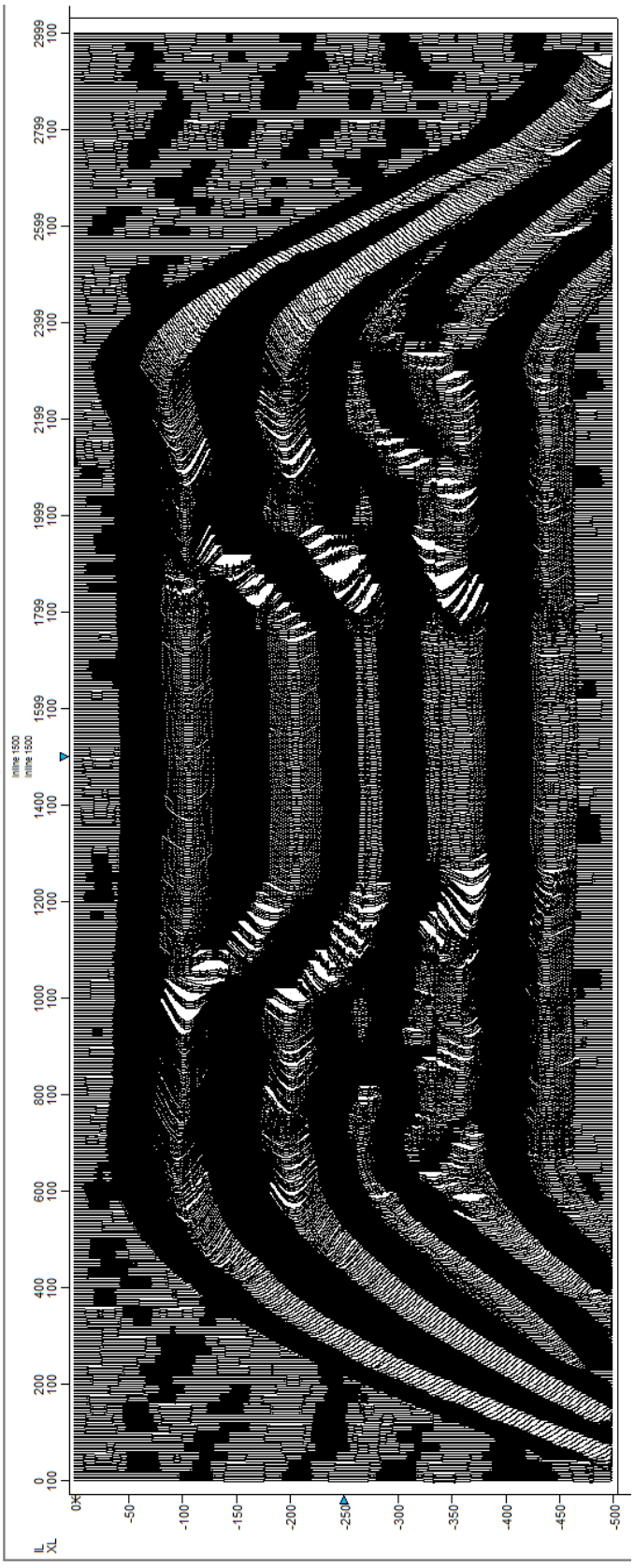

One Dirtying Upward Cycle at Elevated Porosity

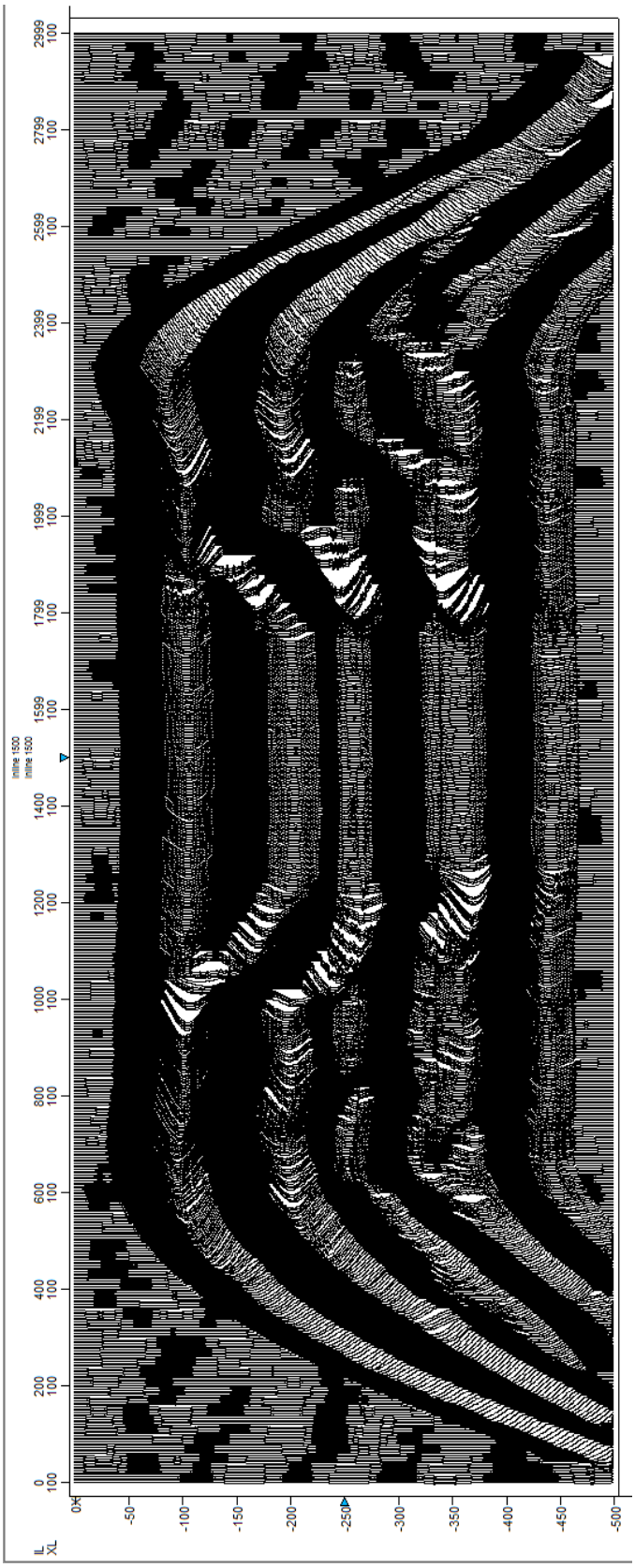

Two Dirtying Upward Cycles at Elevated Porosity

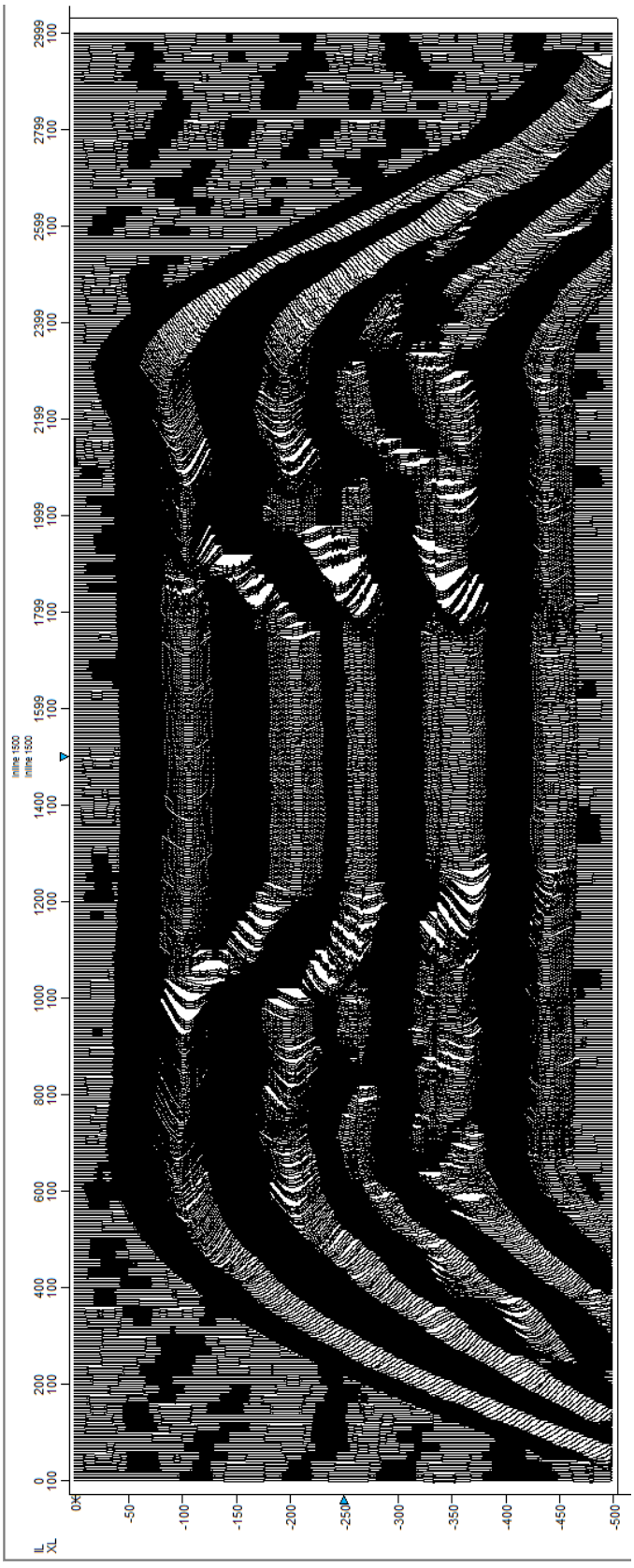

Four Dirtying Upward Cycles at Elevated Porosity

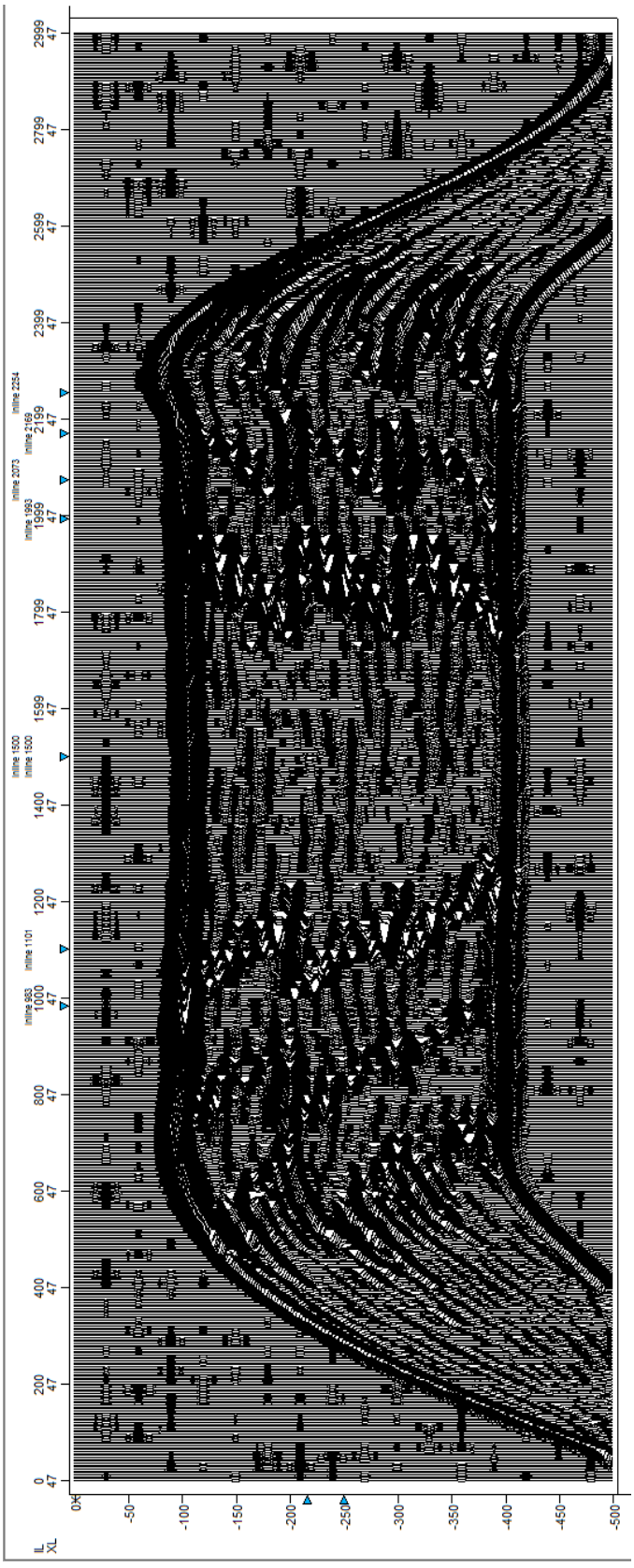

Aggradational Facies Stacking Pattern at 40 Hz